



The role of IL-6 trans-signaling in liver regeneration after partial hepatectomy

Dissertation

This dissertation is submitted for the degree of the Doctor of Philosophy to
the Faculty of Mathematics and Natural Sciences at the Heinrich-Heine-
University Düsseldorf

Presented by

Nastaran Fazel Modares

From Maragheh, Iran

Düsseldorf,

Die Rolle des IL-6 *trans-signalings* bei
Leberregeneration nach partieller Hepatektomie

Dissertation

Dissertation zur Erlangung des Doktorgrades der Mathematisch-
Naturwissenschaftlichen Fakultät der Heinrich-Heine-Universität Düsseldorf

vorgelegt von

Nastaran Fazel Modares

aus Maragheh/Iran

Düsseldorf, den

aus dem Institut für Biochemie und Molekularbiologie II, Medizinische
Fakultät, Heinrich Heine Universität Düsseldorf

Gedruckt mit der Genehmigung der Mathematisch-
Naturwissenschaftlichen Fakultät der Heinrich-Heine-Universität
Düsseldorf

Referent: Prof. Dr. rer. nat. Jürgen Scheller

Korreferent: Prof. Dr. Philipp A. Lang

Tag der mündlichen Prüfung:

Eidesstattliche Erklärung zur Dissertation Hiermit versichere ich, dass die vorliegende Dissertation von mir selbständig und ohne unzulässige fremde Hilfe unter Beachtung der Grundsätze zur Sicherung guter wissenschaftlicher Praxis an der Heinrich-Heine-Universität Düsseldorf verfasst worden ist. Die Dissertation wurde in der vorgelegten oder in ähnlicher Form noch bei keiner anderen Institution eingereicht. Ich habe bisher keine erfolglosen Promotionsversuche unternommen.

Düsseldorf, den

Nastaran Fazel Modares

به پدرم و مادرم

This thesis is dedicated to my parents. For their endless love and support.

“To be idle is a short road to death and to be diligent is a way of life;
foolish people are idle, wise people are diligent.”

Buddha

Table of Content

TABLE OF CONTENT	8
1 INTRODUCTION	11
1.1 Cytokines.....	11
1.2 Interleukin-6 type cytokines.....	11
1.3 Composition of the IL-6/ IL-6R complex and signal transduction.....	12
1.3.1 IL-6/IL-6R complex: Classic signaling.....	12
1.3.2 IL-6/sIL-6R complex: Trans-signaling.....	12
1.3.3 IL-6 Cluster signaling.....	13
1.4 The role of IL-6 in health and disease.....	14
1.5 Blockade of IL-6 signaling as a therapeutic target.....	16
1.6 Liver homeostasis and disease.....	18
1.6.1 Liver anatomy.....	18
1.6.2 Liver function.....	19
1.6.3 Liver diseases.....	19
1.7 Liver regeneration after PHX.....	22
1.8 The role of IL-6 in liver regeneration after PHX.....	23
1.9 Aims.....	25
2 MATERIAL	26
2.8 Materials.....	34
2.9 Surgical tools.....	35
2.10 Methods.....	36
2.11 Mice.....	46
2.11.1 Mouse Experiments.....	46
2.11.2 Serum and organ removal.....	48
3 RESULTS	50
3.1 Generation of soluble IL-6R mice.....	50
3.2 sIL-6R in sIL-6R ^{+/+} mice activates the cells through IL-6 trans-signaling.....	59

3.3 Soluble IL-6R ^{+/+} mice fully compensated disabled IL-6 classic signaling by IL-6 trans-signaling during liver regeneration after partial hepatectomy.....	67
3.4 sIL-6R was enhanced in sIL-6R ^{+/+} mice after PHX.....	72
3.5 IL-6 trans-signaling promotes liver regeneration in sIL-6R ^{+/+} mice.....	74
3.6 Selective inhibition of IL-6 trans-signaling prevents liver regeneration following PHX 77	
3.7 Selective inhibition of IL-6 trans-signaling abrogated STAT3 signaling during liver regeneration following PHX.....	81
3.8 Effect of IL-6 on the function of HSC in liver regeneration upon liver damage	86
3.9 Induced <i>Hgf</i> expression of hepatic stellate cells via IL-6 trans-signaling in mice following PHX	87
3.10 IL-6 Trans-signaling regulates <i>Hgf</i> production	90
4 DISCUSSION	94
4.1 Generation of IL-6 trans-signaling mice.....	95
4.2 sIL-6R in sIL-6R ^{+/+} mice targets the cells through trans-signaling.....	97
4.3 Liver regeneration was normal in sIL-6R ^{+/+} mice	98
4.4 IL-6 trans-signaling initiated JAK/STAT signaling in target cells	99
4.5 IL-6 trans-signaling results in enhanced HGF production by HSCs after PHX	99
4.6 Abrogated liver regeneration upon blockade of IL-6 trans-signaling by sgp130Fc ...	101
4.7 Blockade of IL-6 classic and trans-signaling results in impaired liver regeneration .	103
4.8 The absence of IL-6R results in impede liver regeneration after PHX	105
4.9 IL-6 trans-signaling promotes HGF production in rat HSCs.....	107
4.10 Clinical relevance of the presented work in the context of liver regeneration	108
5 REFERENCES.....	113
6 ZUSAMMENFASSUNG	125

7	SUMMARY	127
8	ABBREVIATIONS	128
9	PUBLICATIONS	132
10	ACKNOWLEDGEMENT	133

1 Introduction

1.1 Cytokines

Cytokines constitute a broad group of small molecules that includes interferons, chemokines, and interleukins [1, 2]. They play an essential role in cell signaling processes such as apoptosis, cell differentiation, and cell growth. Cytokines activate signals through specific receptors present on the cell surface of signal receiving cells [1]. Cytokines are produced and synthesized by different cell types. Expressed cytokines can activate other cytokine-producing cells of the same type in a process known as autocrine signaling; or activates neighboring cells through cell-cell communication known as paracrine signaling [3, 4]. It has been shown that cytokines are involved not only in physiological processes but also in pathophysiological processes such as autoimmune diseases, inflammatory diseases, and cancer [5]. Among the different cytokines, the multifunctional role of the interleukin-6 (IL-6) family of cytokines is well studied [6]. Additionally, based on their fundamental role in the suppression or progression of inflammatory diseases, members of the IL-6 family are attractive therapeutic targets for the treatment of inflammation, autoimmune disorders, and cancer [7].

1.2 Interleukin-6 type cytokines

In the present study, the main investigation center was on interleukin 6, which carries the same name as the family of cytokines to which it belongs. This family of cytokines consist of nine members: IL-6, IL-11, IL-27, IL-31, ciliary neurotrophic factor (CNTF), leukemia-inhibitor-factor (LIF), cardiotrophin-like cytokine (CLC), cardiotrophin-1 (CT-1), and oncostatin M (OSM) [8]. The IL-6 type cytokines are composed of four helical-bundle proteins with an up-up-down-down topology [9]. IL-6 has been described and recognized by different names such as B cell stimulating factor 2 (BSF-2), as it stimulates B cells to produce more immunoglobulins [10]; interferon- β 2 (INF- β 2), which has activity similar to that of INF [11, 12]; and finally, as Sehegal et al. named it, IL-6 [13]. Initially, IL-6 binds to its α -receptor known as IL-6R [14]. IL-6R is a nonsignaling type I transmembrane glycoprotein composed of 468 amino acids with a molecular weight of approximately 80 kD [15]. The binding of IL-6 to IL-6R alone is not enough to initiate signaling in the target cells. Signal transduction by IL-6 is initiated when the IL-6/IL-6R complex interacts with β -receptor glycoprotein 130 (gp130), which is a type I transmembrane receptor consisting of

918 amino acids. Gp130 has five extracellular immunoglobulin (Ig)-like/fibronectin-like domains [16]. During cytokine binding, gp130 forms homodimers to initiate the signal [15]. Notably, all other members of the interleukin-6 family, except IL-31, initiate intracellular signaling through gp130 homodimers or heterodimers [17, 18] (Fig. 1A).

1.3 Composition of the IL-6/ IL-6R complex and signal transduction

IL-6 initiates signaling in the target cells through three different pathways, which are known as 1) classic signaling, 2) trans-signaling, and 3) cluster signaling [3, 19] (Fig. 1B-D).

1.3.1 IL-6/IL-6R complex: Classic signaling

IL-6 binds to its cognate α -receptor known as IL-6R (CD126 or gp80), and the formation of the IL-6/IL-6R complex is needed to activate cells through the so-called classic signaling pathway [3]. IL-6R is composed of three extracellular domains: an extracellular stalk domain, a transmembrane domain, and an intracellular domain. The three IL-6R extracellular domains include an immunoglobulin (IgG)-like domain (D1) and two fibronectin type III domains (D2 and D3) [14, 20]. Site I of IL-6 interacts with IL-6R via the cytokine binding module of the D2 and D3 domains [21]. Subsequently, the IL-6/IL-6R complex interacts with gp130. It is noteworthy that the stalk domain facilitates the interaction of the IL-6/IL-6R complex with gp130 in the target cells [22]. The connection of IL-6/IL-6R with gp130 results in homodimerization of gp130 and leads to the activation of Janus-kinase/signal transducer and activator of transcription (Jak/STAT) [23], phosphatidylinositol-3-kinase (PI3K) and mitogen-activated protein kinase (MAPK) pathways [24]. IL-6R is expressed by few cell types, namely, hepatocytes, B and T cells, neutrophils, macrophages, and monocytes [25-27]. Therefore, IL-6 can activate classic signaling in only a few cell types.

1.3.2 IL-6/sIL-6R complex: Trans-signaling

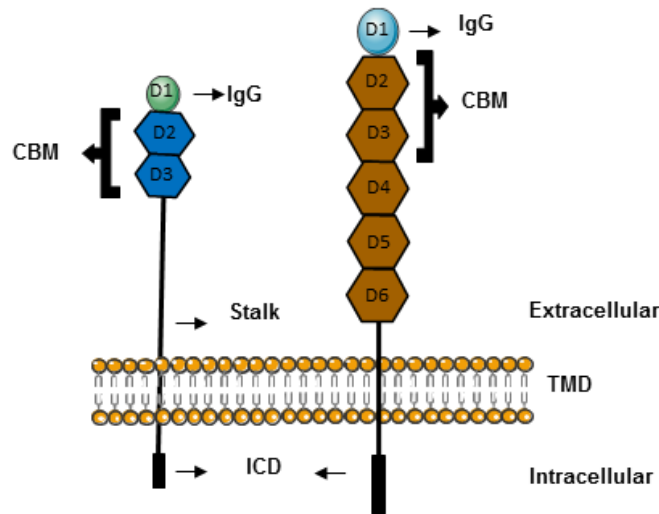
In trans-signaling, IL-6 interacts with the soluble form of IL-6R (sIL-6R), which consists only of the extracellular domains and the stalk region [3]. The IL-6/sIL-6R complexes can also bind and activate gp130, which is ubiquitously expressed. sIL-6R is generated through alternative splicing of IL-6R mRNA or, more frequently, through proteolytic cleavage by different metalloproteases

[28], mainly those of the ADAM protease family, which also cleave many cytokines and receptors such as TNF- α , the TNF receptor, and IL-6R [29]. Disintegrin and metalloproteinases 10 and 17 (ADAM10 and ADAM17) mainly mediate ectodomain shedding of the membrane-bound IL-6R and the production of soluble IL-6R [28]. The IL-6/sIL-6R complex interacts with gp130 to form gp130 homodimers. Homodimerization of gp130 results in the pathway induction of Jak/STAT, PI3K, and MAPK by trans-signaling [24].

1.3.3 IL-6 Cluster signaling

In cluster signaling, IL-6R α is expressed on the surface of cells *in trans*, and IL-6 binds to cells expressing IL-6R α (transmitter cells). Then, the IL-6/IL-6R complexes on the transmitter cells interact with neighboring cells, which are expressing gp130 (receiver cells), and subsequently, IL-6 initiates the signaling in these cells. Therefore, initiation of IL-6 signaling occurs through cell-cell interaction [19].

A



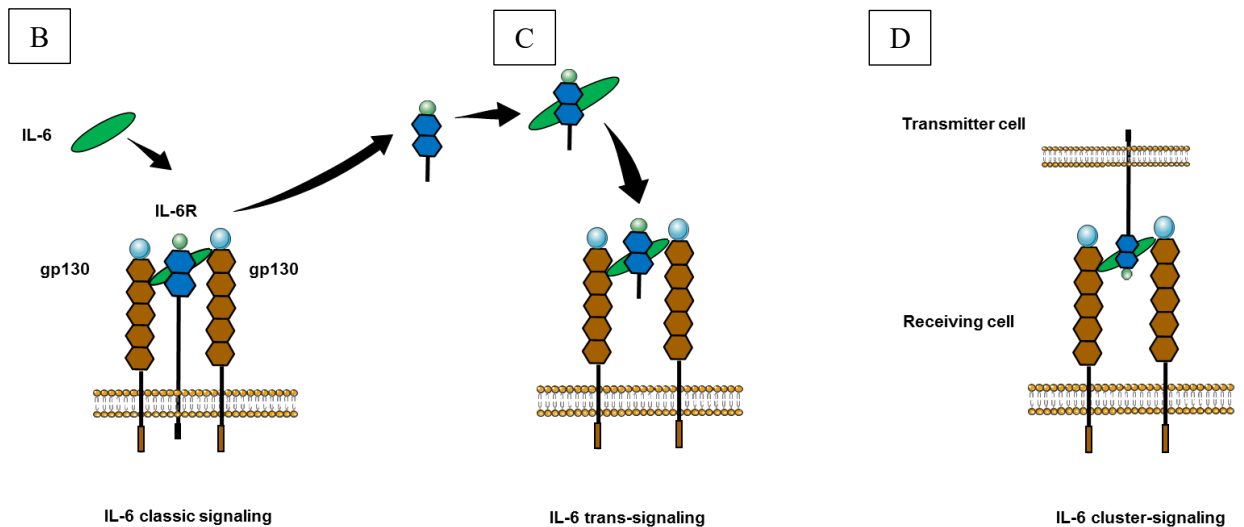


Fig. 1. Structural overview of IL-6R, gp130, and IL-6-induced signal transduction, including the IL-6/IL-6R/gp130 complex formation. (A). Schematic representation of the modular design of IL-6R (blue) and gp130 (brown): IgG domain (IgG, circle), cytokine binding module (CBM), stalk region (black bar), fibronectin type III domains (hexagons), transmembrane domain (TMD), intracellular domain (ICD, black boxes for IL-6R and gp130, respectively). Further explanations are provided in section 1.3. (B) The binding of IL-6 (green oval) to the membrane-bound IL-6R results in the recruitment of two gp130 receptors (brown). The homodimerization of the gp130 leads to the activation of signal transduction in the cell through classic IL-6 signaling. (C) Schematic representation of IL-6/sIL-6R complex formation. Upon IL-6 binding to the soluble form of IL-6R, the IL-6/sIL-6R complex is formed. This complex formation results in the recruitment of two gp130 molecules, which leads to the activation of signal transduction in the cell through IL-6 trans-signaling. (D) IL-6R α is expressed on the surface of cells *in trans*, which are named transmitter cells. These cells interact with neighboring cells expressing gp130, which are called receiving cells. This interaction leads to the activation of signal transduction in the cell through IL-6 cluster signaling. Further explanations are described in Section 1.3. Figure adopted from Grötzinger et al., Chalaris et al., and Rose-John [17, 26, 30].

1.4 The role of IL-6 in health and disease

Interleukin 6 (IL-6), with its pleiotropic features, is involved in a wide range of physiological and pathophysiological processes [31, 32]. It is expressed by B cells, T cells, fibroblasts, endothelial cells, macrophages, and monocytes [33]. IL-6 contributes to neural homeostasis, function maintenance and survival [34-37]. Using IL-6 deficient mice showed 60% reduction in sensory function of these neurons [38]. Furthermore, functional recovery of sensory nerves after injury was

also impaired in the absence of IL-6 [38, 39]. In the cardiovascular system, IL-6 mediates vascular homeostasis and protects myocytes from the consequences of oxidative stress [40]. In the liver, IL-6 regulates synthesis of acute phase proteins as a reduction in acute phase response was observed after IL-6 deficient mice were challenged with LPS [31, 41, 42]. Moreover, IL-6 regulates bone homeostasis through regulation of osteoclast activity [43]. However, IL-6 dysregulation can negatively influence homeostasis and promote inflammatory diseases. In a steady state, IL-6 serum concentration is low (approximately 1-10 pg/ml) [28]. However, upon injury or infection, immune cells are activated, and massive amounts of IL-6 are secreted leading to drastic increases in the levels of circulating IL-6 under pathophysiological conditions (up to 1000 fold) [44]. IL-6 contributes to immune responses by regulating the differentiation of T and B cells. IL-6 affects the differentiation of T cells into T helper 2 (TH2) cells [45]. Presence of IL-6 could also affect the differentiation of naïve CD4⁺ T cells into TH2 cells by inducing IL-4 expression and suppressing IFN- γ via SOCS3. Interestingly, IL-6 maintains the balance in the T cell differentiation into T helper 17 cells (TH17) and into regulatory T (Treg) cells [46-48]. IL-6 also promotes the differentiation of B cells into antibody-producing cells [49, 50]. IL-6 also contributes to the development of autoimmune diseases [51]. Overexpressed IL-6 inhibits TGF- β and redirects the differentiation of naïve CD4⁺ T cells towards becoming T helper cells 17 (TH17), playing important roles in the progression of different immune diseases such as rheumatoid arthritis (RA), which affects the joints and is accompanied by pain. To date, the proinflammatory roles of IL-6 have been studied and best characterized in RA [52, 53]. The infiltration of immune cells during RA enhances the release of proinflammatory mediators, such as IL-6, into the synovium, and the circulating IL-6 levels in the blood and synovial fluid of patients diagnosed with RA are simultaneously and drastically increased [54]. In addition to IL-6, upregulated sIL-6R has also been observed in these patients, facilitating widespread effects of IL-6 in RA [55]. Circulating IL-6 reaches the liver via the bloodstream and induces the production of acute phase proteins, including serum amyloid A (SAA), fibrinogen, and haptoglobin [56] [57]. Furthermore, most patients with RA are also diagnosed with anemia [58]. During progression of this autoimmune disease, IL-6 stimulates the production of hepcidin in the liver. Increased levels of hepcidin reduces iron levels in the serum and cause anemia in these patients. Moreover, overproduction of IL-6 could dysregulate osteoclast activity and develop osteoporosis, as observed in patients with RA [59]. The effect of IL-6 overexpression has been extensively reported in

different inflammatory and autoimmune diseases; however, impaired IL-6 and its signaling component, IL-6R or gp130, may also affect healthy humans; however, this aspect is poorly established [60]. Recently, it was shown that patients with abnormalities in IL-6R expression by genetic mutations in the IL-6R gene developed skin lesions, immune deficiency and atopy coinciding with high levels of IgE [61]. Considering the fundamental role of IL-6 in health and disease, any dysregulation in IL-6, IL-6R, or gp130 expression might affect an individual's health, possibly becoming life-threatening.

In summary, the overexpression of IL-6 has various effects on the progression of RA [59]. Overactive IL-6 is associated not only with joint destruction but also with systemic disorders [62]. Therefore, IL-6 and components of IL-6 signaling have become potential clinical targets to improve the outcome of inflammatory diseases [63].

1.5 Blockade of IL-6 signaling as a therapeutic target

Despite the pivotal role of IL-6 in homeostasis, dysregulation of IL-6 promotes different inflammatory diseases, such as RA [64], inflammatory bowel disease (IBD) [65], and multiple sclerosis [66]. To analyze effects of the inhibition of IL-6 signaling and IL-6 components on the progression of inflammatory diseases, various components have been developed, some of which have had clinical use or have entered the clinical trial phase. The outcomes of RA in animal models were significantly improved using anti-IL-6R antibodies. Successful use of IL-6R antibodies in rodent models of RA has resulted in the development of tocilizumab (TCZ), which is a humanized antibody directed against the IL-6R that blocks binding of IL-6 to its receptor [67]. The efficacy of TCZ has been proved in clinical trials and is currently used clinically in patients diagnosed with RA, castleman's disease, and systemic juvenile idiopathic arthritis (SJIA) [68, 69]. The use of TCZ forced the development of the second antibody, sarilumab against IL-6R [70]. Similar to tocilizumab, sarilumab has been used for the treatment of patients with rheumatoid arthritis [71]. Siltuximab also inhibits the interaction of IL-6 with IL-6R by binding to IL-6 [72]. Furthermore, different therapeutic agents, such as EBI-029 (epitope 2) and olokizumab (epitope 3), bind to IL-6 and prevent the interaction of the IL-6/IL-6R complex with gp130 [73]. However, all antibodies inhibit IL-6 classic, trans-signaling, and cluster signaling with the same magnitude. It is not possible to selectively inhibit IL-6 signaling using these approaches, and globally blocking IL-6 could interfere with its essential roles in the homeostasis in different organs. For example, blocking

classic IL-6 signaling by antibodies could lead to dysregulation of the immune response and subsequently increase the risk of infection in patients diagnosed with rheumatoid arthritis [74, 75]. Therefore, the development of specific therapeutic agents to specifically inhibit IL-6 trans-signaling might have advantages compared to other drugs. To specifically inhibit IL-6 trans-signaling, sgp130Fc has been developed [76] (Fig. 2). Sgp130Fc consists of the extracellular domain of gp130 fused to the Fc region of a human IgG antibody [76]. Mechanistically, sgp130Fc has a high binding affinity to the IL-6/sIL-6R complex [76]. However, sgp130Fc is also found endogenously in human serum with a concentration of approximately 250-400 ng/ml [76, 77]. A recent study showed that this amount of endogenous sgp130 is not able to block IL-6 trans-signaling on the other hand, it might enhance the half-life of IL-6 [78]. Sgp130Fc as a fusion protein has been designed and used in different preclinical studies. Previous studies have investigated the efficiency of sgp130Fc through blockade of IL-6 trans-signaling in improving the outcomes of different inflammatory diseases such as arteriosclerosis [79], asthma [80], chronic intestinal inflammation [65], and RA [81]. Although blocking IL-6 through the use of different antibodies, such as TCZ, could reduce the manifestations of diseases, it could impair homeostasis in different organs [82]. For example, blocking IL-6 activity via TCZ in patients with RA has been reported to cause hepatotoxicity, elevated ALT and AST levels, liver failure in patients [82, 83]. Furthermore, an official report showed that the use of TCZ results in liver failure (Red hand letter, 26 Jun 2019, Roche). As a central organ in the body, the liver has pivotal roles, and its dysfunction causes other accompanying effects on essential biological processes. Therefore, the impact of IL-6 activity blockades through the use of antibodies or sgp130Fc on the vital physiological roles of IL-6 should be taken into account.

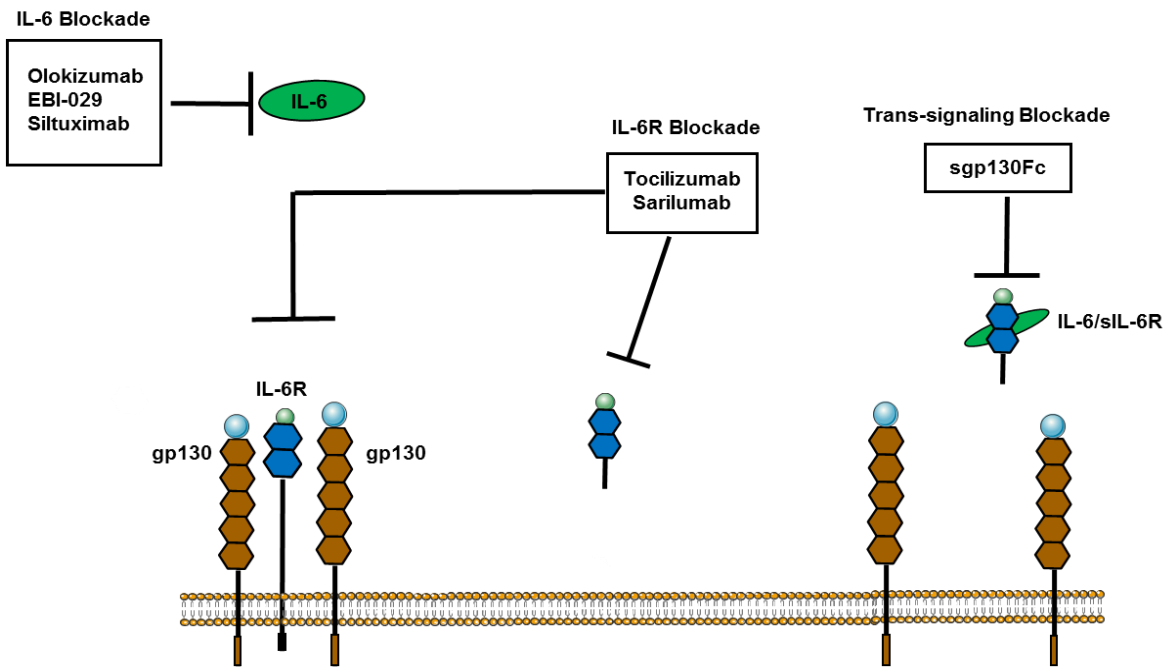


Fig. 2. Therapeutic blockade of IL-6 signal transduction. Various inhibitors with different functions are used for the inhibition of IL-6-induced signal transduction. For the classical and trans-signaling pathway, monoclonal antibodies directed against the IL-6 binding epitopes are used. Siltuximab binds to epitope 1, and EBI-029 binds to epitope 2. Tocilizumab and sarilumab bind to IL-6R (the membrane-bound and soluble forms) and block the IL-6 binding. For selective blockade of the trans-signaling pathway, sgp130Fc is used, which specifically binds to the IL-6/sIL-6R complex. Figure adopted from Hunter & Jones et al. [73].

1.6 Liver homeostasis and disease

1.6.1 Liver anatomy

The liver is the largest organ in the body. The liver is positioned at the right upper quadrant of the abdominal cavity below the diaphragm [84]. The blood supply to the liver is supported by two main sources: the portal vein, which supplies nutrients from other organs such as the spleen, intestine, and pancreas (nutrient-rich and oxygen-poor blood), and the hepatic artery, which is responsible for the oxygen supply (oxygen-rich and nutrient-poor blood) [84-86]. The falciform ligament divides the liver into two distinct lobes, the right and left lobes. In contrast to that of

humans, the murine liver is divided into four lobes: a left lobe, right lobe, caudate lobe, and median lobe [87].

1.6.2 Liver function

Hepatocytes are the largest population of resident cells in the liver [88, 89]. The distribution of hepatocytes is heterogeneous in the liver, and they are categorized into different groups based on their location and their distance from the oxygen-rich portal triad. Periportal hepatocytes contribute to the liver functions of gluconeogenesis, β -oxidation of fatty acids, amino acid catabolism, bile acid secretion and cholesterol, glycogen, and urea synthesis. Periventricular hepatocytes also contribute to glycolysis as well as lipogenesis, detoxification and bile acid synthesis [90-93]. Bile duct canaliculi are presented in the apical sides of the resident hepatocytes where the synthesized bile is secreted and drained into the bile duct [94].

Furthermore, Kupffer cells, known as nonparenchymal cells, are resident macrophages in the liver. They contribute to the regulation of immune responses through cytokine production and eliminate bacteria and viruses by phagocytosis [89, 95, 96]. Finally, presinusoidal cells are found in the perisinusoidal space of the liver. These cells are also known as hepatic stellate cells (HSCs), Ito cells, or fat-storing cells. HSCs compromise 5 to 8% of the total liver mass and are located in the space of Dissé [97]. In addition to vitamin A storage, they are involved in the support of hepatocyte proliferation through the production of hepatocyte growth factor (HGF) [98].

The liver is a central organ in the regulation of metabolism. Regarding the processing of carbohydrates, the liver is involved in glycogen synthesis and gluconeogenesis to maintain the sugar level in the blood [99].

1.6.3 Liver diseases

As described above, the liver plays a critical role in the production of serum proteins, such as acute phase proteins. Consistently, the liver plays an essential role in the conversion of toxic metabolites or food-borne toxins into nontoxic particles [100, 101]. However, pathological circumstances can impair the homeostasis and essential activity of the liver [102, 103]. In general, two main pathological changes result in liver dysfunction: 1) acute and 2) chronic liver damage [103, 104]. Alcohol consumption, viral infection, autoimmune-mediated hepatitis, primary biliary cholangitis,

or genetic disorders can cause chronic liver injury [105]. The progression of chronic inflammation results in fibrosis [106]. Upon liver damage HSCs become active. During this phenotypic changes, HSCs transform to myofibroblast-like cells which is accompanied with losing their vitamin A droplets and expression of α -smooth muscle action (α -SMA) [107-109]. Active HSCs are known source of ECM proteins which is characteristic of fibrotic liver [110, 111]. It has been shown removing active HSCs by induction of apoptosis might help to resolution of fibrosis [112]. At this early fibrosis stage, local inflammation results in the expression of cytokines and growth factors, which induce the regeneration process of the liver, and as a result, the original level of liver function can be restored [113]. However, in advanced stages, fibrosis progresses into liver cirrhosis, which is the end stage of chronic liver injury and causes 1 million deaths per year worldwide [106, 114]. In advance stage of fibrosis, the liver is unable to regenerate and carry out its homeostatic functions. The progression of cirrhosis can result in the development of hepatocellular carcinoma (HCC) in some cases [115, 116]. Liver resection as a curative modality for HCC has been developed [117, 118]. Liver transplantation is another therapeutic approach; in this case, the liver of donors needs to be regenerated to restore the original mass and function [119]. A better understanding of how these regeneration processes are coordinated in the body will help us to improve the clinical tools and treatments for these patients.

As already explained, loss of liver function caused by chronic or acute liver injury initiate and enhance the regeneration process [120]. For deeper insight into liver regeneration and for understanding the underlying mechanism by which to improve therapeutic approaches, different preclinical models have been established. Because of the similarities between rodents and humans, rodent models are used *in vivo* to mimic liver regeneration processes and to achieve a better view of the involved mechanisms [121]. Among cytokines, IL-6 plays an important role in the context of liver diseases and regeneration [122]. As already described, the production of acute phase proteins in the liver is promoted by IL-6 signaling [123, 124], as confirmed in a study with transgenic mice, in which the gp130 receptor was not expressed in hepatocytes. In these mice, induction of liver damage by lipopolysaccharide (LPS) or infection resulted in an abrogated acute phase response [124, 125]. In another study, liver hepatitis was induced by concanavalin A (ConA). Mice treated with IL-6 before ConA administration exhibited less susceptibility to the induced hepatitis. Injection of IL-6 has been shown to protect mice from liver hepatitis after treatment with ConA [126].

Furthermore, the role of IL-6 has been studied in the development of chronic liver injury [127]. Hepatocellular carcinoma (HCC) has been mostly observed in males [128-130]. Similar disparity of HCC has been shown in rodent HCC model [131, 132]. It has been studied that estrogen treatment in male mice inhibits progression of HCC induced by diethyl nitrosamine (DEN) [133, 134]. Furthermore, it has been shown that induction of HCC with DEN in wt male mice resulted in higher hepatic injury characterized by increased levels of ALT, higher necrosis and apoptosis as compared to wt female and IL-6 deficient male mice [135, 136]. The influence of gender and IL-6 production on hepatic injury has been observed in carbon tetrachloride (CCl₄)-induced HCC model which resulted in an increased level of circulating IL-6 in the serum of male mice as compared to female mice. [137].

Moreover, the DEN model was combined with a high-fat diet (HFD), which led to higher levels of IL-6 expression [138]. Normally, IL-6 expression is negatively regulated by SOCS3 [139, 140]. Interestingly, using SOCS3-deficient mice resulted in higher levels of IL-6 and STAT3, which enhanced the proliferation of hepatocytes and contributed to the progression of the HCC [141]. Moreover, in humans, the level of IL-6 expression correlates with the progression of fulminant liver failure or chronic liver injury [135, 142, 143]. These data suggest that IL-6 plays an important role in the progression of liver diseases. Despite its role in the progression of liver cancer, another study showed that IL-6 had a protective role in liver injury such as fibrosis. Using IL-6-deficient mice or conditional gp130-deficient mice and the induction of fibrosis by a single dose of CCl₄ resulted in higher levels of liver injury, hepatocyte dysfunction, and impaired cell proliferation [143, 144]. Accordingly, the protective effect of IL-6 in these models was investigated by treatment with IL-6 [145]. To determine the protective role of IL-6, the liver was subjected to intoxication by intracellular uridine depleting drug (D-gal), and the subsequent results were analyzed. In this model, liver injury forced oval cells to proliferate and induce liver regeneration [146]. Interestingly, it has been shown that administration of D-gal and injection of Hyper IL-6, a fusion protein consisting of IL-6 and soluble IL-6R, before treatment resulted in higher survival rates and less extensive liver damage in rats; however, treatment with IL-6 alone did not show these results [147]. In addition to the protective roles of IL-6 described in the context of liver disease models, its fundamental role in the initiation of liver regeneration upon injury has also been studied in the PHX model.

1.7 Liver regeneration after PHX

In 1931, Higgins and Anderson proposed the PHX model in rodents *in vivo*. This model became famous because the remaining lobes of the liver were not damaged and were not associated with necrosis. Furthermore, the exact timing of regeneration could also be studied [148, 149]. For a 70% partial liver dissection, different cells, cytokines, and growth factors regulate hepatocytes to proliferate [150]. Finally, the liver is restored to its original size and function within 7 days [151].

Partial hepatectomy predominantly triggers the proliferation of hepatocytes [148, 152]. Under steady-state conditions, hepatocytes do not proliferate and remain in the G0 phase [150, 153]. Upon injury induced by PHX, different factors force approximately 95% of the total hepatocytes to enter the cell cycle [150, 154]. The hepatocytes proliferation has been shown to be regulated by different factors, and after two or three rounds of replication, the hepatocytes reenter the G0 phase [150, 155]. In the first 24 hours postoperation, hepatocytes located close to the portal vein of the liver lobule enter the cell cycle, followed by the hepatocytes distributed around the central vein [154, 156]. In contrast, DNA is synthesized in nonparenchymal cells, such as Kupffer cells, at later points of regeneration (approximately 48 to 96 hours postoperation) [117, 157, 158]. In detail, lipopolysaccharides (LPS) derived from the gastrointestinal tract induce TNF- α expression, and TNF- α interacts with its receptors on the surface of Kupffer cells and subsequently activates the NF- κ B pathway in the Kupffer cells, resulting in the production of IL-6 by the Kupffer cells and other innate immune cells [159-163]. IL-6 mediates the priming of hepatocytes that initiate liver regeneration. Interaction of IL-6 with IL-6 receptor or sIL-6R activates STAT3 signals via gp130 in hepatocytes [155, 164, 165]. This STAT3 activation results in the upregulation of many genes, including proinflammatory and anti-inflammatory cytokines (IL-6, TNF, and IFN), metabolism-related genes (sodium/ bile acid cotransporter, *saa3*, and *saa5*), cell cycle genes (DNA binding protein, MyD 118, and histone 3), and growth factors (hepatocyte growth factor (HGF)) [166]. In this phase, hepatocytes are primed to enter the cell cycle. In the case of mice, the priming phase continues for 4 hours after PHX. The next phase induces the expression of different receptors such as EGFR, c-Met, and TNFR, which leads to the replication of hepatocytes. Finally, the replication is terminated when hepatocytes reenter the G0 phase [148, 165]. To terminate the replication of hepatocytes, inhibitory genes such as P21, P53, P102, and SOCS3 are upregulated during the last phase of regeneration. In general, the regeneration process continues until the liver reaches its

original size, which is accomplished approximately 7 days after a partial hepatectomy [155, 157, 167].

1.8 The role of IL-6 in liver regeneration after PHX

Consistent with the protective role of IL-6 in fibrosis, its fundamental role in liver regeneration was suggested after the elevated levels of IL-6 were observed in the serum upon liver damage caused by PHX [168, 169]. In detail, the upregulated IL-6 interacts with the IL-6R and gp130 expressed on the surface of resident cells in the liver, mainly hepatocytes, and subsequently STAT3 is phosphorylated, which enhances the expression of target genes involved in liver regeneration [170, 171]. Interestingly, using IL-6-deficient mice undergoing PHX showed that the absence of IL-6 significantly reduced DNA synthesis in hepatocytes and the survival rate of the mice. To corroborate the role of IL-6 in the improvement of regeneration, IL-6-deficient mice were exogenously treated with IL-6, which resulted in the induction of STAT3 phosphorylation and the subsequent increase in hepatocyte proliferation and liver regeneration [41]. Different studies have shown that IL-6 exerts its pathophysiological effects through trans-signaling [28]. However, Peters et al. were the first to illustrate the protective role of IL-6 trans-signaling in liver regeneration. They designed HIL-6 as a fusion protein consisting of IL-6/sIL-6R to activate cells through IL-6 trans-signaling. Mice were treated with HIL-6 and subjected to 70% PHX. Treatment with HIL-6 resulted in accelerated liver regeneration upon PHX. Later, Galun et al. studied liver regeneration in mice treated with IL-6, HIL-6, and untreated controls. After performing 70% PHX, liver proliferation was evaluated by BrdU, and HIL-6 was shown to significantly accelerate liver regeneration; however, this process was comparable in all experimental groups after one week, indicating that exogenous reinforcement of IL-6 trans-signaling had a positive effect on liver regeneration [147, 172, 173], as demonstrated by another study in which induction of IL-6 trans-signaling, but not IL-6 alone, induced the proliferation of hepatocytes accompanied by an upregulation in the observed level of hepatocyte growth factor (HGF). Conversely, blocking IL-6 trans-signaling by hydrodynamic injection of sgp130Fc plasmid reduced the level of HGF and the subsequent proliferation of hepatocytes in the hepatectomized liver [174]. The findings described above suggest that IL-6, through trans-signaling, might play an important role in liver regeneration upon injury. However, to determine the contribution of IL-6 trans-signaling to liver regeneration,

further models are needed. Furthermore, the effect of the IL-6 trans-signaling blockade on the liver in the context of different inflammatory diseases, such as RA, needs to be precisely studied.

1.9 Aims

IL-6 plays essential roles in homeostasis, regeneration, metabolism, and inflammation. Dysregulation of IL-6 signaling is common in inflammatory diseases. Furthermore, concerning the role of IL-6 in liver regeneration, previous studies demonstrated that IL-6 i) induces acute phase proteins, ii) primes hepatocytes and forces them to enter the cell cycle, and iii) reduces necrotic cell death. IL-6 influences target cells through IL-6 classic signaling, trans-signaling, or cluster signaling. However, to the best of our knowledge, it is not clear which signaling pathway of IL-6 (classic or trans-signaling) is essential for liver regeneration after PHX.

To obtain a specific answer requires different preclinical models in which IL-6 trans-signaling or classic signaling can be specifically inhibited. However, studies have shown that exogenous injection of HIL-6 could accelerate hepatocyte proliferation and subsequent liver regeneration. Using a specific inhibitor of IL-6 trans-signaling, sgp130Fc, reduced hepatocyte proliferation after PHX, suggesting a positive role for IL-6 trans-signaling upon PHX. However, to confirm this suggestion, a clear model is still needed in which only trans-signaling can influence liver cells. Using an ADAM hyperactive mouse model is not suitable for obtaining an exact answer about the contribution of IL-6 trans-signaling in liver regeneration. Because ADAM activity is not only limited to the shedding of IL-6R; it also influences TNFR, Notch, and EGFR-ligands. Therefore, the effect of PHX in these mice would not be restricted to a single substrate. Thus, in a subsequent study, a novel mouse model will be generated in which all membrane-bound IL-6 receptors are genetically converted into soluble IL-6R. In this mouse model, the cells can be activated only by trans-signaling and not by classic signaling. In this regard, the effect of only IL-6 trans-signaling on liver regeneration after PHX will be precisely investigated. In addition, to gain a better understanding, the regeneration process of IL-6 trans-signaling in mice will be compared to that in IL-6R-deficient mice. The role of IL-6R has not been studied in liver regeneration after PHX.

Furthermore, to gain deeper insight into the contribution of IL-6 trans-signaling and the effect of blocked trans-signaling on the liver regeneration caused by PHX, IL-6 will be globally blocked by IL-6 mAb or specifically by sgp130Fc, which is currently being tested in clinical trial phase II.

2 Material

2.1 Primary antibodies

Anti-pSTAT3 (Y705) (D3A7)	100 µg/ml, 1:500, Western blotting; Cell Signaling Biotechnology, Frankfurt, Germany
Anti-STAT3 (124H6)	100 µg/ml, 1:1000, Western blotting; Cell Signaling Biotechnology, Frankfurt, Germany
Anti-STAT3 (79D7)	100 µg/ml, 1:1000, Western blotting; Cell Signaling Biotechnology, Frankfurt, Germany
Anti-γ-tubulin (T5326)	1 mg/ml, 1:2000, Western blotting; Sigma-Aldrich, Missouri, USA
Anti-GFP	100 µg/ml, 1:1000, Western blotting; Roche, Mannheim, Germany
Anti-IL-6Rα (H-7)	200 µg/ml, 1:200, Immunocytochemistry; Santa Cruz Biotechnology, Texas, USA
Anti-PCNA (<i>D3H8P</i>)	100 µg/ml, 1:200, Immunocytochemistry; Cell Signaling Biotechnology, Frankfurt, Germany
Anti-HGF (80429-R052)	0.2 µm filter solution , 1:200 Immunocytochemistry; Sino Biological, Wayne, USA
Anti-Mouse IL-6Ra (DY1830)	50.0 ng/ml, ELISA; R&D Systems, Minneapolis, MN, USA

Anti-mouse/rat HGF	ELISA; R&D Systems, Minneapolis, MN, USA
Anti-mouse HGF (DY2207)	ELISA; R&D Systems, Minneapolis, MN, USA

2.2 Secondary antibodies

Anti-Mouse IgG-POD	1 mg/ml, 1:5000, Western blotting; Thermo Scientific, Waltham, USA
Anti-Rabbit IgG-POD	1 mg/ml, 1:5000, Western blotting; Thermo scientific, Waltham, USA
Cy3 Goat anti-rabbit	1 mg/ml, 1:200, Immunocytochemistry; Jackson ImmunoResearch, Cambridge, UK

2.3 Chemicals

Acrylamide, 30% solution	Sigma-Aldrich, Steinheim, Germany
Bovine Serum Albumin (BSA)	Biomol, Hamburg, Germany
Ethanol	Merck, Darmstadt, Germany
Methanol	Merck, Darmstadt, Germany
Triton X-100	VWR, Radnor, USA
Trypan blue	Bio-Rad, München, Germany

Tween 20	Sigma-Aldrich, Steinheim, Germany
Complete Protease Inhibitor Cocktail	Roche, Mannheim, Germany
Ammonium Persulfate (APS)	Merck KGaA, Darmstadt, Germany
Glycerol	Carl Roth GmbH, Darmstadt, Germany
Isopropanol	AppliChem GmbH, Darmstadt, Germany
β -Mercaptoethanol	Sigma-Aldrich, Steinheim, Germany
Skimmed milk powder	Carl Roth GmbH & Co. KG, Karlsruhe, Germany
Sodium Dodecyl Sulfate (SDS)	Carl Roth GmbH & Co. KG, Karlsruhe, Germany
Sucrose	Merck KGaA, Darmstadt, Germany
Acetone	Merck, Darmstadt, Germany
Betaisodona	TVA OP inventory, USA
Oligo-(dT)-Primer	Fermentas, St. Leon-Rot, Germany
Percoll	Sigma-Aldrich, Taufkirchen, Germany
Paraformaldehyde	Merck KGaA, Darmstadt, Germany
Penicillin/streptomycin	Genaxxon Bioscience, Ulm, Germany
Streptavidin-HRP Solution	R&D Systems, Wiesbaden, Germany
Surfactant P20	GE Healthcare, Freiburg, Germany
Tetramethylethylenediamine (TEMED)	Sigma-Aldrich, Steinheim, Germany

Tris	Carl Roth GmbH & Co. KG, Karlsruhe, Germany
Sodium chloride	Applichem, Darmstadt, Germany
Sodium fluoride	Sigma-Aldrich, Steinheim, Germany
Sodium orthovanadate	Sigma-Aldrich, Steinheim, Germany
Sodium pyrophosphate	Sigma-Aldrich, Steinheim, Germany
Sodium hydroxide (NaOH)	Sigma-Aldrich, Steinheim, Germany

2.4 Kits

iTaq™ Universal Probes One-Step Kit	Bio-Rad, California, USA
iTaq™ Universal SYBR Green One-Step Kit	Bio-Rad, California, USA
Mouse IL-6Ra	R&D Systems, Minneapolis, MN, USA
Mouse/Rat HGF	R&D Systems, Minneapolis, MN, USA
Mouse HGF	R&D Systems, Minneapolis, MN, USA

2.5 Buffers

PBS	137 mM NaCl 2.7 mM KCl 1.5 mM KH ₂ PO ₄ 8.1 mM Na ₂ HPO ₄
-----	--

	pH 7.4
TBS-T	0.5 M Tris-HCl 1.5 M NaCl pH 7.5
5x Laemmli buffer	62.5 mM Tris-HCl 10% Glycerol 2% SDS 5% β -Mercaptoethanol pH 6.8 Bromophenol blue
Blocking buffer	5% Milk powder in TBS-T
ELISA blocking buffer	PBS 1% BSA 5% Sucrose
ELISA washing buffer	PBS 0.05% Tween
IP buffer	50 mM Tris-HCl 150 mM NaCl 1 mM EDTA 1 mM EGTA

	<p>1 mM Na₃VO₄</p> <p>2.5 mM Na-Pyrophosphate</p> <p>1 mM β-Glycerophosphate</p> <p>1% TritonX100</p> <p>complete protease inhibitor cocktail</p> <p>(one tablet/50 ml)</p> <p>pH 7.5</p>
Lysis buffer (WB)	<p>1% Triton X-100</p> <p>protease inhibitors</p> <p>PhosSTOP (1 tablet/10 ml)</p>
Lysis buffer (ELISA)	<p>50 mM HEPES (11.9 g)</p> <p>150 mM NaCl (8.8 g)</p> <p>Glycerol 10% (100 ml)</p> <p>Triton X-100 (10 ml)</p>
Nano-lysis buffer	<p>20 mM Tris-HCL pH 7.5</p> <p>150 mM NaCl</p> <p>0.5 mM EDTA</p> <p>2 mM PMSF</p> <p>0.5% NP-40</p>

SDS running buffer	25 mM Tris-HCl 192 mM Glycine 0.1% SDS pH 8.3
Separating buffer	1.5 M Tris-HCl 0.4% SDS pH 8.8
Stacking buffer	0.5 M Tris-HCl 0.4% SDS pH 6.8
Stripping buffer	62.5 mM Tris-HCl 2% SDS 0.1% β -Mercaptoethanol pH 6.8

2.6 Recombinant cytokines and inhibitors

IL-6	Conaris Research Institute AG, Kiel, Germany
Hyper-IL-6	Conaris Research Institute AG, Kiel, Germany

Sgp130Fc	Conaris Research Institute AG, Kiel, Germany
IL-6 monoclonal antibody 20F3 (IL-6 mAb)	InVivo Bio Tech Services GmbH, Hennigsdorf, Germany

2.7 Devices

7500 Real-Time-PCR	System Applied Biosystems, Warrington, UK
ChemoCam Imager	Intas, Göttingen, Germany
Heracell VIOS 250i CO2 Incubator	Thermo Fisher Scientific, Waltham, MA, USA
Mastercycler	Eppendorf, Hamburg, Germany
Multichannel Pipette	Eppendorf, Hamburg, Germany
Multipipette	Eppendorf, Hamburg, Germany
Nano drop ND-2000	Thermo Fisher Scientific, Waltham, MA, USA
pH-Meter	Sartorius, Göttingen Plate, Germany
Centrifuge	Eppendorf, Hamburg, Germany
Roll mixer	Neolab, Heidelberg, Germany
Tecan infinite M200 PRO reader	Tecan, Crailsheim, Germany
Thermo block	Eppendorf, Hamburg, Germany
Vortexer	Neolab, Heidelberg, Germany

Water bath	Aqualine Lauda, Lauda-Königshofen, Germany
Spotchem EZ: SP-4430	Axonlab, Stuttgart, Germany

2.8 Materials

Stainless Steel Beads	Qiagen, Hilden, Germany
Eppendorf tubes (1.5 and 2 ml)	Eppendorf AG, Hamburg, Germany
Falcon tubes (15 and 50 ml)	BD Biosciences, Franklin Lakes, USA
Nitra-Tex Gloves	Ansell Healthcare, Brüssel, Belgium
Whatman paper	VWR International GmbH, Darmstadt, Germany
Thread: Premilene DS 16 4-0	BBD Äskulap, Melsungen, Germany
Thread: Safil HR13 5-0	BBD Äskulap, Melsungen, Germany
Thread: Dragofil DS19 5-0	BBD Äskulap, Melsungen, Germany
Needles	Brown, Wertheim, Germany
Compresses/swabs/cotton swabs	TVA OP inventory, Zett, USA
StarFrost slides	VWR, Darmstadt, Germany
SuperFrost Plus slides	Thermo Scientific, Braunschweig, Germany
Spotchem II Liver-1 (test strips)	Arkray, Amstelveen, NL

2.9 Surgical tools

All surgical tools used in this study were purchased from Fine Science Tools (F.S.T.) (USA).

Walton scissors (curved/sharp/9.5 cm)	F.S.T., Foster, USA
Vannas spring scissors (curved/10.5 cm)	F.S.T., Foster, USA
Retractor blunt 10 cm (Heiss)	F.S.T., Foster, USA
Baby Allis Hemostat Clamp (4x5/12 cm)	F.S.T., Foster, USA
Micro scissors	F.S.T., Foster, USA
Needle holder (13 cm)	F.S.T., Foster, USA
Suture tying forceps (flat handle/straight/13 cm)	F.S.T., Foster, USA
Adson-DeBakey standard pattern forceps	F.S.T., Foster, USA
Eye dressing forceps (curved / 9.5 cm)	F.S.T., Foster, USA

2.10 Methods

2.10.1 Molecular methods

2.10.1.1 RNA extraction

Total RNA was extracted from liver and spleen using TRIzol (Thermo Fisher Scientific, Waltham, MA, USA) [175]. Samples were incubated in TRIzol at room temperature for 5 min. Then, 200 μ l of chloroform was added, and the tube was vortexed for 15 sec. Samples were incubated at room temperature for 3 min before centrifugation at 12000 x g for 15 min at 4°C. Three phases were formed: a clear upper layer, an interphase, and a red organic phase. The red phenol-chloroform phase at the bottom of the tube contained proteins, the white interphase layer included DNA, and RNA was in the clear upper layer. The upper layer was carefully transferred to a fresh tube containing 500 μ l of isopropanol. The tube was vortexed for 10 sec and incubated at room temperature prior to centrifugation at 12000 x g for 10 min at 4°C. The RNA pellet was washed with 75% ethanol and then with 100% ethanol. After the final washing step and centrifugation at 7500 x g for 5 min at 4°C, the supernatant was discarded, and the pellet was dried at room temperature for 20 min. The pellet was diluted in 101 μ l of water.

2.10.1.2 Measurement of RNA concentration

After RNA extraction, 1 μ l of the sample was used for quantification. The concentration was measured using a NanoDrop 2000c spectrophotometer (Thermo Scientific, Waltham, MA, USA, cat. #172-5140). The 260 to 280 nm absorption ratio showed the purity of the nucleic acid. To obtain the same RNA concentration in all samples, the concentration was adjusted to 100 ng/ μ l. The pellet was dissolved with dH₂O, and the samples were stored at -80°C for further analysis.

2.10.1.3 cDNA synthesis

Five micrograms of total RNA (in a final volume of 12.5 μ l) was incubated with 2 μ l of oligo (dT) at 65°C for 5 min. A master mix was prepared (Table 1). RiboLock was used to inhibit the activity of RNases and protect the RNA from degradation during cDNA synthesis. RNA was reverse transcribed at 42°C for 1 h. At the end of the reaction, RNA was denatured at 70°C for 10 min. Synthesized cDNA was stored at -20°C.

Table 1: cDNA master mix

Reagent (company)	Volume per sample (µl)
Oligo(dT) (0.5 µg/µl) (MWG)	2.0
5x RT buffer (Thermo Scientific)	4.0
dNTP (10 mM of each) (Thermo Scientific)	2.0
RiboLock (Thermo Scientific)	0.5
Revert Aid reverse transcriptase (Thermo Scientific)	1.0

2.10.1.4 Quantitative real time-PCR

To determine the expression of specific genes, iTaq™ Universal Probes One-Step Kit or iTaq™ Universal SYBR Green One-Step Kit (Bio-Rad, California, USA) was used. The master mix was prepared according to the manufacturer's instructions. Five microliters of iTaq universal probe reaction mix (2x), 0.25 µl of iScript advanced reverse transcriptase, 0.25 µl of primers, and 100 ng of RNA were used. The total volume of the mixture was adjusted to 10 µl by adding nuclease-free H₂O. For relative quantification, the expression levels of all target genes were normalized to the expression level of the housekeeping gene glyceraldehyde 3-phosphate dehydrogenase (*Gapdh*), and gene expression levels were calculated using the $\Delta(Ct_1)$ method: Ratio= $\frac{((\text{Efficiency}_{(\text{target})} \times 0.01) + 1)^{-(Ct_{\text{target}})}}{((\text{Efficiency}_{(\text{reference})} \times 0.01) + 1)^{-(Ct_{\text{reference}})}}$.

The expression level of target genes was determined by an ABI 7500 Real-Time PCR System (Thermo Fisher Scientific, Waltham, MA, USA)). The following primer pairs were used in this study (Tables 2-3).

Table 2: Real time PCR primers

TaqMan probe	(reference number)
<i>Hgf</i>	(Mm01135184_m1)
<i>IL-6R</i>	(Mm01211445_m1)
<i>Gapdh</i>	(Mm9999915_g1)

Table 3: Real-time PCR primers

SYBR Green Probe	Forward primer	Reverse primer
<i>Gapdh</i>	5'-GAAGGGCTCATGACCACAGT-3'	5'-CCTTCTTGATGTCATCATATTTGG-3'
<i>Gp130</i>	5'-GGCTCTGAGTCTTGA-3'	5'-GAAGCCATTCTGGTC-3'
<i>IL-6R (Ex5)</i>	5'-CTGCCAACCTTGTGG-3'	5'-GCAGCAAGTAGTAACTCGGGT-3'
<i>IL-6R (Ex7+ Ex8 + Ex9)</i>	5'-CCACCCCGGCAGGAAT-3'	5'-GCACTGGGGCGAGGA-3'

2.10.1.5 Cell surface detection of the IL-6R

Cell surface expression of IL-6R was detected as described in previous studies [176]. In detail, 100 μ l from mouse peripheral blood was taken from wt, sIL-6R^{fl/fl}, sIL-6R^{+/+} and IL-6R^{-/-} mice. Cells were blocked with Fc-block (anti-CD16/CD32, eBioscience, cat. #14-0161-86, working concentration of 1:50) for 10 min at room temperature. After the incubation, antibodies were added, including anti-IL-6R (working concentration of 1:50, PE, cat. #D7715A7, eBioscience), anti-CD3 (PE-Cy7, eBioscience, cat. #25-0031-82), anti-Ly6C (PerCP, eBioscience, cat.: #45-5932-82), anti-B220 (APC, eBioscience, cat. #17-0452-81), anti-Ly6G (FITC, eBioscience, cat. #11-5931-85), and anti-CD11b (APC-Cy7, eBioscience, cat. #47-0112-82, working concentration of 1:300) for 15 min at room temperature in FACS buffer (PBS containing 1% FCS, 0.5 mM EDTA). Then, red blood cells were lysed using 2 mL of prewarmed (37°C) BD lysis buffer (BD Biosciences, cat. #349202) for 10 min at 37°C. Cells were washed twice with FACS buffer and

analyzed by flow cytometry (BD FACSCanto II flow cytometer, BD Biosciences, San Jose, CA, USA). Data were analyzed using FlowJo software (FlowJo LLC, Oregon, USA).

2.10.1.6 Histology

This technique allows visualization of the cells expressing target protein(s) in a fixed cell or tissue [177]. Using primary antibodies, it is possible to determine the localization of the protein of interest. The liver was placed in a tissue cassette and fixed in 4% formaldehyde overnight at 4°C before embedding in paraffin. Sections with 5 to 7 µm thickness were cut using a microtome. Slides were incubated overnight at 65°C. Paraffin was removed from the slides by incubating the samples 3 times for 10 min in 100% xylol. The tissues were rehydrated in a series of alcohol solutions for 2 min in 100% ethanol (2x), followed by 2-min incubation in 95% ethanol (2x) and 2-min incubation in 70% ethanol (2x). Finally, slides were incubated in PBS for 10 min. Antigen retrieval was performed by heating to 100°C for 15–20 min in 10 mM sodium citrate buffer. Slides were blocked using 5% BSA (bovine serum albumin, Carl Roth, Karlsruhe, Germany) in PBS (100 µl per slide) and incubated in a wet chamber for at least 45 min at room temperature. The primary antibodies including anti-phospho-STAT3 (Tyr705) D3A7, cat. #9145, 1:200 dilution; anti-PCNA (*D3H8P*), cat. #13110, 1:200 dilution (Cell Signaling, Frankfurt, Germany); anti-IL-6Rα (H-7), cat. #sc-373708, 1:200 dilution (Santa Cruz Biotechnology, Texas, USA); and purified mouse anti-E-cadherin, cat. # clone 36/E, 1:100 dilution (BD Biosciences, San Jose, CA, USA) were diluted in 5% BSA-PBS and incubated overnight at 4°C. Slides were washed three times with PBS, and secondary antibodies were applied, namely, Cy3 goat anti-rabbit (Jackson ImmunoResearch, Cambridge, UK), cat. #111-165-144, 1:200 and goat anti-rabbit (Invitrogen, California, USA), cat. #51445A, 1:200. Slides were mounted in DAPI mounting solution (cat. #H-1200, Vector, Burlingame, USA). For each staining, 10 visualization fields were analyzed from whole sections of the liver in the different animal groups.

Images were taken using an Axiocam 506 digital camera connected to a Zeiss ApoTome 2 system microscope. Images were analyzed using ZEN 2.3 imaging software and Fiji software to quantify the signal.

2.10.1.7 Hematoxylin and eosin staining

Hematoxylin staining facilitates monitoring tissue structure and morphological changes and determination of different cell types in fixed tissue samples. Hematoxylin has a deep blue purple color and stains the cell nucleus. Eosin has pink color and stains the cytoplasm and extracellular matrix [178]. In this study, the liver was fixed, and sections were prepared as described above. Sections were deparaffinized and rehydrated as described earlier. Subsequently, samples were incubated in hematoxylin buffer for 3 min. This step was followed by a 2-sec incubation in 0.1% HCl. To remove the remaining hematoxylin, samples were incubated in dH₂O for 3 min. To stain the cytoplasm, sections were incubated in eosin buffer for 3 min and then rinsed with tap water for 3 min. After completing the nuclear and cytoplasmic staining, the color was fixed using a series of alcohol solutions: 70% ethanol (1x) for 3 min, 80% ethanol (1x) for 3 min, and 100% ethanol (1x) for 3 min. Finally, samples were incubated in xylol for 5 min. The mounting solution was warmed up, and samples were mounted by mounting solution prior to detection. Pictures were analyzed by using image J software.

2.10.2 Protein methods

2.10.2.1 Tissue and cell lysis

2.10.2.1.1 Tissue lysis for western blotting

Liver tissue was lysed in PBS containing 1% Triton X-100, protease inhibitors (Sigma, Taufkirchen, Germany), and PhosSTOP (1 tablet/10 ml). To obtain a homogenous lysate, Mixer Mill MM 400 was used. The tissue breakup process was performed for 3 min with a frequency of 30 Hz. After obtaining homogenous mixtures, the lysates were centrifuged. The supernatants were used to determine the total protein concentration.

2.10.2.1.2 Tissue and cell lysis for ELISA

To prepare samples for this assay, a lysis buffer was used containing 50 mM HEPES (11.9 g), 150 mM NaCl (8.8 g), 10% (100 ml) glycerol, and 10 ml Triton X-100 dissolved in 1 l of dH₂O. Prior to use, 1:100 PMSF and half of a proteinase inhibitor tablet were added to 50 ml of this buffer.

Liver samples and HSC cell pellets were lysed. After centrifugation, the supernatant was transferred to a new reaction tube.

2.10.2.2 Measurement of protein concentration with advanced protein assay reagent

Protein concentrations were determined using Advanced Protein Assay Reagent (5X) (Cytoskeleton Inc., Denver, USA). Advanced Protein Assay Reagent was diluted with water and adjusted to a 1x solution. Then, 150 μ l of Advanced Protein Assay Reagent and 150 μ l of water were transferred into a 96-well plate. One microliter of the lysate sample was loaded in triplicate. The Advanced Protein Assay Reagent served as a blank control. The concentration was determined by measuring the absorbance at a range of 570–615 nm by a Tecan Infinite M200pro fluorimeter (Tecan, Crailsheim, Germany).

2.10.2.3 Nano-Trap

The GFP-nanobody binding protein coupled to NHS-Sepharose was washed 3 times with 500 μ l of ice-cold dilution buffer and centrifuged at 2700 g for 2 min. The supernatant was discarded, and the beads were resuspended in dilution buffer. Fifty microliters of the beads were used for each sample. Next, the lysate and beads were mixed and incubated on a roller for 2 h at room temperature. After incubation, the tube was centrifuged for 3 min at 2700 g at 4°C. Then, the beads were washed 2 times with 500 μ l of dilution buffer at 4°C and centrifuged 2700 g. In the last step, 15 μ l of 5X laemmli buffer was added to the lysate and supernatant, and 30 μ l of laemmli buffer was added to the beads. All samples were boiled at 95°C for 10 min. The samples were analyzed by SDS-PAGE and Western blotting.

2.10.2.4 Sodium dodecyl sulfate-gel electrophoresis (SDS)

SDS allows the separation of biological macromolecules such as proteins. Proteins are separated according to their length and charge [179]. To linearize and negatively charge the proteins, sodium dodecyl sulfate (SDS) was used. Technically, during electrophoresis, negatively charged proteins move to the positive electrode and are separated according to the molecular weight. In this study, STAT3 phosphorylation was analyzed. Therefore, 50 μ g of liver lysate or 20 μ g of HSC lysate were diluted with LDS sample buffer (4X) and boiled for 10 min at 95°C. A 10% gel containing

stacking gel and separating gel was prepared for SDS-PAGE. The separating gel consisted of 8 ml of dH₂O, 6.6 ml of acrylamide, 5.2 ml of separating buffer, 10% APS, and 8 µl of TEMED. The stacking gel consisted of 3.4 ml of dH₂O, 1 ml of acrylamide, 1.5 ml of stacking buffer, 60 µl of 10% APC, and 6 µl of TEMED. A 1.5 mm gel was poured containing a separating gel of approximately 6 cm and a stacking gel of approximately 1 cm. Ten or 15 combs were placed in the stacking gel, and the samples were loaded after the gel was set. Protein separation was performed using a Mini-PROTEAN tetra system with a constant voltage of 80 V.

2.10.2.5 Western blotting

To detect the target proteins, the proteins were transferred from the SDS gel to a nitrocellulose membrane (Thermo Fisher Scientific, Waltham, MA, USA). The nitrocellulose membrane has a high protein-binding capacity. The membrane was activated using dH₂O for 5 min prior to use. In this study, a semiwet blotting system was used. Therefore, the gel was first placed in ice-cold transfer buffer. Whatman paper sheets (4 pieces for each side of the gel) were preincubated in transfer buffer. A transfer sandwich was prepared according to the manufacturer's protocol. The transfer cassette was closed and vertically transferred to the tank containing stainless steel/platinum electrodes and was filled with ice-cold transfer buffer. Protein was transferred to the membrane from the SDS gel for approximately 1 h and 30 min with 100 V at RT. Afterwards, the membrane was blocked in 5% fat-free dried skimmed milk (Carl Roth, Karlsruhe, Germany) in TBS (10 mM Tris-HCl (Carl Roth, Karlsruhe, Germany) 7.6 pH, 150 mM NaCl (AppliChem, Darmstadt, Germany)) for 1 h at room temperature. Rabbit anti-phospho-STAT3 (Tyr705) (D3A7) (1:1000, cat. #9145), rabbit anti-STAT3 (79D7) (1:1000, cat. #4904), and mouse anti- γ -tubulin (Sigma-Aldrich, cat. #T5326) mAbs were diluted in 5% fat-free dried skimmed milk (Carl Roth, Karlsruhe, Germany) in TBS-T (10 mM Tris-HCl (Carl Roth, Karlsruhe, Germany), 7.6 pH, 150 mM NaCl (AppliChem, Darmstadt, Germany), 0.5% Tween 20 (Sigma Aldrich, Munich, Germany)) and were incubated overnight at 4°C. The next day, the blot was washed with TBS-T 3 times for 10 min. The blot was incubated with a secondary peroxidase-conjugated antibody (Thermo Fisher Scientific, Waltham, MA, USA, cat. #31462, cat. #31451) at a working dilution of 1:2,500 in 5% fat-free dried skimmed milk in TBS-T for 1 h at room temperature. The washing step was repeated. Finally, the blot was washed and incubated in TBS prior to detection. PageRuler Prestained Protein Ladder (Thermo Fisher Scientific, Waltham, MA, USA, cat. #26616) was used

as a molecular weight (MW) marker. The Immobilon™ Western Chemiluminescent HRP substrate (Merck Chemicals GmbH, Darmstadt, Germany) and the ChemoCam Imager (INTAS Science Imaging Instruments GmbH, Göttingen, Germany) were used for signal detection.

2.10.2.6 Removal of antibody from the membrane (Stripping)

To detect another protein on the blot with another antibody, the membrane was stripped. Briefly, the stained membrane was incubated in 62.5 mM Tris-HCl (Carl Roth, Karlsruhe, Germany), 6.8 pH, 2% SDS (Carl Roth, Karlsruhe, Germany) and 0.1% β -mercaptoethanol (Sigma-Aldrich, Munich, Germany) in a water bath for 30 min at 60°C. After incubation, the membrane was washed with TBS-T (3x) for 10 min and then blocked and restained with another primary antibody as described.

2.10.2.7 Enzyme-linked immunosorbent assay (ELISA)

ELISAs were performed to test and quantify the presence of specific proteins in solution [180]. Among the different types of ELISA, sandwich ELISAs were used. In this technique, microwell plates are covered with an antibody known as capture antibody. Samples containing the antigen (target protein) were added and bound to the capture antibody. Subsequently, a conjugated biotinylated secondary antibody was added. This antibody recognized the antigen. Herein, a sandwich complex was formed containing the primary antibody, antigen, and secondary conjugated antibody. To determine the amount of protein of interest within the serum, conjugate streptavidin-horseradish peroxidase was used, which binds to the biotin-conjugated antibody. In the presence of peroxidase, adding 3, 3', 5, 5'-tetramethylbenzidine (TMB) substrate results in catalysis of an enzymatic color reaction. Each reaction was terminated by adding 2N sulfuric acid (H₂SO₄), and the color intensity was determined photometrically at 450 nm using a microplate reader.

2.10.2.7.1 ELISA for interleukin-6 receptor

To perform this assay, whole blood was obtained as described, and serum was extracted from different experimental groups at the indicated time points after PHX. To quantify the level of sIL-6R in mouse serum, an enzyme-linked immunosorbent assay (Mouse IL-6Ra DuoSet, cat. #DY1830, R&D Systems, Minneapolis, MN, USA) was performed. In detail, microtiter plates

(Nunc Maxisorb, Sigma-Aldrich, Munich, Germany) were incubated overnight with goat anti-mouse IL-6R α capture antibody diluted in PBS (R&D Systems, 1.6 μ g/ml working concentration, 1:180). The plates were washed 3 times with 300 μ l of washing buffer (R&D Systems, cat. #WA12). Subsequently, plates were blocked with 300 μ l of 1% BSA-PBS and incubated for at least 1 h prior to addition of the sample. One hundred microliters of serum from wt, sIL-6R^{fl/fl}, sIL-6R^{+/+} and IL-6R^{-/-} mice were diluted and loaded onto each well. After 2 h of incubation, the plates were washed three times with washing buffer (R&D Systems, cat. #WA12). Bound sIL-6R was detected by biotinylated goat anti-mouse IL-6R α mAb (R&D Systems, at a working concentration of 50 ng/ml). The plates were washed 3 times with 300 μ l of PBS-T and incubated with streptavidin-horseradish peroxidase at a working dilution of 1:200 (R&D Systems) for 30 min at RT. The washing step was repeated prior to starting the enzymatic reaction with soluble peroxidase substrate (BM blue POD, Roche, Mannheim, Germany). To stop the reaction, 50 μ l of 1.8 N H₂SO₄ was added to each well. The absorbance was determined at 450 nm by the Tecan Infinite M200pro fluorometer (Tecan, Crailsheim, Germany).

2.10.2.7.2 Hepatocyte growth factor (HGF) ELISA

To quantify the level of HGF protein in liver lysates of mouse tissue samples, enzyme-linked immunosorbent assays were performed with the supernatants of cultured rat HSCs or lysates of cultured rat HSCs (mouse/rat HGF cat. #MHG00, or mouse HGF cat. #DY2207, R&D Systems, Minneapolis, MN, USA) following the manufacturer's instructions. In detail, 50 μ l of assay diluent RD1-38 (R&D Systems) was loaded in each well of polystyrene microplates (R&D Systems). Subsequently, wells were incubated with 50 μ g of liver samples or 20 μ g of HSC lysates. This step was followed by 4 washing steps with 400 μ l of washing buffer (R&D Systems). Subsequently, the samples were incubated with 100 μ l of mouse/rat HGF conjugated antibody for 2 h. The plates were washed with 400 μ l of washing buffer (R&D Systems). To prepare the substrate solution, equal amounts of color reagents A and B (R&D Systems) were mixed 15 min before use. Samples were incubated with 100 μ l of substrate solution for 30 min at room temperature. To stop the reaction, 100 μ l of stop solution (R&D Systems) was added to each well. The absorbance was determined at 450 nm by the Tecan Infinite M200pro fluorometer (Tecan, Crailsheim, Germany).

2.10.2.8 HSC culture and stimulation assay

2.10.2.8.1 Cell culture

Freshly isolated HSCs were cultured in Dulbecco's modified Eagle's medium (DMEM) supplemented with 10% fetal calf serum and 1% Antibiotic Antimycotic Solution (Merck). One day after isolation, cells were washed with DMEM supplemented with 1% ITS+3 Liquid Media Supplement (Merck).

2.10.2.8.2 Cytokine stimulation of HSCs

One day after isolation, hepatic stellate cells were washed with DMEM and stimulated using 100 ng/ml Hyper IL-6Fc, 100 ng/ml IL-6 or 1 µg/ml sgp130Fc for 3 days under serum-free conditions. The number of HSCs was quantified by taking three different images after each stimulation.

The supernatant of the culture was collected and frozen. Cell pellets were collected for different purposes such as RNA extraction or lysate preparation.

2.10.2.8.3 Histology of HSCs

To detect the target protein in HSCs, cells were seeded at the indicated time points, supernatants were collected, and HSCs were washed with PBS supplemented with 60 mg/l penicillin and 100 mg/l streptomycin (Genaxxon Bioscience GmbH, Ulm, Germany) to prevent contamination. Then, samples were fixed with methanol for 5 min or with 4% PFA for 15 min. Subsequently, cultured HSCs were washed with 1X PBS supplemented with 60 mg/l penicillin and 100 mg/l streptomycin (Genaxxon Bioscience GmbH, Ulm, Germany) and were directly covered with PBS supplemented with 60 mg/l of penicillin and 100 mg/l of streptomycin (Genaxxon Bioscience GmbH, Ulm, Germany) and then sealed tightly using paraffin film. Fixed HSCs can be stored for up to 2 weeks at 4°C. To perform immunohistochemistry on fixed HSCs, after fixation and washing, samples were incubated overnight with primary antibodies against IL-6Rα ((H-7), cat. #sc-373708, 1:200 dilution (Santa Cruz Biotechnology, Texas, USA)) diluted in PBS or recombinant rat HGF ((cat. #80429-R052, 1:200 dilution (Sino Biological, Wayne, USA)) at 4°C. The next day, samples were washed 3 times and incubated with Cy3 goat anti-rat antibody for 1 h at RT. After incubation, samples were washed 3 times with PBS and mounted using mounting

solution containing DAPI mounting solution (cat. #H-1200, Vector, Burlingame, USA). Then, HSCs were covered with a cover slide, and the protein of interest was detected.

2.11 Mice

2.11.1 Mouse Experiments

2.11.1.1 Animals

WT and IL-6R^{-/-} mice [181] were obtained from Jackson Laboratory and the Animal Research Facility of the Heinrich-Heine University of Dusseldorf. sIL-6R^{fl/fl} mice were generated at inGenious targeting laboratory (www.genetargeting.com). The experiments of this study were carried out according to the LANUV-NRW requirements, Germany, with an approval number 84-02.04.2015.A462.

All mice were kept under specific pathogen-free conditions and handled according to the regulations defined by FELASA and the National Animal Welfare Bodies Committee (GV-SOLAS) (www.gv-solas.de). All transgenic animals were based on a C57BL/6N background. Mice were fed a standard laboratory diet and given autoclaved tap water *ad libitum*. Mice were kept in an air-conditioned room with controlled temperature (20-24°C), humidity (45-65%), and day/night cycle (12 h light, 12 h dark).

2.11.1.2 Partial hepatectomy (PHX)

In all experimental groups, 70% (2/3) partial hepatectomy (PHX) was performed under sterile conditions according to the protocol described previously [182].

2.11.1.3 Anesthesia

During partial hepatectomy and sham surgery, anesthesia was performed by isoflurane mask.

2.11.1.4 Surgical procedure

After performing anesthesia with isoflurane, mice were placed on a thermal plate at 37°C. The abdomen was shaved by a razor and cleaned using Betaisodona. Subsequently, mice were covered with sterile towels and gauzes. To open the abdominal cavity, one centerline incision below the

sternum was performed. The abdominal cavity was opened, and a retractor was placed. To have better access to the liver, *Xiphoid* was flipped up and fixed using an operation clamp. Then, the *falciform ligament* was cut until the *V. cava superior*, so that the liver was accessible. Using a wet Q-Tip with sterile NaCl (0.9%), the right and left liver lobes were carefully lifted without touching any other organ. A surgical thread (DS 19 Dragofil 5-0) was placed as proximal as possible in the hilum area of the ingrown lobes. The end of the thread was knotted with three knots. From the knots, the right upper lobe, left upper lobe and left lower lobe of the liver were resected together with the gallbladder through one-step ligature (approximately 7% of the total liver mass). After resection, the abdominal cavity was rinsed with sterile NaCl (0.9%). The peritoneum was sutured by a continuous suturing method (HR 13 Safil 5-0). The outer skin was closed (DS 16 Premilene 4-0) and disinfected with Betaisodona. Due to fluid loss during PHX, 2 ml of sterile NaCl (0.9%) was injected subsequently into the flank.

2.11.1.5 Analgesia

To reduce the pain resulting from the operation, mice received Rimadyl® in a single dosage of 5 mg/kg of body weight (5 mg/ml) SC in a volume of 1 µl/g of body weight directly after operation. Analgesia was repeated 24 and 48 h post operation. Mice with pain symptoms were excluded from the experiment.

2.11.1.6 Inhibition of IL-6 classic signaling and trans-signaling

To selectively inhibit IL-6 signaling, mice were treated with IL-6 mAb and/or sgp130Fc. To specifically inhibit classic IL-6 signaling, mice received intraperitoneal (i.p.) injections of 250 µg of IL-6 monoclonal antibody 20F3 (IL-6 mAb) in 200 µl of PBS (BD Bioscience, Heidelberg, Germany). To specifically inhibit IL-6 trans-signaling, 50 µg of sgp130Fc in a total volume of 200 µl was injected intraperitoneally (i.p.) into the mice.

Injections were performed 16 h prior to the operation and every 2 days post operation. Sgp130Fc was produced and secreted by stably transduced CHO cells and was purified through protein A affinity columns followed by size exclusion chromatography (performed by Robin Polz).

2.11.1.7 Liver regeneration following PHX

After PHX, liver regeneration in rodents was completed within 7-10 days [164]. To study the regeneration process, animals were kept in the experiment until 12 days following PHX. At day 12, mice were sacrificed by puncturing of the *venae cava inferior* and *i.p.*-injecting ketamine/xylazine anesthesia (400 μ l, 10 mg/ml ketamine, 1 mg/ml xylazine) or through cervical dislocation. To analyze the mechanisms involved in the regeneration process, WT and sIL-6R^{+/+} animals were sacrificed 0, 3, 6, 12, 24, and 48 h after PHX. IL-6R^{-/-} mice and WT mice treated with sgp130Fc and WT mice treated with IL-6mAb were sacrificed at the following intervals: 0, 12, and 24 h. Subsequently, organs were removed and stored at -80°C for further analysis. Serum was extracted and stored for further analysis.

2.11.2 Serum and organ removal

2.11.2.1 Blood analysis

Blood analysis was performed by preparing serum from experimental groups at different time points after PHX.

2.11.2.2 Whole blood uptake and serum extraction

To take the whole blood sample, mice were first injected with anesthetics. The abdominal cavity was opened. *Vena cava inferior* was punctured using a 20 G cannula caudal at the mouth of the hepatic vein. A blood sample with a volume of approximately 100-150 μ l was obtained.

To extract the serum from the whole blood, samples were incubated for 30 min at room temperature. Subsequently, the samples were centrifuged for 15 min at 3000 rpm. The upper layer was transferred to a new reaction tube followed by centrifugation for 6 min at 12,000 rpm. Serum was stored at -20°C for further analysis.

2.11.2.3 Determination of serum parameters

Serum parameters were determined using the automated biochemical analyzer Spotchem EZ SP-4430 (Arkray, Amstelveen, Netherlands). Using various reagent strips, the following parameters were measured from a 100- μ l serum sample: aspartate aminotransferase (AST/GOT) and alanine

aminotransferase (ALT/GPT). The reagent strips consisted of a multilayer test field containing the necessary reagents.

2.11.2.4 Organ removal

After the whole blood extraction, organs such as liver, spleen, colon, and lung were removed from each mouse. The organs were snap-frozen by liquid nitrogen and stored at -80°C for further analysis.

2.11.2.5 Liver weight to body weight ratio

To calculate the liver weight to body weight ratio, the weight of the remnant and regenerated liver was divided by the total body weight after PHX at the indicated time points.

2.11.2.6 Statistical analyses

For all statistical analyses of IF staining and Western blotting the GraphPad Prism 5.0 and Fiji software was used. In order to analyze the differences between two different groups, the student's t test was used. In order to analyze the significant differences of experimental groups for different time points ANOVA was applied. Data are expressed as mean \pm S.E.M. Relevant significances are displayed in the figures * $p \leq 0.05$; ** $p \leq 0.01$; *** $p \leq 0.001$.

3 Results

3.1 Generation of soluble IL-6R mice

As previously discussed, IL-6 plays essential roles in liver regeneration. Current data suggest that IL-6 trans-signaling is crucial in the context of liver regeneration, which was also observed from a study using a hydrodynamic injection of sgp130Fc cDNA into mice. Blockade of IL-6 trans-signaling resulted in impaired hepatocyte proliferation after PHX [174]. In keeping with this finding, Peters and colleagues showed that treatment with HIL-6 accelerated liver regeneration followed by PHX [173]. In the present study, novel transgenic mice called sIL-6R mice were generated. In sIL-6R^{+/+} mice, all endogenous membrane-bound IL-6R is converted into the soluble form of IL-6R (sIL-6R). Therefore, IL-6 can only activate target cells through trans-signaling. The use of sIL-6R^{+/+} mice enabled this study to investigate the specific contribution of IL-6 trans-signaling in liver regeneration induced by PHX while IL-6 classic signaling is abrogated.

In detail, the gene for IL-6R (gene ID: 16194) consists of 10 exons. Exon 9 codes for the transmembrane domain and the first part of the intracellular domain of IL-6R. Additionally, exon 10 codes for the last part of the intracellular domain of the IL-6 receptor and continues the 3' UTR (Fig. 3A). Through deletion of intron 9 (5420 bp) in the targeting vector, exons 9 and 10 were fused (Fig. 3B). The existence of intron 9 in the targeting vector could result in complications and difficulties with IL-6R gene modification. In addition, the stop codon located in exon 10 in the original reading frame of IL-6R was exchanged for the 2A-peptide fragment, which has self-cleaving properties. The 2A-peptide fragment consists of 16 amino acids and is derived from the foot-and-mouth disease virus [183]. Insertion of the 2A-peptide within a fusion protein cotranslationally results in the generation of two separate proteins from one open reading frame. This fragment was fused to a KDEL-tagged GFP resulting in the E9-E10c-GFP-E10u cassette. During cotranslation processes, GFP and IL-6R are cleaved into two separate proteins. Next, insertion of the furin cleavage site in the 2A-peptide fragment results in cleavage by the protease furin. The FRT-neomycin-resistance-FRT cassette was fused to the E9-E10c-GFP-E10 cassette, which was flanked by loxP sites (Fig. 3B). Stem cells carrying a modified sequence were microinjected into Balb/c blastocysts. Chimeras with a high percentage of black coat color were mated to wild-type C57BL/6N mice, resulting in the generation of mice containing sIL-6R^{fl/fl}NEO.

The first generation of transgenic mice was crossed to a mouse expressing flippase recombinase (FLP) to delete the neomycin-resistant FRT cassette.

Further breeding of NEO-deleted sIL6R^{fl/fl} mice resulted in homozygous sIL-6R^{fl/fl} mice (Fig. 3C). Breeding to Cre-expressing mice finally resulted in homozygous sIL-6R^{+/+} mice. The Cre-Lox recombination within the IL-6R gene allows the direct expression of the IL-6R in its soluble form, which lacks the transmembrane and intracellular domains in homozygous sIL-6R^{+/+} mice (Fig. 3D). In wt mice, the IL-6R gene remained unchanged and was not modified. Genetic modification of the IL-6R should not alter the expression of IL-6R in sIL-6R^{fl/fl} mice such that IL-6 can activate the cells through classic signaling by binding to the membrane-bound IL-6R or by trans-signaling via sIL-6R. In mice, sIL-6R is generated by ectodomain shedding, mainly through ADAM protease activity (Fig. 3E). However, in generated sIL-6R^{+/+} mice, IL-6R is produced and secreted in its soluble form, and cells could be activated only through IL-6 trans-signaling (Fig. 3F).

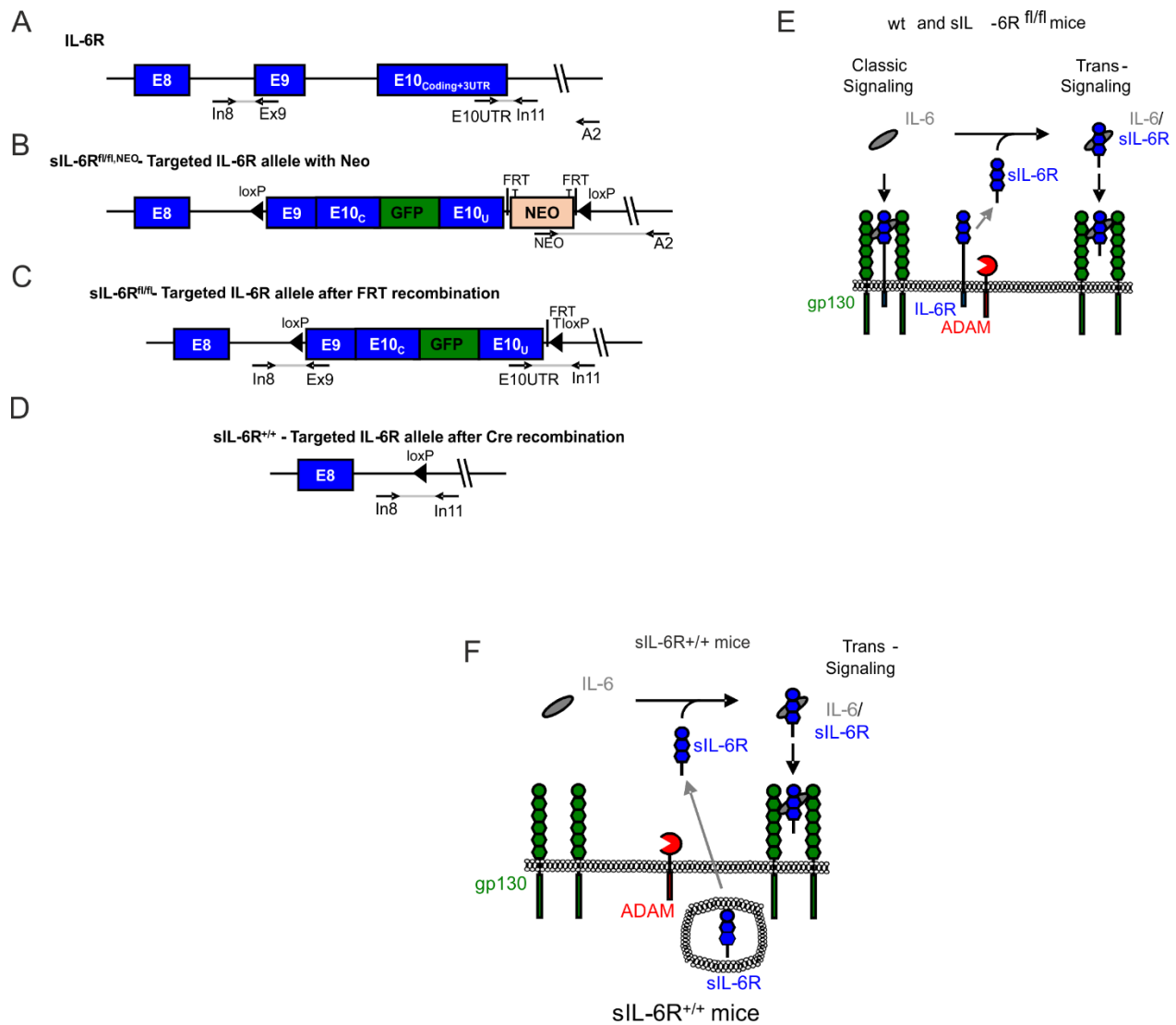


Fig. 3. Generation of sIL-6R^{+/+} mice

(A) Schematic representation of the targeting strategy for the generation of sIL-6R^{fl/fl} and sIL-6R^{+/+} mice. The arrows indicate the locations of primers used for genomic PCR. E8 to E10: Exon 8 to Exon 10 (blue); Exon 9 codes for the transmembrane domain and the first part of the intracellular domain of the IL-6R. Exon 10 codes for the intracellular domain of the IL-6R (coding, C) and the 3' untranslated region (3'UTR, U). (B+C) In sIL-6R^{fl/fl} mice, exon 9 and exon 10 were fused. The natural stop codon of IL-6R was replaced by a 2A-GFP-KDEL (green) followed by the 3'UTR of exon 10. (D) After Cre recombination, the E9-E10-GFP cassette was deleted, resulting in the generation of a mRNA coding only for the soluble IL-6R. Schematic illustration of classic and trans-signaling in wt and sIL-6R^{fl/fl} (E) and sIL-6R^{+/+} mice (F). IL-6 (in gray) in complex with membrane-bound IL-6R (blue) and gp130 (green) induce classic signaling. (E) In mice, sIL-6R (blue) is only produced by shedding of the membrane-bound IL-6R by ADAM proteases

(red). (F) In sIL-6R^{+/+} mice, sIL-6R is produced and secreted. IL-6 in complex with sIL-6R and gp130 induces trans-signaling. These figures were taken from *Fazel Modares, N., et al. hepatology, 2019.*

To confirm that the modified sequence was correctly inserted in the expected part of the IL-6R gene, different PCRs were performed (Fig. 4A-B). To this end, primers binding to different exons and introns of IL-6R were designed, namely, primer set 1 and primer set 2.

As previously explained, exon 9, which codes the transmembrane domain of IL-6R, was supposed to be deleted from the original frame of the IL-6R gene after cre recombination. To confirm the deletion of exon 9 and exon 10, primer set 1 (In8 + Ex9) binding to intron 8 and exon 9 was used. DNA was isolated from mouse tails, and PCR was performed. Due to the lack of exon 9 in sIL-6R^{+/+} mice, no PCR product was expected. Since the original reading frame of IL-6R remained unchanged in wt mice, a PCR product of 399 bp was expected. In sIL-6R^{fl/fl} mice, a PCR product of 456 bp was expected because of the lox-p site. As shown in Fig. 4A, the detected product was 399 bp in wt mice. Furthermore, PCR data from sIL-6R^{+/+} mice confirmed that the exon 9 and exon 10 had been successfully deleted from the original reading frame of IL-6R in generated sIL-6R^{+/+} mice. Last, PCR data confirmed that IL-6R was correctly modified in sIL-6R^{fl/fl} mice (Fig. 4A).

Furthermore, to confirm the correct modification of IL-6R, a multiplex PCR by primer set 2, which binds to In8, In11, E10UTR, and In11, was performed. By multiplex PCR, different fragments can be amplified in a single PCR reaction tube. In this instance, In8 to E10UTR and In11 to In11 could be amplified. Therefore, DNA was isolated from wt, sIL-6R^{+/+}, and sIL-6R^{fl/fl} mice, and PCR was performed. In wt mice, only a small fragment could be amplified by primer (In11 and E10UTR), resulting in a fragment of 181 bp. However, the amplification of the larger fragment from In8 to In11 was not possible. Concerning sIL-6R^{+/+} mice, primer set 2 (In8 + In11) amplified a fragment of approximately 480 bp. In sIL-6R^{fl/fl} mice, the amplified fragment resulting from the presence of the loxP site was expected to be 358 bp, which is presented in Fig. 4B.



Fig. 4. Confirmation of genetic modification in sIL-6R^{+/+} mice

DNA was isolated from wt, sIL-6R^{+/+}, and sIL-6R^{fl/fl} mice. (A) PCR was performed with Primer set 1 binding to In8+ Ex9 and (B) multiplex PCR primer set 2 binding to In8+ In11; E10UTR + In11. These figures were taken from *Fazel Modares, N., et al. J hepatology, 2019.*

As previously mentioned, the sIL-6R^{fl/fl} mouse carries a 2A-GFP-KDEL coding sequence. By assessing GFP protein in these mice, we confirmed that the modified sequence was correctly inserted into sIL6R^{fl/fl} mice. Unfortunately, due to the low signal, GFP could not be detected by immunohistochemistry on the liver or spleen. However, by immunoprecipitation and Western blotting, detection of GFP was possible. Therefore, liver and spleen lysates were prepared from wt, sIL-6R^{fl/fl}, and sIL-6R^{+/+} mice. After concentrating GFP in liver and spleen lysate via NanoTrap, Western blotting was performed. Fifty micrograms of liver or spleen lysates were incubated with the primary anti-GFP antibody. The obtained GFP detection results are presented in Fig. 5. The upper panel shows Western blotting of liver lysates from wt, sIL-6R^{fl/fl}, and sIL-6R^{+/+} mice. GFP protein has a molecular weight about 25 kDa. As expected, by using an anti-GFP antibody, 25 kDa GFP protein was observed in liver lysates of sIL-6R^{fl/fl}, which confirmed that modified sequences carrying GFP were fused to the IL-6R gene in these mice. However, no GFP protein was detected in liver lysates of wt or sIL-6R^{+/+} mice. The absence of GFP in the liver lysates of sIL-6R^{+/+} mice also demonstrated that the GFP sequence was successfully deleted in homozygous sIL-6R^{+/+} mice (Fig. 5A). The lower panel indicates Western blotting of spleen lysates from wt, sIL-6R^{+/+} and sIL-6R^{fl/fl} mice. As presented in Fig. 5B, GFP was detected in spleen lysates from sIL-6R^{fl/fl} mice. However, GFP was not detected in spleen lysates from wt mice. Through genetic modification, the GFP coding cassette was deleted in sIL-6R^{+/+} mice; therefore, no GFP was detected in the spleen of sIL-6R^{+/+} mice. As a loading control, Baf/3 cells were transfected with GFP. Cell lysates were prepared and loaded with liver or spleen lysates (Fig. 5B).

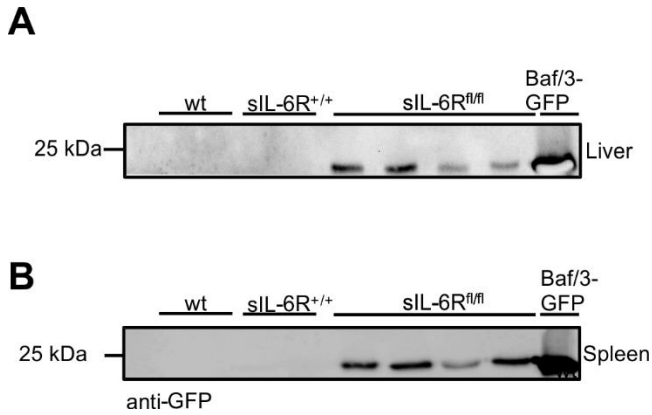


Fig. 5. Western blot of liver lysates against GFP.

(A) Upper panel liver lysates prepared from wt (n=2), sIL-6R^{fl/fl} (n=4) and sIL-6R^{+/+} (n=2) mice. (B) Lower panel spleen lysates prepared from wt (n=2), sIL-6R^{fl/fl} (n=4) and sIL-6R^{+/+} (n=2) mice. Lysates of Baf/3 cells expressing GFP protein serve as the loading control. These figures were taken from *Fazel Modares,*

N., et al. hepatology, 2019.

Next, the expression of IL-6R was assessed by immunohistochemistry. Therefore, paraffin-embedded liver sections from wt, sIL-6R^{fl/fl}, sIL-6R^{+/+}, and sIL-6R^{fl/fl} Alb-Cre⁺ mice were prepared. IL-6R was stained in red, and the nucleus was stained with DAPI in blue. Pictures were taken with different magnification; the left panel shows 20x, and larger magnification is presented on the right panel (63x). As shown in Fig. 6A, the positive signal for IL-6R was detected in the liver sections of wt mice. The specificity of the IL-6R staining was tested with the liver tissues from the IL-6R knockout mice. As expected, no cells were stained positive for IL-6R in the IL-6R^{-/-} mice, which confirmed that staining was specific (Fig. 6A). Next, liver sections of sIL-6R^{+/+} mice were stained for IL-6R. No IL-6R-expressing cells were detected in the liver sections of sIL-6R^{+/+} mice, which demonstrated that all the membrane-bound IL-6R was converted to its soluble form (sIL-6R) and rapidly secreted.

Furthermore, the expression of IL-6R was also analyzed in IL-6R-knockout mice in hepatocytes, known as sIL-6R^{+/+} Alb-Cre⁺. Staining of liver sections revealed that no IL-6R-expressing cells were detected in sIL-6R^{+/+} Alb-Cre⁺ mice, which further confirmed the cre deletion strategy.

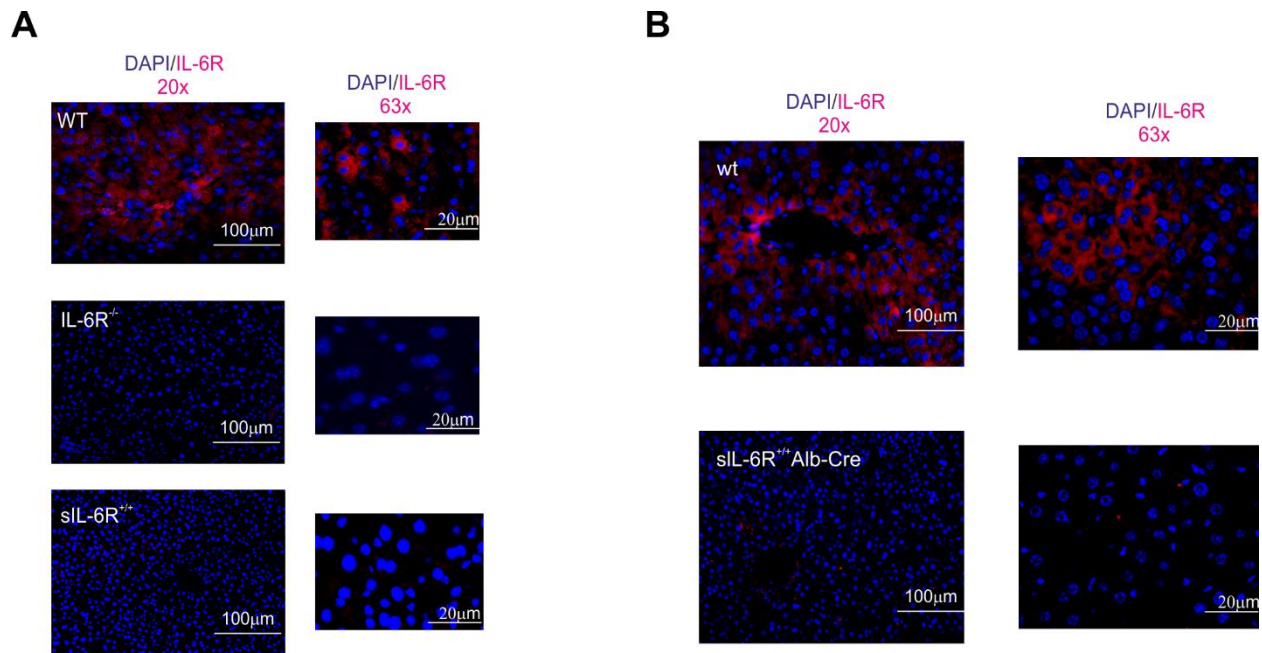


Fig. 6. IL-6R visualization by immunohistochemistry in liver

Paraffin-embedded sections of (A) liver from wt (n=2), IL-6R^{-/-} (n=2), sIL-6R^{+/+} (n=2) mice were prepared. (B) Liver sections of wt (n=2) and sIL-6R^{+/+} Alb-Cre (n=2) were prepared. Samples were stained for IL-6R in red and DAPI in blue. Pictures were taken with two different magnifications: left panel x20 and right panel x63. One representative of n=2 is shown. These figures were taken from *Fazel Modares, N., et al. hepatology, 2019.*

Further, the overall expression of IL-6R was analyzed. Moreover, to confirm that the Cre-mediated deletion strategy was efficient, sIL-6R^{fl/fl} mice were crossed with Alb-Cre and LysM-Cre mice, which resulted in the deletion of the IL-6R on the hepatocytes or monocytes, macrophages, and granulocytes, respectively. Next, the mRNA expression levels of IL-6R were quantified by RT-PCR. Therefore, livers from wt, sIL-6R^{fl/fl}, sIL-6R^{+/+}, mice were isolated, and RNA was extracted. A set of primers binding to exon 5 of IL-6R was designed. The modification of IL-6R should not interfere with the amplification of IL-6R using this primer. As expected, IL-6R was expressed in wt mice, and its expression was not impaired in sIL-6R^{fl/fl} and sIL-6R^{+/+} mice (Fig. 7).

Concerning sIL-6R^{+/+} mice, the mRNA expression levels of IL-6R exhibited an increase, which might be due to increased mRNA stability (Fig. 7). Notably, the interaction of microRNAs with the 3'UTR of the IL-6R gene might have regulatory effects on IL-6R expression. In this applied strategy, the deletion of the 3'UTR in sIL-6R^{+/+} mice may interfere with the regulatory effects of

microRNAs, which might be the reason for the exacerbated IL-6R expression in sIL-6R^{+/+} mice. These data suggested that the insertion of the GFP cassette and modification of the IL-6R original reading frame did not impair the overall expression of IL-6R in sIL-6R^{fl/fl} and sIL-6R^{+/+} mice.

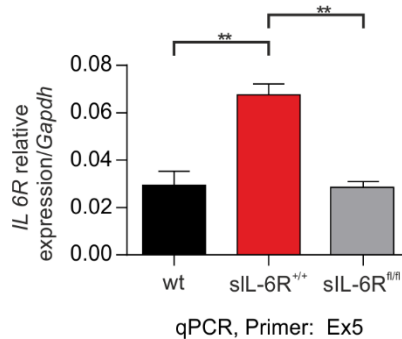


Fig. 7. Quantification of IL-6R mRNA levels

Livers were isolated from wt, sIL-6R^{+/+} and sILR^{fl/fl} mice (n=3). RNA was extracted (n=3). RT-PCR from wt (black bar), sIL-6R^{+/+} (red bar) and sILR^{fl/fl} (gray bar) mice was performed. IL-6R expression levels were normalized to *Gapdh* expression. The result is presented as the mean \pm S.E.M. This figure was taken from *Fazel Modares, N., et al. hepatology, 2019.*

As mentioned previously, the GFP cassette was fused to exon 9 and exon 10 of IL-6R, which was deleted in homozygous sIL-6R^{+/+} mice. To examine the deletion of GFP and the expression of IL-6R in its soluble form, RT-PCR was performed. To this end, livers from wt, sIL-6R^{+/+}, IL-6R^{-/-} and sIL-6R^{+/+} Alb-Cre⁺ were isolated, and RNA was extracted. Primer binding to Ex7, Ex8, and Ex9 were used. IL-6R was amplified only in wt mice by using the EX7 + Ex8 + Ex9 primer. However, genetic modification resulted in the deletion of exon 9 from the IL-6R gene in sIL-6R^{+/+}; therefore, no expression of IL-6R was detected. This observation confirmed that IL-6R is expressed only in its soluble form in sIL-6R^{+/+} mice. Furthermore, IL-6R expression was abrogated in IL-6R^{-/-} mice, which confirmed the results obtained by immunohistochemistry. Concerning sIL-6R^{+/+} Alb-Cre⁺, IL-6R expression was significantly reduced compared to observed IL-6R expression levels in wt mice, which confirmed that via Cre-deletion, IL-6R was successfully deleted from the liver in sIL-6R^{+/+} Alb-Cre⁺ (Fig. 8).

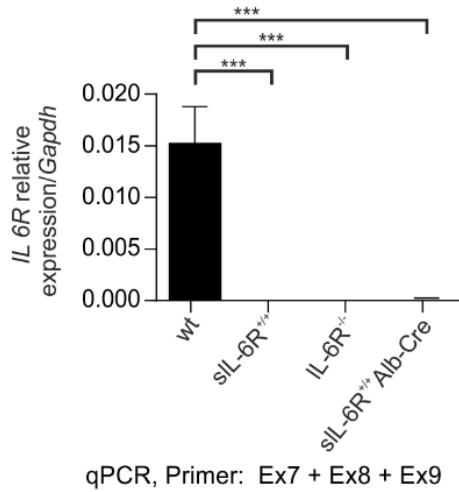


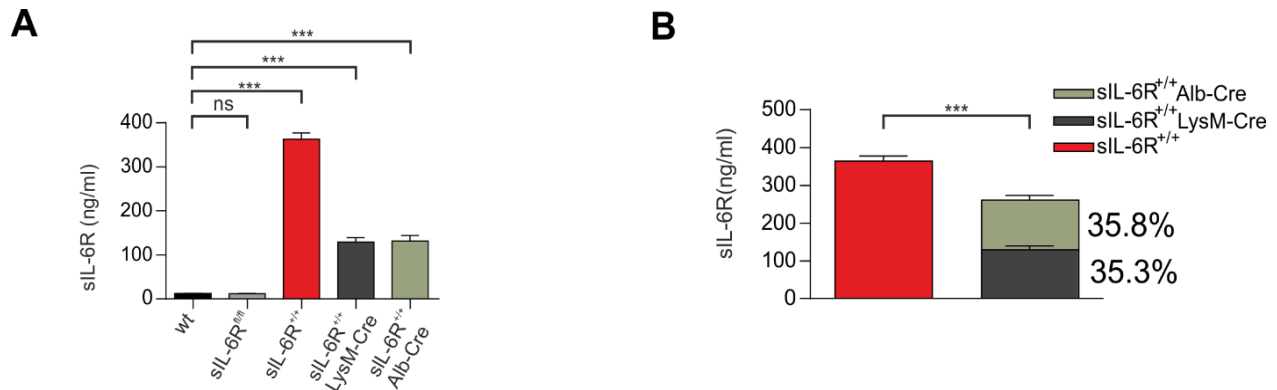
Fig. 8. Quantification of IL-6R mRNA levels

Livers were isolated from wt, sIL-6R^{+/+}, IL-6R^{-/-} and sIL-6R^{+/+} Alb-Cre mice using primers coding Ex7+ Ex8 + Ex9 of IL-6R. Relevant significances are displayed, ***p≤ 0.001. The results are presented as the mean ± S.E.M. This figure was taken from Fazel Modares, N., et al. *hepatology*, 2019.

Next, sIL-6R expression was quantified on the protein level by ELISA. Therefore, blood was taken from *Vena cava* from wt, sIL-6R^{fl/fl}, sIL-6R^{+/+}, sIL-6R^{+/+} Alb-Cre⁺ and sIL-6R^{+/+} LysM-Cre⁺ mice. Serum was extracted from whole blood, and ELISA was performed. The detected amounts of sIL-6R from wt mice were approximately 11 ng/ml in the serum, which was consistent with previous findings (Fig. 9) [174].

Concerning sIL-6R^{fl/fl} mice, nearly identical amounts of sIL-6R were observed in the serum (Fig. 9). This observation further confirmed that genetic modification of IL-6R did not affect its expression in sIL-6R^{fl/fl} mice. The RT-PCR results demonstrated that IL-6R expression was enhanced in sIL-6R^{+/+} mice about 2-fold. Interestingly, the level of sIL-6R on the protein levels was also notably elevated and reached 363 ng/ml, which showed 33-fold induction compared to wt mice (Fig. 9). Furthermore, ELISA results from sIL-6R^{+/+} Alb-Cre⁺ and sIL-6R^{+/+} LysM-Cre⁺ mice demonstrated that sIL-6R reached up to 128 and 129 ng/ml in the serum of sIL-6R^{+/+} Alb-Cre⁺ and sIL-6R^{+/+} LysM-Cre⁺ mice, respectively (Fig. 9A). Interestingly, previous studies illustrated that sIL-6R in the serum is completely generated by hepatocytes and neutrophils/macrophages. This finding was obtained by using Alb-Cre-recombined IL-6R^{-/-} mice and LysM-Cre-recombined IL-6R^{-/-} mice, which presented 67.95% and 39.95% of sIL-6R levels of wt mice [181]. Based on ELISA results, the sum of sIL-6R displayed in sIL-6R^{+/+} Alb-Cre⁺ (128 ng/ml) and sIL-6R^{+/+} LysM-Cre⁺ (129 ng/ml) has only a 70.8% contribution to the total sIL-6R levels observed in sIL-6R^{+/+} mice. These data suggested that sIL-6R^{fl/fl} mice and wt mice

displayed identical levels of sIL-6R in the serum. However, the sIL-6R levels were strongly elevated in sIL-6R^{+/+} mice compared to wt mice. Using sIL-6R^{+/+} LysM-Cre⁺ and sIL-6R^{+/+} Alb-



Cre⁺ may alleviate that effect; in addition to hepatocytes, neutrophils, and macrophages, other cells in wt mice produce sIL-6R and contribute to the detected levels of sIL-6R in the serum.

Fig. 9. Quantification of sIL-6R

Serum levels of sIL-6R in wt (black bar), sIL-6R^{fl/fl} (gray bar), sIL-6R^{+/+} (red bar), sIL-6R^{+/+} LysM-Cre (dark gray) and sIL-6R^{+/+} Alb-Cre (green bar) mice were determined by ELISA. The results are presented as the mean \pm S.E.M. of at least 7 animals/group. Relevant significances are displayed, ***p \leq 0.001. These figures were taken from *Fazel Modares, N., et al. hepatology, 2019.*

3.2 sIL-6R in sIL-6R^{+/+} mice activates the cells through IL-6 trans-signaling

Previous data illustrated that treatment of wild-type mice with recombinant IL-6 initiated IL-6 trans-signaling in the colon, liver, and lung [184]. In this study, sIL-6R^{+/+} mice exhibited significantly higher levels of sIL-6R compared to wt or sIL-6R^{fl/fl} mice under steady-state conditions. Higher levels of sIL-6R led to the hypothesis that only IL-6 trans-signaling could target the cells in sIL-6R^{+/+} mice. To prove this hypothesis, naïve sIL-6R^{+/+} mice were intraperitoneally (i.p.) injected with 5 μ g of recombinant IL-6. In addition, naïve sIL-6R^{+/+} mice were coinjected with sgp130Fc or IL-6 mAb to inhibit IL-6 signaling. To analyze the signal transduction of IL-6 trans-signaling in sIL-6R^{+/+} mice, pSTAT3 and STAT3 were monitored via Western blotting. Ninety min after treatment, the liver, lung, and colon were isolated from mice treated with recombinant IL-6, coinjected with sgp130Fc or IL-6 mAb or left untreated. Next, lysates were

prepared. γ -tubulin was used as the loading control. Representative blots of liver lysates are shown on the left panel (Fig. 10A). Furthermore, pSTAT3 detected on the blots was analyzed by calculating the ratio of pSTAT3 to total protein with Fiji software presented in Fig. 10B. pSTAT3 has a molecular weight of 83 kDa. No pSTAT3 protein was detected in liver lysates of untreated mice (Fig. 10A). However, exogenous injection of recombinant IL-6 significantly increased STAT3 phosphorylation compared to pSTAT3 levels detected in untreated mice (Fig. 10A). Furthermore, blockade of IL-6 signaling via sgp130Fc reduced STAT3 phosphorylation (Fig. 10A-B). Consistent with this result, coinjection with IL-6 mAb also reduced levels of pSTAT3 in sIL-6R^{+/+} mice, which were comparable to pSTAT3 levels in control mice. Furthermore, immunohistochemistry was performed to visualize pSTAT3-positive cells. Therefore, paraffin-embedded liver sections from sIL-6R^{+/+} mice treated with recombinant IL-6, coinjected with sgp130Fc or IL-6 mAb or left untreated, were prepared. Samples were collected from three different animals, and three nonconsecutive sections were analyzed per animal. Ten pictures were quantified from each section. Samples were stained for pSTAT3 in red and DAPI in blue. Consistent with this approach, this observation was quantified as presented in Fig. 10C-D.

As presented in Fig. 10C, no pSTAT3-positive cells were observed in the liver sections of wt mice. However, after treatment with recombinant IL-6, positive cells for pSTAT3 were frequently observed, and the number of positive cells reached significance compared to untreated mice. Importantly, treatment with sgp130Fc reduced the number of positive cells for pSTAT3 in the liver sections of sIL-6R^{+/+} mice. Consistent with this finding, blockade of IL-6 signaling by IL-6 mAb exhibited a similar pattern, and the number of positive cells was significantly reduced. This observation was in agreement with the results obtained from Western blotting of liver lysates. Overall, these data suggest that the liver is targeted by IL-6 trans-signaling in sIL-6R^{+/+} mice upon exogenous treatment with recombinant IL-6.

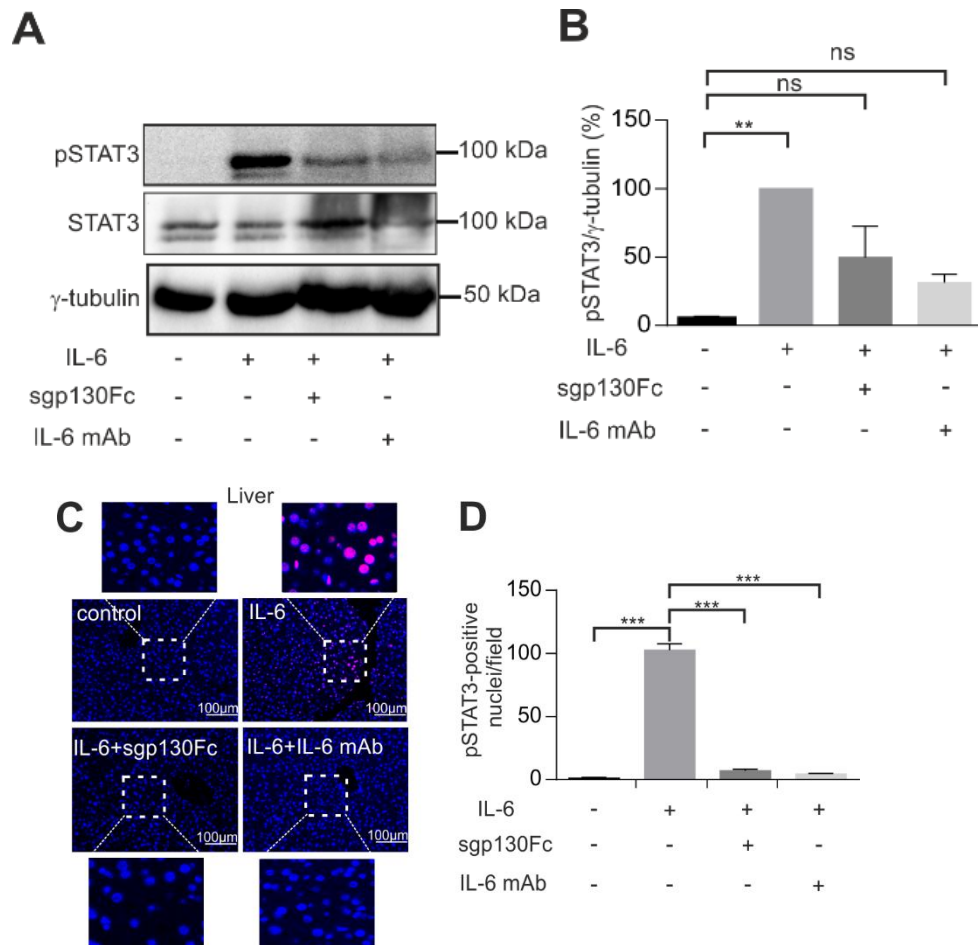


Fig. 10. IL-6 activates STAT3 signaling in the liver of sIL-6R^{+/+} mice through trans-signaling

sIL-6R^{+/+} mice were intraperitoneally injected with PBS (control), IL-6, combination treatment of IL-6 and sgp130Fc or combination treatment of IL-6 and IL-6 mAb. Mice were sacrificed 90 min after injection. (A) Liver lysates were prepared and stained for STAT3, pSTAT3, and γ -tubulin by Western blot analysis. Representative blot is shown. (B) Quantification of (A) of all samples. The results are presented as the mean \pm S.E.M. of 3 animals/group. Relevant significances are displayed $**p \leq 0.01$. (C) Sections of paraffin-embedded liver tissue were stained for pSTAT3. Dotted lines indicate higher magnification of each picture (10 μ m). (D) Quantification of (C) was performed from 10 visual fields per mouse (30 visual fields). The results are presented as the mean \pm S.E.M. of 3 animals/group. Relevant significances are displayed, $***p \leq 0.001$, and the results are presented as the mean \pm S.E.M. one representative of $n=3$ is show. These figures were taken from *Fazel Modares, N., et al. hepatology, 2019*.

Next, colons of sIL-6R^{+/+} mice treated with recombinant IL-6, coinjected with sgp130Fc or IL-6 mAb or left untreated were isolated. Lysates were prepared as described previously. Phosphorylation of STAT3 was analyzed by Western blotting. Representative blots are shown on the left panel in Fig. 11A. The results obtained from Western blotting were quantified by analyzing the ratio of pSTAT3 to the ratio of total protein by Fiji software. Data are presented in Fig. 11B.

In colon lysates of untreated sIL-6R^{+/+} mice, a weak signal was detected for pSTAT3. However, injection with recombinant IL-6 induced STAT3 phosphorylation in the colon of sIL-6R^{+/+}. An apparent reduction of pSTAT3 levels was observed after blockade of trans-signaling with sgp130Fc. pSTAT3 levels after the siege of IL-6 trans-signaling were comparable to pSTAT3 levels observed in untreated mice. Conversely, the pSTAT3 signal was not completely abolished in treated mice with IL-6 mAb, indicating that IL-6 signaling was partly blocked in the colon of sIL-6R^{+/+} mice (Fig. 11B). Notably, this increase was not significant and was still comparable to the pSTAT3 levels detected in untreated mice.

Furthermore, to confirm the Western blotting results, pSTAT3-expressing cells were visualized by immunohistochemistry. Therefore, paraffin-embedded colon sections were prepared, and immunohistochemistry was performed. Samples were stained for pSTAT3 in red and DAPI in blue. Samples were collected from three different animals. Three nonconsecutive sections were analyzed per animal. Ten visualized fields were quantified. As shown in Fig. 11C, recombinant IL-6 induced the number of positive cells for pSTAT3 in the colon of sIL-6R^{+/+} mice. However, no pSTAT3-positive cells were observed upon blockade of IL-6 trans-signaling in sIL-6R^{+/+} mice. Similarly, STAT3 phosphorylation was abrogated in the colon of sIL-6R^{+/+} mice upon treatment with IL-6 mAb.

Taken together, Western blotting data demonstrated that exogenous treatment with recombinant IL-6 induced STAT3 phosphorylation in the colon of sIL-6R^{+/+} mice, which was also confirmed by immunohistochemistry. Conversely, a weak signal of STAT3 phosphorylation was detected in treated mice with sgp130Fc or IL-6 mAb. However, immune staining showed that IL-6 signaling was completely blocked, and no pSTAT3-positive cells were detected in the colons of sIL-6R^{+/+} mice.

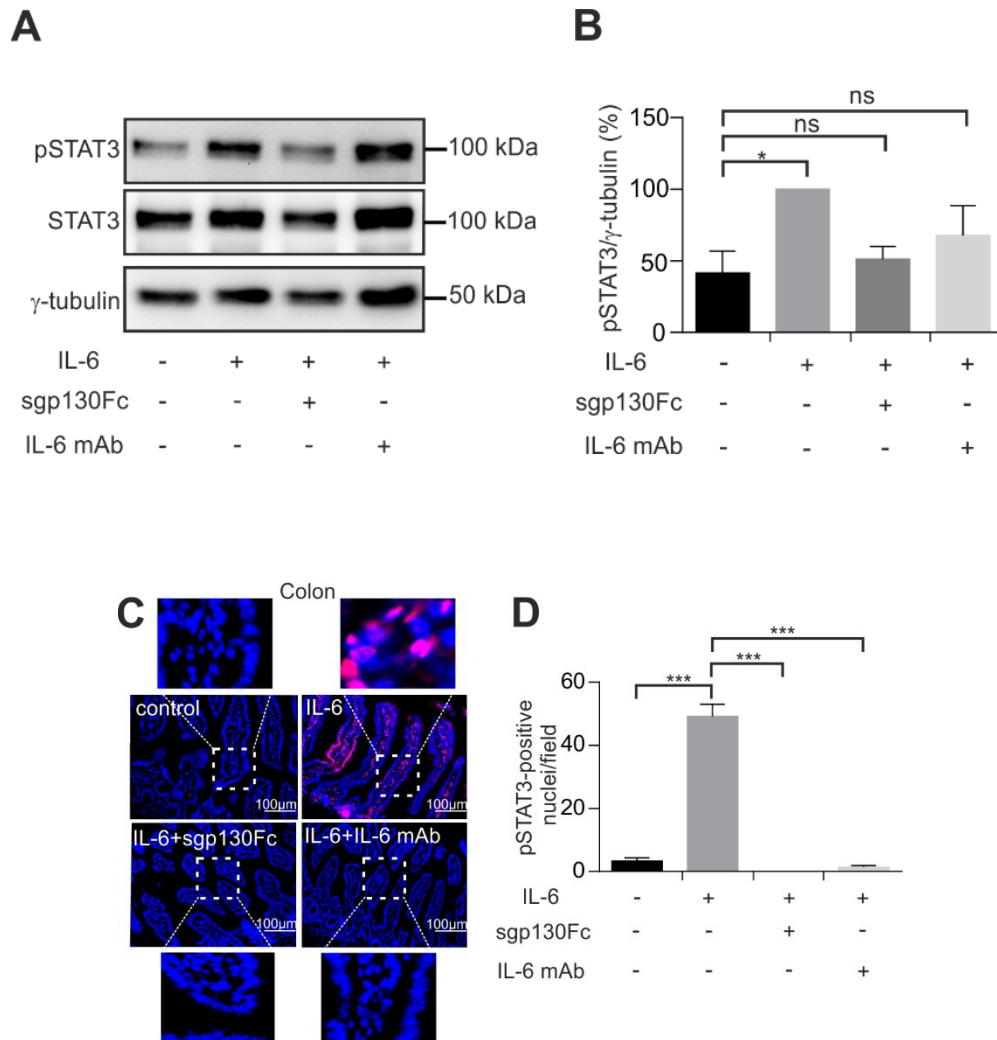


Fig. 11. IL-6 activates STAT3 signaling in the colon of sIL-6R^{+/+} mice through trans-signaling

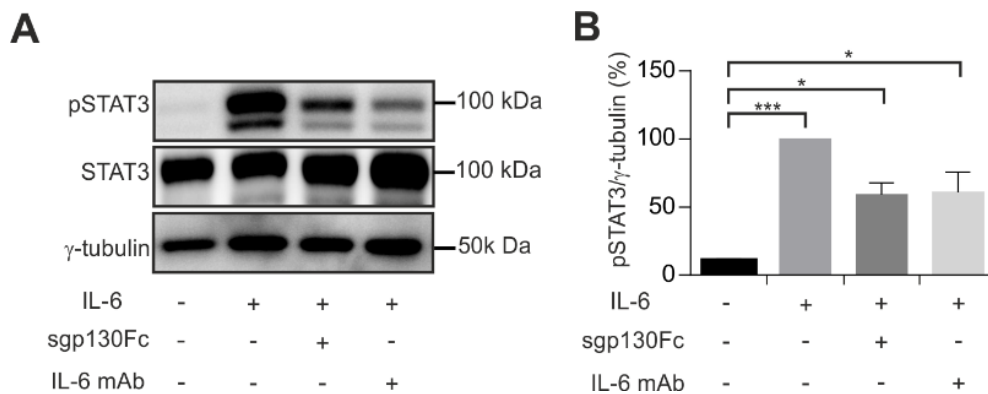
(A) Colon lysates were prepared and stained for STAT3, pSTAT3, and γ -tubulin by Western blot analysis. Representative blot is shown. (B) Quantification of (A) for all samples. The results are presented as the mean \pm S.E.M. of 3 animals/group. Relevant significances are displayed * $p \leq 0.05$. (C) Sections of the paraffin-embedded colon were stained for pSTAT3. Higher magnification of each picture is indicated by dotted lines (10 μ m). One representative of $n=3$ is shown. (D) Quantification of (C) was performed from 10 visual fields per mouse (30 visual fields). The results are presented as the mean \pm S.E.M. of 3 animals/group. Relevant significances are displayed, *** $p \leq 0.001$. These figures were taken from *Fazel Modares, N., et al. J hepatology, 2019.*

Moreover, lysates from the lung tissue were prepared. STAT3 phosphorylation was monitored via Western blotting (Fig. 12A). Western blotting data were quantified by calculating the pSTAT3

ratio to total protein ratio presented in Fig. 12B. No pSTAT3 was detected in lung lysates of untreated animals (Fig. 12B). Similar to colon and liver tissues, treatment with recombinant IL-6 also induced significant STAT3 phosphorylation in lung lysates from sIL-6R^{+/+} mice.

Moreover, treatment with sgp130Fc did not completely block the pSTAT3 signal in the lung lysates. Furthermore, a weak signal for pSTAT3 was also detected after treatment with IL-6 mAb in lung lysates (Fig. 12A-B). Next, positive cells for pSTAT3 were visualized by immunohistochemistry (Fig. 12C-D). Lung samples were collected from three different animals, and three nonconsecutive sections were analyzed per animal. Ten visualized fields were quantified per animal. Positive cells for pSTAT3 are shown in red and DAPI in blue. No positive cells for pSTAT3 were detected in untreated mice (Fig. 12C-D). However, more cells were positive for pSTAT3 in the sections of treated mice with recombinant IL-6 and the number of pSTAT3-positive cells, leading to significant generation of pSTAT3 compared to untreated mice (Fig. 12C-D). However, the number of cells positive for pSTAT3 was decreased upon blockade of IL-6 trans-signaling with sgp130Fc compared to treated mice with recombinant IL-6 (Fig. 12C-D).

Nevertheless, the complete reduction was not observed by Western blotting. Treatment with IL-6 mAb resulted in the reduction of pSTAT3 positive cells in comparison to the treated mice with recombinant IL-6 (Fig. 12C-D). These data suggested that IL-6 trans-signaling could activate lung cells through trans-signaling in sIL-6R^{+/+} mice, which demonstrated that boosted sIL-6R is biologically active in these mice. Nevertheless, the amount of injected IL-6 mAb and sgp130Fc were not able to completely inhibit this pathway.



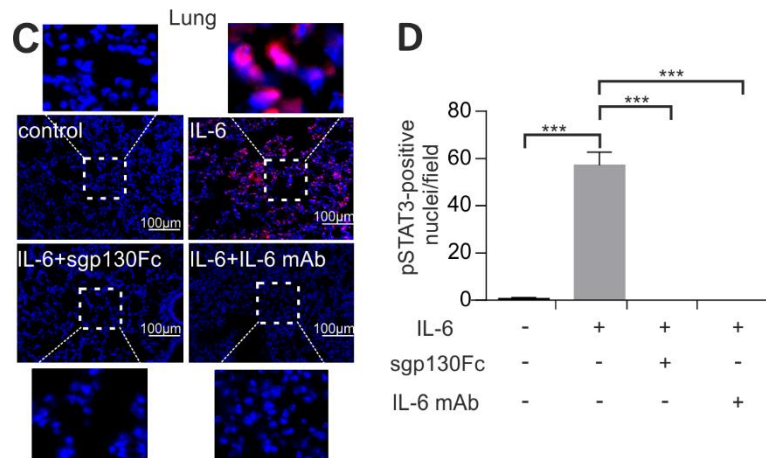


Fig. 12. IL-6 activates STAT3 signaling in the lungs of sIL-6R^{+/+} mice through trans-signaling

(A) Lung lysates were prepared and stained for STAT3, pSTAT3, and γ -tubulin by Western blot analysis. Representative blot is shown. (B) Quantification of (A) of all samples. The results are presented as the mean \pm S.E.M. of 3 animals/group. Relevant significances are displayed, * $p \leq 0.05$ and *** $p \leq 0.001$. (C) Sections of the paraffin-embedded lung were stained for pSTAT3. Higher magnification of each picture is indicated by dotted lines (10 μ m). (D) Quantification of (C) was performed from 10 visual fields per mouse (30 visual fields). The results are presented as the mean \pm S.E.M. of 3 animals/group. Relevant significances are displayed, *** $p \leq 0.001$. One representative of $n=3$ is shown. These figures were taken from *Fazel Modares, N., et al. J hepatology, 2019*.

As previously mentioned, IL-6 promotes the production of acute phase proteins, such as SAA, through classic signaling [168]. To analyze whether boosted sIL-6R could alter the production of acute phase proteins, mRNA expression levels of *Saa* were measured. Furthermore, the results obtained in sIL-6R^{+/+} mice were compared to wt mice. Therefore, sIL-6R^{+/+} mice and wt mice were treated with 5 μ g recombinant IL-6. Mice injected with PBS served as control mice. Ninety minutes post injection, livers were isolated, RNA was extracted, and RT-PCR was performed. As shown in Fig. 13, IL-6 treatment significantly induced the expression levels of *Saa* in the livers of wt mice.

Interestingly, IL-6 induced the expression levels of *Saa* in sIL-6R^{+/+} mice, as well. The upregulated levels of *Saa* in the liver of wt mice were comparable to *Saa* expression levels observed in sIL-6R^{+/+} mice (Fig. 13).

Taken together, these data suggest that IL-6 trans-signaling regulates the production of acute phase proteins, confirming that IL-6 trans-signaling compensates for the lack of IL-6 classic signaling in sIL-6R^{+/+} mice.

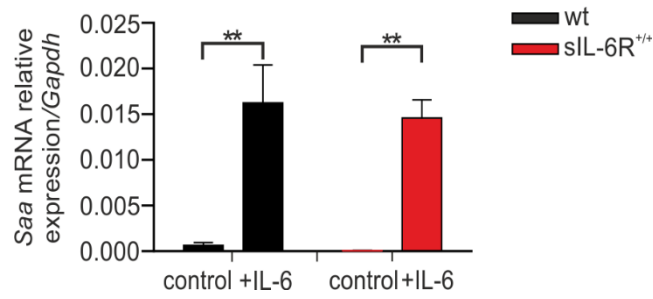


Fig. 13. Enhanced expression levels of *Saa* in sIL-6R^{+/+} mice

sIL-6R^{+/+} mice were intraperitoneally injected with PBS or IL-6 in PBS. Mice were sacrificed 90 min after injection. RNA was isolated, and RT-PCR was performed. Quantification of *Saa* mRNA levels in wt and sIL-6R^{+/+} mice after injection of 5 µg IL-6. The results are presented as the mean ± S.E.M. of 3 animals/group. Relevant significances are displayed **p ≤ 0.01. These figures were taken from *Fazel Modares, N., et al. hepatology, 2019*

3.3 Soluble IL-6R^{+/+} mice fully compensated disabled IL-6 classic signaling by IL-6 trans-signaling during liver regeneration after partial hepatectomy

To answer the question which signaling pathway of IL-6 (classic or trans-signaling) is essential for liver regeneration, the early phase of liver regeneration was precisely analyzed in sIL-6R^{+/+} mice. To date, the results obtained from this study showed that sIL-6R^{+/+} is biologically active and that IL-6 only affected the cells through trans-signaling. Therefore, these mice helped us to study only the contribution of IL-6 trans-signaling in liver regeneration. To this end, sIL-6R^{+/+} mice were subjected to 70% PHX (regeneration model), and liver regeneration was analyzed in wt, sIL-6R^{+/+}, sIL-6R^{fl/fl}, and IL-6R^{-/-} mice. In each group, 10 mice were operated. Hepatectomized mice were monitored for 12 days, and the survival rate was assessed. Upon PHX, wt animals showed approximately 80% survival, which is to analyze consistent with previous reports [169] (Fig. 14). Interestingly, sIL-6R^{fl/fl} mice also showed an 80% survival rate after PHX. Surprisingly, sIL-6R^{+/+} mice showed a survival rate of 80% after induction of liver regeneration by PHX, which was comparable to the survival rate observed in wt mice (Fig. 14). Conversely, the IL-6R-deficient mice did not survive until the end of the experiment (12 days after the operation) and showed a survival rate of 20%. Of note, mice with low health scores were excluded from the analysis and were characterized as not surviving mice.

Taken together, these data demonstrated that the survival rates of sIL-6R^{+/+} mice and wt mice are comparable after 70% PHX, which confirms that IL-6 trans-signaling promotes liver regeneration in the absence of IL-6 classic signaling upon PHX. Moreover, for the first time, liver regeneration of IL-6R-deficient mice was analyzed in the PHX model. IL-6R^{-/-} mice showed not only that IL-6 is essential for the initiation of liver regeneration but also that IL-6R is vital for liver regeneration after PHX, as indicated by the low survival rate after PHX.

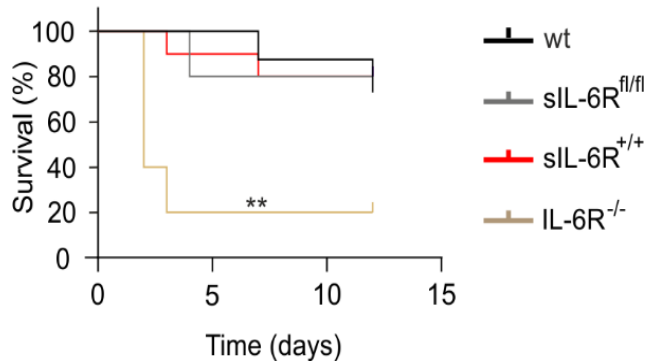


Fig. 14. High survival rate in sIL-6R^{+/+} mice after PHX

Mice were subjected to 70% PHX, and the survival rate was monitored for 12 days. Wt mice (n=10, black), IL-6R^{-/-} mice (n=10, brown), sIL-6R^{fl/fl} mice (n=10, gray) and sIL-6R^{+/+} mice (n=10, red). This figure was taken

from Fazel Modares, N., et al. *hepatology*, 2019.

Based on the survival rate of the experimental groups after PHX, the regeneration process was assessed in more detail. To continue, morphological alterations of the regenerated liver from wt and sIL-6R^{+/+} mice 12 h and 24 h after PHX were analyzed and compared to IL-6R^{-/-} mice. First, five animals were operated in each group. Livers were collected 12 h post-PHX, and H&E staining was performed. For each section, 10 visualized fields were quantified (Fig. 15A-B). As expected, the morphology of liver tissues did not show pathological alterations 12 h post-operation in wt mice (Fig. 15A-B). Interestingly, regenerated liver from sIL-6R^{+/+} mice also did not show pathological alterations 12 h after PHX. Consistently, the number of necrotic scores was comparable in sIL-6R^{+/+} mice compared to wt mice 12 h after PHX. Next, liver sections of IL-6R^{-/-} mice were stained with H&E. Interestingly, necrotic scores were significantly increased 12 h after surgery in the liver of IL-6R^{-/-} mice. Consistently, morphological alterations of wt, sIL-6R^{+/+} and IL-6R^{-/-} mice were also analyzed 24 h after PHX. Concerning wt mice, the regenerative liver was not associated with pathophysiological alteration 24 h after PHX analyzed by H&E. Interestingly, a similar pattern was observed in sIL-6R^{+/+} mice, as well. However, the morphology of the liver was changed in IL-6R^{-/-} mice 24 h after PHX. The number of necrotic scores was significantly increased 24 after PHX (Fig. 15A-B).

These data suggested that PHX resulted in less survival and more necrotic scores in IL-6R^{-/-} mice. However, liver morphology did not change during regeneration in sIL-6R^{+/+} mice. The number of necrotic scores was comparable to the number observed in wt mice.

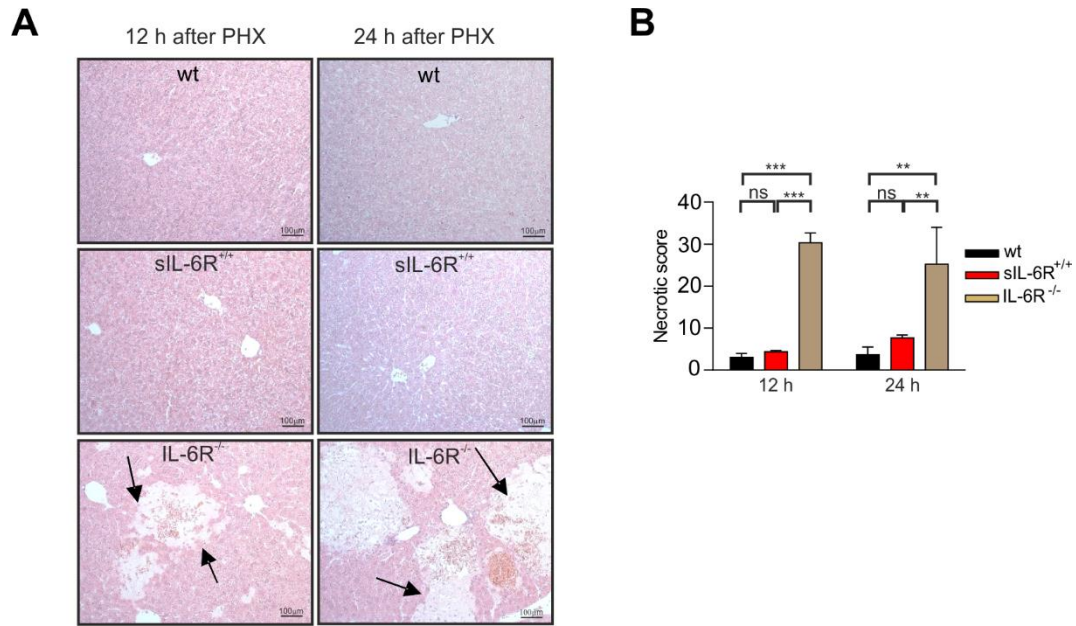


Fig. 15. Less morphological alterations of the regenerative liver in sIL-6R^{+/+} mice after PHX

(A) Paraffin-embedded tissues were collected from wt, sIL-6R^{+/+} and IL-6R^{-/-} mice. H&E staining was performed 12 h and 24 h after PHX. Necrotic areas are marked with arrows. One representative picture is shown. (B) Quantification of (C). Relevant significances are displayed, **p ≤ 0.01, ***p ≤ 0.001. The results are presented as the mean ± S.E.M. of 5 animals/group. These figures were taken from *Fazel Modares, N., et al. hepatology, 2019.*

Moreover, elevated liver enzymes, such as alanine transaminase (ALT) and aspartate transaminase (AST), indicate liver damage and liver diseases. Therefore, along with H&E staining, ALT and AST levels were also measured 12 h and 24 h after PHX. Blood was obtained from hepatectomized mice taken 12 h and 24 h after PHX. Serum was extracted. Elevated levels of AST were less pronounced in wt and sIL-6R^{+/+} mice 12 h after PHX (Fig. 16A). AST levels slightly increased 12 h after PHX in IL-6R^{-/-} mice but did not reach significance compared to wt mice (Fig. 16A). Twenty-four hours after PHX, a slight increase was detected in the level of AST in wt mice. In contrast, AST levels were slightly decreased in sIL-6R^{+/+} mice 24 h after PHX but did not reach significance compared to wt mice. Moreover, AST levels in IL-6R^{-/-} mice were significantly increased compared to sIL-6R^{+/+} mice (Fig. 16A). Furthermore, ALT levels were also measured in the serum of hepatectomized mice. Similarly, blood was obtained from wt, sIL-6R^{+/+} and IL-6R^{-/-} mice taken 12 h and 24 h after PHX. Serum was extracted. In contrast to the observed pattern for AST, ALT levels did not increase 12 h after PHX in wt mice and sIL-6R^{+/+} mice. However, the

level of ALT significantly increased as early as 12 h postsurgery in IL-6R^{-/-} mice compared to wt mice. At 24 h postsurgery, the level of ALT did not differ in wt, sIL-6R^{+/+} mice, and IL-6R^{-/-} mice (Fig. 16B).

Taken together, along with an increased number of necrotic areas, AST levels also increased 24 h and ALT levels 12 h in IL-6R^{-/-} mice after PHX. ALT levels did not increase in wt and sIL-6R^{+/+} mice.

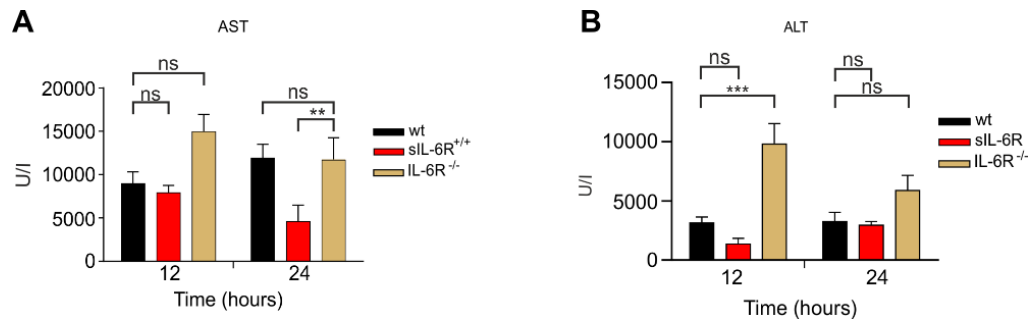


Fig. 16. Decreased levels of AST and ALT in sIL-6R^{+/+} mice after PHX

Whole blood was extracted from wt, sIL-6R^{+/+} and IL-6R^{-/-} mice (A) AST levels were measured 12 h and 24 h after PHX in wt, sIL-6R^{+/+} and IL-6R^{-/-} mice. Relevant significances are displayed, **p ≤ 0.01 and results are the mean ± S.E.M. of 5 animals/group. (B) ALT levels were determined 12 h and 24 h after PHX in wt, sIL-6R^{+/+} and IL-6R^{-/-} mice (n=5). Relevant significances are displayed, **p ≤ 0.01, ***p ≤ 0.001, and results are presented as the mean ± S.E.M. These figures were taken from *Fazel Modares, N., et al. hepatology, 2019.*

Along with pathological factors of the liver, the correlation between liver mass and body weight was analyzed after PHX. To this end, the body and regenerated liver of wt, sIL-6R^{+/+} and IL-6R^{-/-} mice were weighed 0, 12 h and 24 h after PHX. The ratio of Lw/Bw was consistently calculated and presented as a percentage. No differences in this rate were observed 0 h after PHX between wt, sIL-6R^{+/+}, and IL-6R^{-/-} mice (Fig. 17). A similar pattern was observed when the ratio was calculated in wt, sIL-6R^{+/+}, and IL-6R^{-/-} mice 12 h after PHX (Fig. 17).

Furthermore, the ratio of Lw to Bw was calculated 24 h after PHX, and no differences were observed. One explanation for the unchanged Lw/Bw ratio could be that at early time points, such as 12 h and 24 h after PHX, cell proliferation and regeneration process is not complete. Therefore,

the liver mass did not show differences 12 h and 24 h after PHX. Thus, the correlation between liver and body weight could be analyzed at a later time point when regeneration is complete.

Additionally, wt mice and sIL-6R^{+/+} mice were subjected to 70% PHX. The mice were kept until 7 days after PHX. The ratio of Lw/Bw was evaluated at the end of the experiment (168 h after PHX). Concerning IL-6R^{-/-} mice due to high mortality at early time points after PHX, it was not possible to compare the obtained results with IL-6R^{-/-} mice. Interestingly, the Lw/Bw ratio was significantly increased 168 h after PHX in wt mice and sIL-6R^{+/+} mice, which further confirmed that liver regeneration in sIL-6R^{+/+} mice is comparable to wt mice (Fig. 17).

Taken together, in the early time points after PHX, no difference was observed in the Lw/Bw ratio between wt, sIL-6R^{+/+} and IL-6R^{-/-} mice. However, Lw/Bw significantly increased 168 h after PHX in wt and sIL-6R^{+/+} compared to the observed ratio 0 h after PHX. This observation confirmed that liver weight correlated with body weight, indicating the progression of liver regeneration in sIL-6R^{+/+} mice.

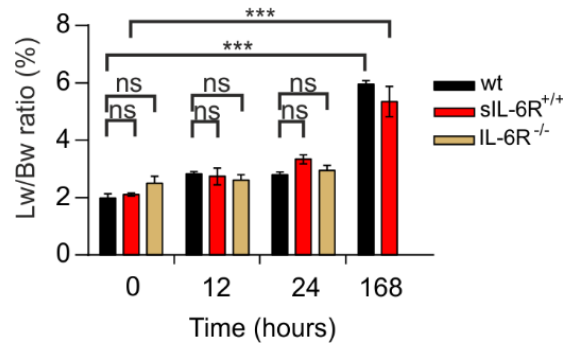


Fig. 17. Correlation of liver weight to body weight during liver regeneration in sIL-6R^{+/+} mice

Liver weight and body weight were calculated in wt, sIL-6R^{+/+} mice, and IL-6R^{-/-} mice after PHX. Liver/body The Lw/Bw ratio was determined at 0, 12, and 24 after PHX in wt, sIL-6R^{+/+} mice and IL-6R^{-/-} mice (n=5). The Lw/Bw ratio was determined at 0 and 168 h after PHX in wt and sIL-6R^{+/+} (n=3). Relevant significances are displayed, ***p ≤ 0.001, results are presented as the mean ± S.E.M. This figure was taken from Fazel Modares, N., et al. *hepatology*, 2019.

3.4 sIL-6R was enhanced in sIL-6R^{+/+} mice after PHX

Under steady-state conditions, sIL-6R levels were upregulated in sIL-6R^{+/+} mice as compared to wt mice, as shown in Fig. 9A. Consistently, it was revealed that high amounts of sIL-6R were biologically active and could activate target cells through IL-6 trans-signaling in the liver of naïve sIL-6R^{+/+} mice (Fig. 10). Furthermore, by using a regeneration model (PHX), we showed that sIL-6R^{+/+} mice had comparable survival rate to wt mice after PHX, which was accompanied by less necrotic scores and low levels of ALT and AST after PHX in compare to IL-6R deficient mice (Fig. 14-16). To determine whether PHX could induce the serum levels of sIL-6R in sIL-6R^{+/+} mice, ELISA was performed. Therefore, wt, sIL-6R^{+/+}, and IL-6R^{-/-} mice were subjected to 70% PHX. Blood was taken through the *vena cava*, and subsequently, serum was extracted, and ELISA was performed. Concerning wt mice, a 1.5-fold increase was detected in the levels of sIL-6R from 12 to 24 h post-operation. sIL-6R levels increased from 11 ng/ml to 15 ng/ml compared to sIL-6R levels detected directly after surgery in wt mice (Fig. 18A). This observation is in good agreement with the previous report, showing elevated sIL-6R levels during the first 48 h after PHX [174]. Due to the lack of IL-6R, no soluble form of IL-6R was detected in the serum of IL-6R^{-/-} hepatectomized mice 12 h and 24 h post-PHX (Fig. 18B). Interestingly, sIL-6R was drastically increased as early as 12 h after PHX in sIL-6R^{+/+} mice (Fig. 18C). sIL-6R levels displayed a 3.2-fold increase compared to IL-6R levels measured directly after PHX. Therefore, sIL-6R levels reached 1200 ng/ml 12 h after PHX (Fig. 18C), and 24 h after PHX, its levels returned to those observed directly after PHX (Fig. 18C). Taken together, these data suggest that PHX significantly induced sIL-6R in sIL-6R^{+/+} mice.

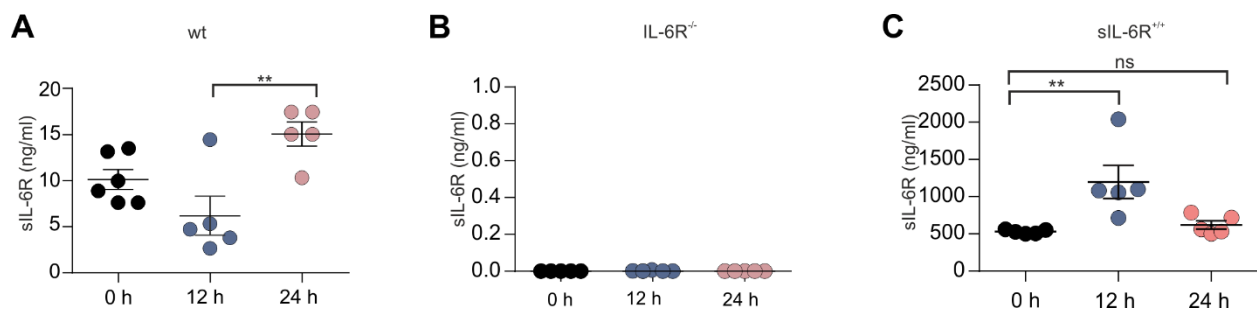


Fig. 18. Enhanced expression of sIL-6R in the serum of hepatectomized mice

0, 12 h and 24 h after PHX, sIL-6R serum levels were determined in wt (A), IL-6R^{-/-} (B) and sIL-6R^{+/+} (C) mice by sIL-6R ELISA (n=5). Relevant significances are displayed, **p ≤ 0.01 and data are presented as the mean ± S.E.M. These figures were taken from *Fazel Modares, N., et al. J hepatology, 2019.*

Since no membrane-bound IL-6R is expressed in sIL-6R^{+/+} mice, enhanced expression levels of sIL-6R should originate transcriptionally and directly be secreted. Therefore, the mRNA levels of *IL-6R* were analyzed, and the results were compared with the expression observed 0 h after PHX. To this end, wt and sIL-6R^{+/+} mice were subjected to 70% PHX, and livers were isolated 0, 3, 6, 12 h and 24 h after PHX. RNA was extracted, and RT-PCR was performed. In wt mice, *IL-6R* expression gradually increased and reached the maximal level of expression as early as 6 h after PHX (Fig. 19A). The expression levels of *IL-6R* returned to basal levels 24 h post-PHX in wt.

Remarkably, *IL-6R* expression steadily increased following PHX in the liver of sIL-6R^{+/+} mice. As early as 3 h after PHX, *IL-6R* expression significantly exceeded the expression observed directly after PHX, resulting in a significantly enhanced expression level ($p < 0.001$) (Fig. 19A). Similar to wt mice, expression of IL-6R reverted to basal levels 24 h after PHX.

Previous data have shown the contribution of the spleen to liver regeneration through the migration of specific macrophages to the liver, which exacerbates IL-6 production and subsequently induces liver regeneration (Behnke et al., 2018). In this study, *IL-6R* expression was also analyzed after PHX in the spleens of sIL-6R^{+/+} and wt mice. Therefore, mice were subjected to 70% PHX. To analyze the kinetics of IL-6R expression in the spleen of hepatectomized mice 0, 3, 6, 12 h and 24 h postoperation, spleens were isolated, and RNAs were extracted. The obtained results were compared to IL-6R expression observed directly after PHX. Generally, PHX-induced expression of IL-6R was less pronounced in the spleens of wt and sIL-6R^{+/+} mice (Fig. 19B). An increase was observed as early as 6 h after PHX but did not reach statistical significance compared to the expression levels observed 0 h after PHX. Notably, *IL-6R* expression was not induced at early time points after PHX in the spleen of wt mice (Fig. 19B). In the sIL-6R^{+/+} mice, the expression levels of *IL-6R* increased from time point 0 to 24 h after PHX, resulting in a significantly enhanced expression level compared to the expression level observed directly after PHX (Fig. 19B).

These data confirmed that PHX induced the transcriptional activity of IL-6R, resulting in elevated expression of sIL-6R in sIL-6R^{+/+} mice. In wt mice, the production of sIL-6R is mainly mediated by ADAM protease activity. This effect might result in delayed upregulation in IL-6R expression compared to the kinetics of IL-6R expression in sIL-6R^{+/+} mice.

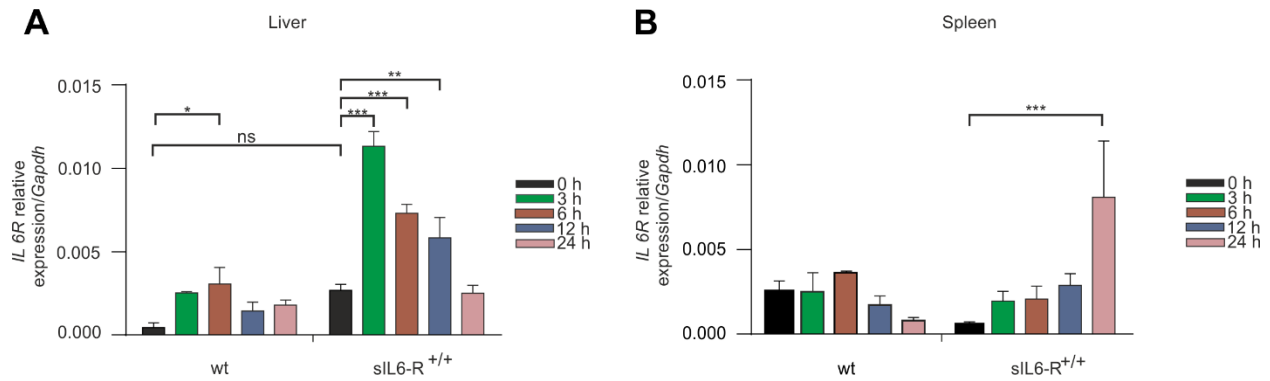


Fig. 19. Enhanced IL-6R expression in hepatectomized sIL-6R^{+/+} mice

(A) Total RNA was extracted from the liver of wt, and sIL-6R^{+/+} mice at 0, 3, 6, 12 h and 24 h after PHX and mRNA levels of IL-6R were determined by quantitative RT-PCR (n=5). Relevant significances are displayed, **p ≤ 0.01, ***p ≤ 0.001, and data are presented as the mean ± S.E.M. (B) Total RNA was extracted from the spleen of wt and sIL-6R^{+/+} mice 0, 3, 6, 12, and 24 h after PHX, and mRNA levels of IL-6R were determined by quantitative RT-PCR (n=5). Relevant significances are displayed, ***p ≤ 0.001 and the results are presented as the mean ± S.E.M. These figures were taken from *Fazel Modares, N., et al. J hepatology, 2019.*

3.5 IL-6 trans-signaling promotes liver regeneration in sIL-6R^{+/+} mice

PHX-induced transcriptional activity of IL-6R, resulting in enhanced sIL-6R during liver regeneration in sIL-6R^{+/+} mice. Previously, it was shown that enhanced sIL-6R could target liver cells through trans-signaling, leading to increased STAT3 phosphorylation (Fig. 10A-D). In this study, the activity of elevated sIL-6R and subsequent signal transduction was investigated to verify the underlying mechanism of regeneration in sIL-6R^{+/+} mice. The activity of sIL-6R through trans-signaling was studied by monitoring STAT3 phosphorylation during liver regeneration via immunohistochemistry and Western blotting. To this end, wt, sIL-6R^{+/+} and IL-6R^{-/-} mice were subjected to 70% PHX. Paraffin-embedded tissues from the liver were prepared directly after 12 h and 24 h after PHX. Samples were stained for pSTAT3 and DAPI. Samples were collected from five different animals for each group. For each group, five nonconsecutive sections were analyzed. In fifty pictures positive cells for pSTAT3 were quantified by using image J. At 0 h after PHX, only a few cells stained positive for pSTAT3 (Fig. 20A-B). The number of positive cells markedly increased from time point 0 to 12 h after operation. Similar numbers of pSTAT3-positive cells

were observed at 24 h after PHX (Fig. 20A-B). In sIL-6R^{+/+} mice, immunostaining was performed similarly to what has been described for wt mice. Less pSTAT3-positive cells were observed at time point 0 after PHX. Interestingly, PHX significantly induced pSTAT3-positive cells 12 h and 24 h post PHX compared to the observed level followed by PHX (Fig. 20A-B). PHX did not alter the number of pSTAT3-positive cells compared to the basal level observed 0 h after PHX (Fig. 20A-B). Additionally, no apparent increase in the strength of the pSTAT3 signal in positive cells was observed following PHX in IL-6R^{-/-} mice (Fig. 20A-B).

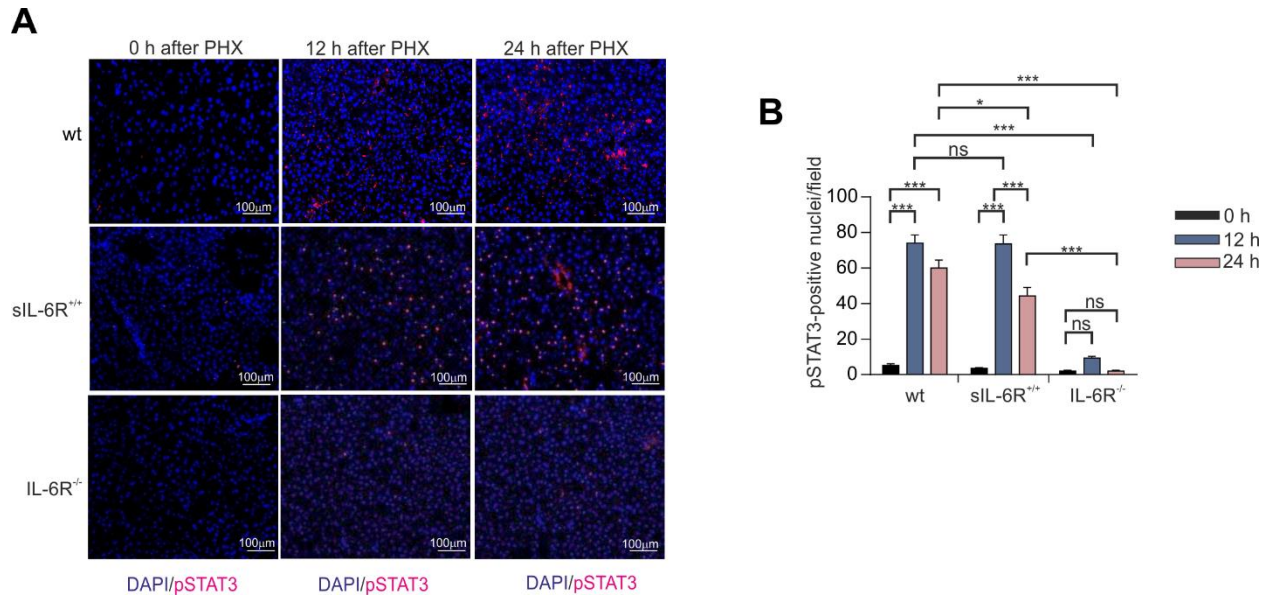


Fig. 20. Abrogated pSTAT3 in IL-6R^{-/-} mice but not in sIL-6R^{+/+} mice upon PHX

(A) Sections of paraffin-embedded liver tissues from wt, IL-6R^{-/-}, and sIL-6R^{+/+} mice were stained for pSTAT3 at 0, 12 h and 24 h after PHX. Representative slides are shown (n=5 mice per group). (B) Quantification of (A) from 10 visual fields of every mouse (n=5). Relevant significances are displayed, *p ≤ 0.05 and ***p ≤ 0.001. Data are presented as the mean ± S.E.M. One picture as representative is shown in each group. These figures were taken from *Fazel Modares, N., et al. J hepatology, 2019.*

Furthermore, to confirm the obtained results from immunohistochemistry, Western blotting was performed. Therefore, livers from sIL-6R^{+/+} and IL-6R^{-/-} mice were isolated 0 h and 12 h after PHX. Lysates were prepared, and Western blotting was performed. Representative blots are shown in Fig. 21A. Furthermore, the ratio of pSTAT3 to γ -tubulin was calculated using Fiji software. Western blot analysis revealed that PHX induced STAT3 phosphorylation in sIL-6R^{+/+} mice 12 h

after PHX, resulting in significant expression compared to the ratio observed in IL-6R^{-/-} mice (Fig. 21B).

These data illustrated that IL-6, through IL-6R trans-signaling, targets liver cells and induces the signal through the STAT3 pathway.

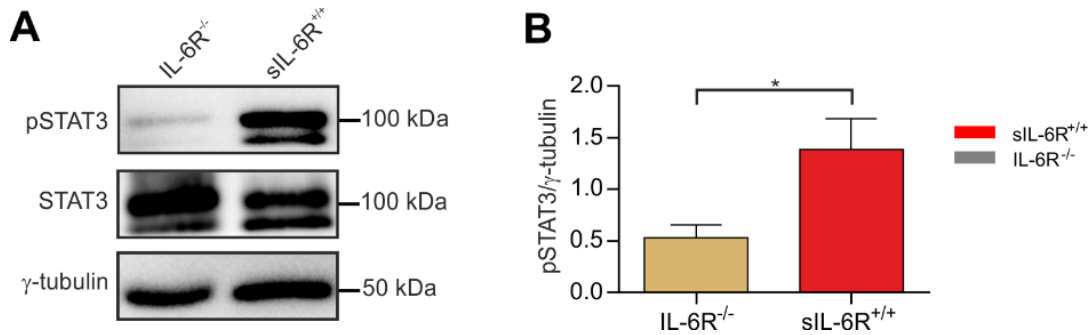


Fig. 21. Enhanced pSTAT3 levels in sIL-6R^{+/+} after PHX

(A) Liver lysates from IL-6R^{-/-} and sIL-6R^{+/+} mice were prepared and stained for pSTAT3 in Western blotting 12 h after PHX. Representative slides are shown (n=5 mice per group). (B) Quantification of (A) Western blots of 5 mice for each time point are shown. Relevant significances are displayed *p \leq 0.05. These figures were taken from *Fazel Modares, N., et al. J hepatology, 2019.*

The obtained data illustrated that PHX induced sIL-6R in the liver of sIL-6R^{+/+} mice, resulting in enhanced STAT3 phosphorylation through trans-signaling. The contribution of IL-6 through trans-signaling in liver proliferation was further studied by analyzing the proliferation rate of liver cells after PHX. To this end, wt, sIL-6R^{+/+} and IL-6R^{-/-} mice were subjected to 70% PHX, and the livers were collected from five different animals in each group. Paraffin-embedded tissue was prepared. Proliferating cells were monitored using proliferating cell nuclear antigen (PCNA) antibody. Ten pictures were taken from each section, and in total, quantification was performed from 50 visualized fields by image J software. 0 h after PHX, few positive cells were detected for PCNA in wt mice. The number of PCNA-positive cells gradually increased during PHX, leading to a continuous increase until 24 h after PHX (Fig. 22A-B). A few PCNA-positive cells were observed directly after PHX in sIL-6R^{+/+} mice. Interestingly, the number of positive cells was induced significantly from 12 h to 24 h after PHX compared to the number of proliferating cells observed directly after PHX in sIL-6R^{+/+} mice (Fig. 22A-B). In IL-6R^{-/-} mice, PHX did not induce the

amount of PCNA-positive cells compared to positive cells detected directly after PHX (Fig. 22A-B). Additionally, no apparent increase in the strength of the PCNA signal in positive cells was observed during PHX.

These data together suggested that boosted IL-6 trans-signaling concomitantly induced STAT3 phosphorylation and the number of proliferating cells after PHX in sIL-6R^{+/+} mice. However, a lack of IL-6R was associated with impaired IL-6 signaling and abrogated STAT3 phosphorylation, resulting in impeded cell proliferation after PHX in IL-6R^{-/-} mice.

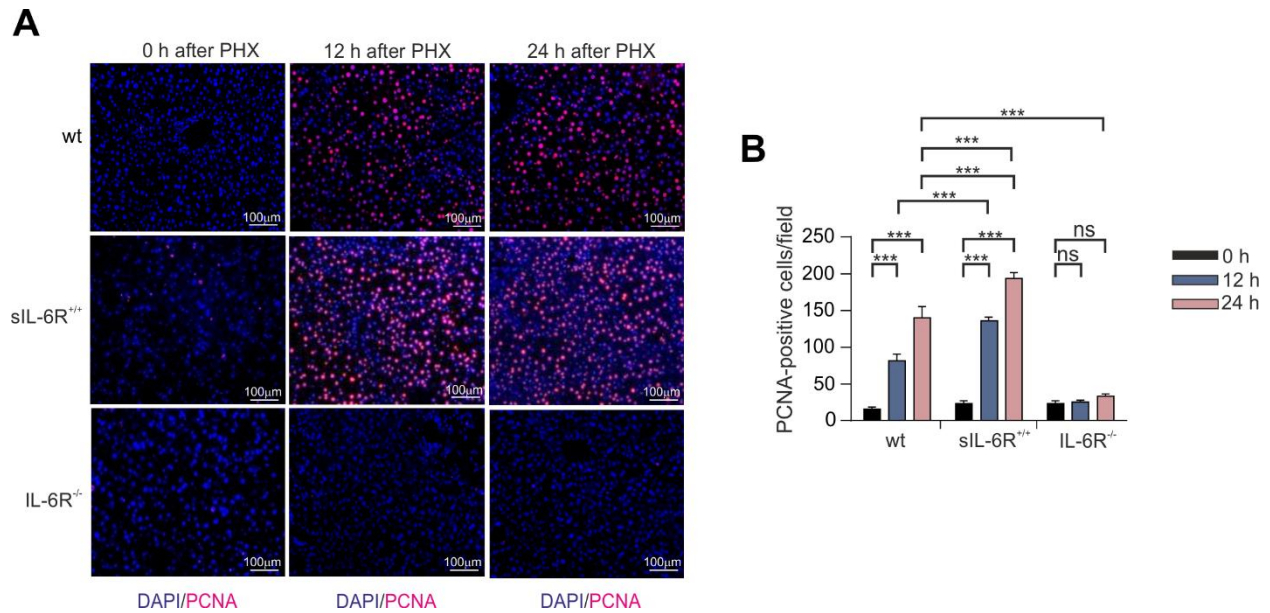


Fig. 22. Abrogated PCNA levels in IL-6R^{-/-} but not in sIL-6R^{+/+} mice after 70% PHX

(A) Sections of paraffin-embedded liver tissues from wt, IL-6R^{-/-}, and sIL-6R^{+/+} mice were stained for PCNA at 12 h and 24 h after PHX. Representative visual fields are shown (n=5 mice per group). (B) Quantification of (A) from 10 visual fields of every mouse (n = 5) is shown. Relevant significances are displayed, *p ≤ 0.05 and ***p ≤ 0.001. Data are presented as the mean ± S.E.M. presented. One representative picture is shown in each group. These figures were taken from Fazel Modares, N., et al. *J hepatology*, 2019.

3.6 Selective inhibition of IL-6 trans-signaling prevents liver regeneration following PHX

In the first part of the presented work, the positive correlation of IL-6 trans-signaling to liver regeneration after PHX was investigated. PHX-induced sIL-6R promotes cell proliferation through

the STAT3 signaling pathway in sIL-6 trans-signaling mice. Next, by distinguishing between IL-6 classic and trans-signaling, we attempted to confirm the positive correlation of IL-6 trans-signaling to liver regeneration in wt mice. Therefore, blockade of IL-6 signaling is required. To this end IL-6 mAb and sgp130Fc were applied in this study. IL-6 mAb neutralizes IL-6, leading to blockade of IL-6 classic and trans-signaling. Furthermore, sgp130Fc trapped the IL-6/sIL-6R complex, resulting in a specific block of IL-6 trans-signaling.

To study the effects of global blockade of IL-6 on liver regeneration, mice were intraperitoneally (i.p.) injected with high doses of IL-6 monoclonal antibody 250 $\mu\text{g}/\text{mouse}$ before and every 2 days after PHX. Previously, a low dose of sgp130Fc was shown to be sufficient to block trans-signaling; therefore, in this study, 50 $\mu\text{g}/\text{mouse}$ sgp130Fc was applied. Wt mice treated with IL-6 mAb and wt mice treated with sgp130Fc were subjected to 70% PHX. We examined the survival rate of mice after PHX. As expected, wt mice showed 80% survival after PHX. However, global blockade of IL-6 with IL-6 mAb and every two days injection after PHX led to a decreased survival rate of 10% (Fig. 23). This observation is consistent with the low survival rate observed after PHX in IL-6R-deficient mice (shown in Fig. 14).

Interestingly, blockade of only IL-6 trans-signaling by sgp130Fc and every two days injection after PHX resulted in a low survival rate of 20% (Fig. 23).

These data confirmed the pivotal role of IL-6 in liver regeneration. Furthermore, blockade of IL-6 trans-signaling resulted in a lower survival rate, corroborating the importance of trans-signaling in liver regeneration confirmed by sIL-6R^{+/+} mice.

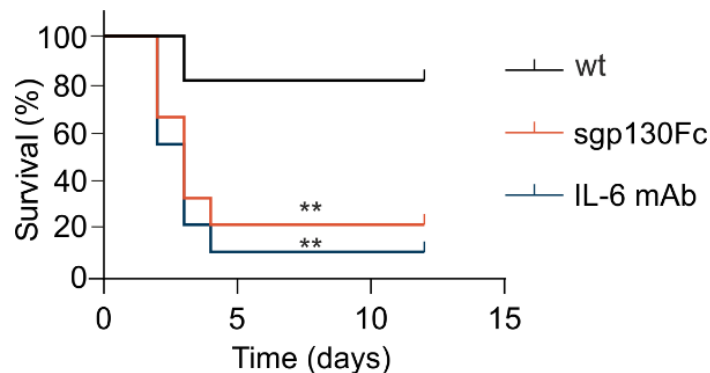


Fig. 23. Abrogated liver regeneration in mice treated with IL-6 mAb and sgp130Fc after 70% PHX

(A) Mice were subjected to 70% PHX, and survival was monitored for 12 days, wt mice (n=10), wt mice +sgp130Fc (n=10), and wt mice +IL-6 mAb (n=10). This figure was taken from *Fazel Modares, N., et al. J hepatology, 2019.*

Blockade of IL-6 signaling with IL-6 mAb or sgp130Fc leads to abrogated liver regeneration. To further analyze liver tissue in these mice, morphological alterations were monitored after PHX. To this end, H&E staining was performed. Mice were treated with IL-6 mAb and sgp130Fc 16 h before PHX and then subjected to 70% PHX. Liver samples were collected from five different animals in each group, and paraffin-embedded tissues were prepared 12 h and 24 h after PHX.

On the liver sections of treated mice with sgp130Fc, larger necrotic areas were detected. The number of necrotic areas increased from 12 h after PHX to 24 h after PHX, leading to significant differences compared to the necrotic regions observed in age-matched control mice (Fig. 24A-B).

Blockade of IL-6 signaling with IL-6 mAb resulted in even more significant and higher necrotic areas in the hepatectomized liver. The number of necrotic scores increased gradually until 24 h after PHX (Fig. 24A-B).

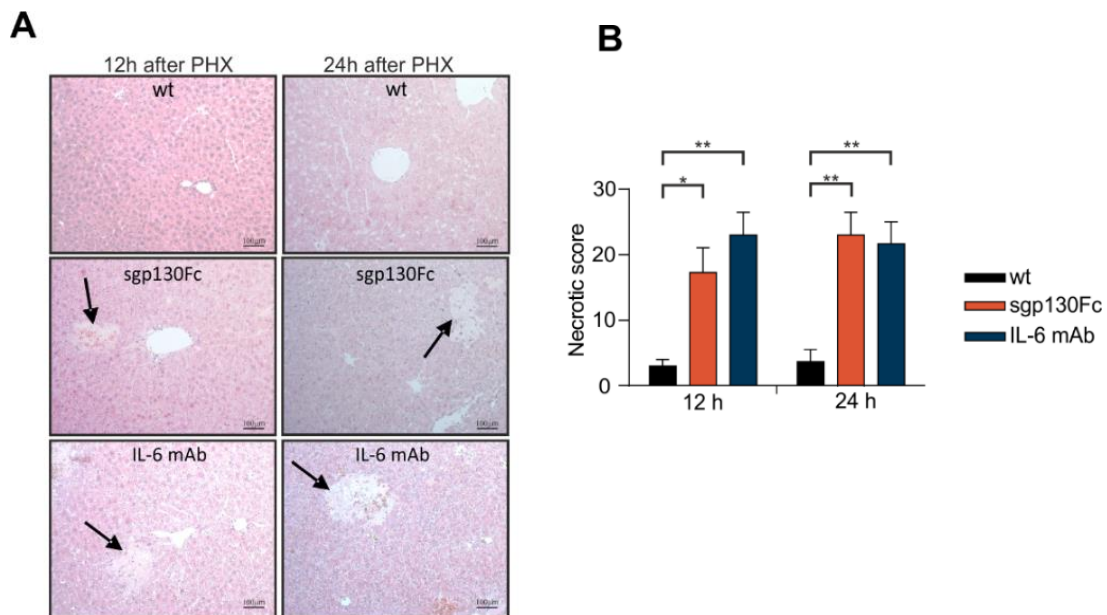


Fig. 24. Enhanced necrotic scores in the liver of treated mice with IL-6 mAb and sgp130Fc followed by PHX

(A) Liver sections from wt, wt+sgp130Fc, and wt+IL-6 mAb mice were stained for H&E (n=3). Necrotic areas are marked with arrows. (B) Quantification of (A) is shown. Relevant significances are displayed, * $p \leq 0.05$, ** $p \leq 0.01$. The results represent the mean \pm SEM. These figures were taken from *Fazel Modares, N., et al. J hepatology, 2019*.

Along with increased necrotic areas in the liver of treated mice with sgp130Fc and IL-6 mAb, the liver enzymes ALT and AST were measured. Therefore, whole blood was taken from *vena cava* 12 h and 24 h after PHX, and serum was extracted. Furthermore, the ALT and AST levels were analyzed in the serum of experimental groups. Blockade of IL-6 trans-signaling or blockade of IL-6 trans-signaling did not result in significant induction of ALT and AST levels in the serum of partially hepatectomized mice (Fig. 25A-B).

Together, liver damage was assessed by enhancing the numbers of necrotic areas in treated mice with IL-6 mAb and sgp130Fc. No significant increase in ALT and AST levels was detected.

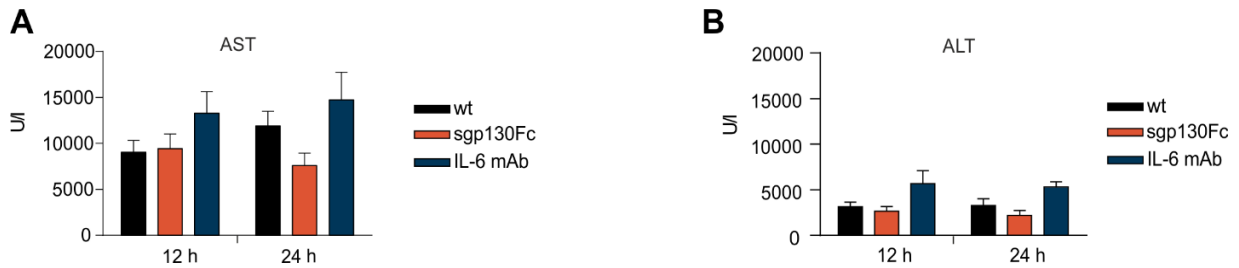


Fig. 25. Enhanced ALT and AST levels in the serum of hepatectomized mice after IL-6 inhibition

(A) AST levels were determined 12 h and 24 h after PHX in wt, wt+sgp130Fc, wt+IL-6 mAb mice. Five mice were analyzed in each group. (B) ALT levels were measured 12 h and 24 h after PHX in wt, wt+sgp130Fc, and wt+IL-6 mAb mice (n=5). P values are indicated as follows: * $p \leq 0.05$, ** $p \leq 0.01$, *** $p < 0.001$, and the results are displayed as the mean \pm SEM. These figures were taken from *Fazel Modares, N., et al. J hepatology, 2019*.

Moreover, the correlation between liver mass and body weight ratio was analyzed in treated mice with IL-6 mAb, sgp130Fc, and wt mice 0 h, 12 h, and 24 h after the operation. The Lw/Bw ratio

was analyzed as described for transgenic mice. The ratio of Lw/Bw did not differ significantly among the experimental group.

Taken together, these results indicate that whereas the number of necrotic areas increased after PHX in treated mice with sgp130Fc or IL-6 mAb, blockade of IL-6 signaling had no significant influence on the Lw/Bw ratio at early time points after PHX.

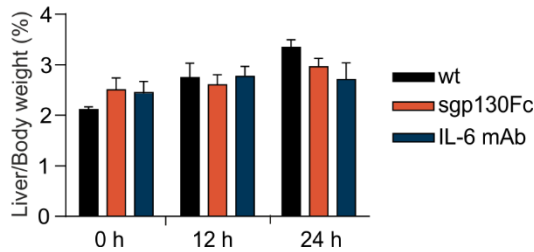


Fig. 26. No alteration in the Lw/Bw ratio after blockade of IL-6 signaling upon PHX

Liver/body weight ratio of wt mice, wt mice +sgp130Fc, and wt mice +IL-6 mAb after 70% PHX were determined at 0, 12, and 24 after PHX (n=5). The results are displayed as the mean \pm SEM. This figure was taken from *Fazel Modares, N., et al. J hepatology, 2019.*

3.7 Selective inhibition of IL-6 trans-signaling abrogated STAT3 signaling during liver regeneration following PHX

The results obtained in this study demonstrate that blockade of IL-6 via IL-6 mAb or specific inhibition of IL-6 trans-signaling via sgp130Fc impaired liver regeneration accompanied by loss of function, impaired cell proliferation, and higher mortality after PHX. The impact of IL-6 in liver regeneration through STAT3 signaling was shown in previous parts of this work; therefore, STAT3 mediation of liver regeneration was comparatively assessed. Mice were treated with IL-6 mAb or sgp130Fc to inhibit IL-6 signaling or specifically trans-signaling. Next, mice were subjected to 70% PHX. 0, 12 h and 24 h after PHX, livers were collected from five different animals in each group. Next, pSTAT3 was assessed via Western blotting and immunohistochemistry. Paraffin-embedded tissue was prepared. Samples were stained for pSTAT3 and DAPI for each animal, and 10 pictures were taken from each section.

0 h after the operation, few positive cells were observed for pSTAT3. The number of pSTAT3-positive cells increased at 12 h post-PHX, leading to a continuous increase until 24 h after operation in the livers of wt mice (Fig. 27A-B). Importantly, blockade of IL-6 trans-signaling with sgp130Fc treatment abrogated the phosphorylation of STAT3, leading to a decreased number of pSTAT3-positive cells 12 h after PHX compared to the observed level in wt mice 12 h after PHX

(Fig. 27A-B). STAT3 phosphorylation levels were constantly decreased until 24 h after PHX (Fig. 27A-B). Similar to wt mice, few cells positive for pSTAT3 were observed directly after PHX in mice treated with IL-6 mAb. PHX-induced STAT3 phosphorylation was less pronounced 12 h after surgery in treated mice with IL-6 mAb. Decreased STAT3 phosphorylation continued until 24 h after PHX, which was comparable to the levels observed 0 h after PHX (Fig. 27A-B).

Taken together, these results demonstrate that inhibiting IL-6 signaling via IL-6 mAb or specific blockade of IL-6 trans-signaling via sgp130Fc resulted in hampered liver regeneration consisting of higher necrotic cells, decreased levels of STAT3 phosphorylation and higher mortality.

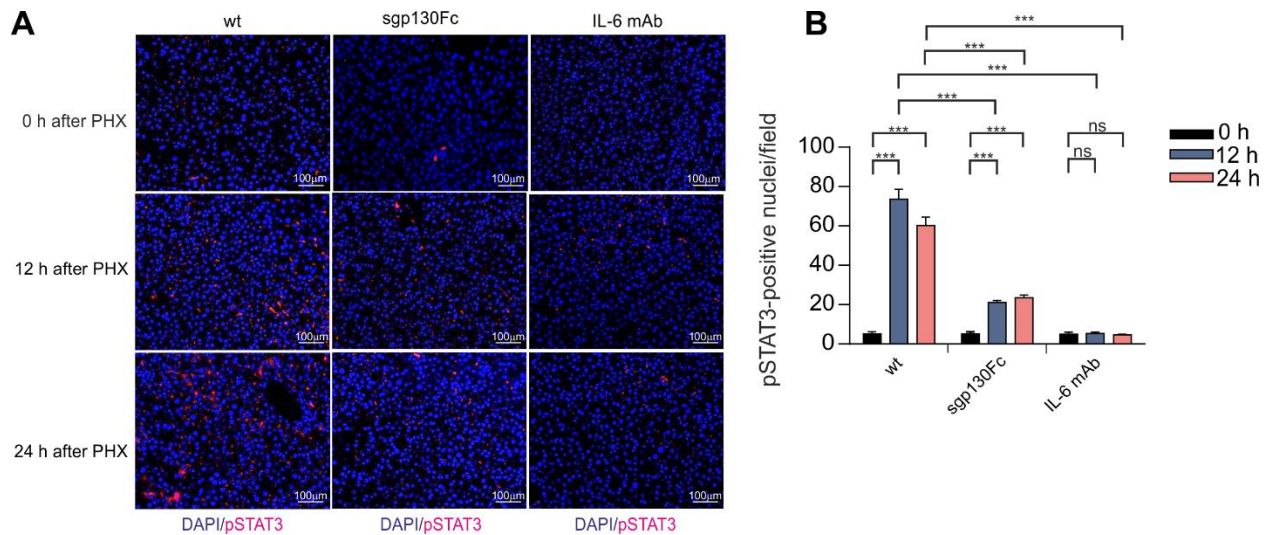


Fig. 27. Abrogated pSTAT3 in wt mice treated with sgp130Fc and IL-6 mAb after 70% PHX

(A) Sections of paraffin-embedded liver tissues from wt mice, wt mice+sgp130Fc and wt mice+IL-6 mAb were stained for pSTAT3 at 0,12 h and 24 h after PHX. Representative slides are shown (n=5 mice per group). (B) Quantification of (A) from 10 visual fields of every mouse (n=5). Relevant significances are displayed, *** $p \leq 0.001$. These figures were taken from *Fazel Modares, N., et al. J hepatology, 2019*.

Furthermore, Western blotting was performed to assess the effect of IL-6 blockade on the level of STAT3 phosphorylation. Liver lysates were prepared from collected livers of wt mice and wt mice treated with sgp130Fc and IL-6 mAb 12 h and 24 h after PHX. Western blotting was performed, and the ratio of pSTAT3 to γ -tubulin was calculated as described for sIL-6R^{+/+} mice.

The first increase in STAT3 phosphorylation occurred 12 h after operation, leading to a continuous increase until 24 h after PHX in wt mice, confirming the increased number of pSTAT3-positive cells observed by immune staining (Fig. 28A-D).

Blockade of IL-6 trans-signaling via sgp130Fc resulted in significantly decreased levels of pSTAT3 compared to wt mice 12 h after PHX. Furthermore, treatment with IL-6 mAb resulted in a reduced amount of STAT3 phosphorylation 12 h after PHX. Notably, STAT3 phosphorylation levels were comparable in mice treated with IL-6 mAb or treated with sgp130Fc 12 h after PHX (Fig. 28A-B).

Along with abrogated STAT3 phosphorylation, 12 h after PHX, the level of STAT3 phosphorylation was also significantly decreased 24 h after PHX in mice treated with IL-6 mAb or sgp130Fc compared to control mice (Fig. 28C-D).

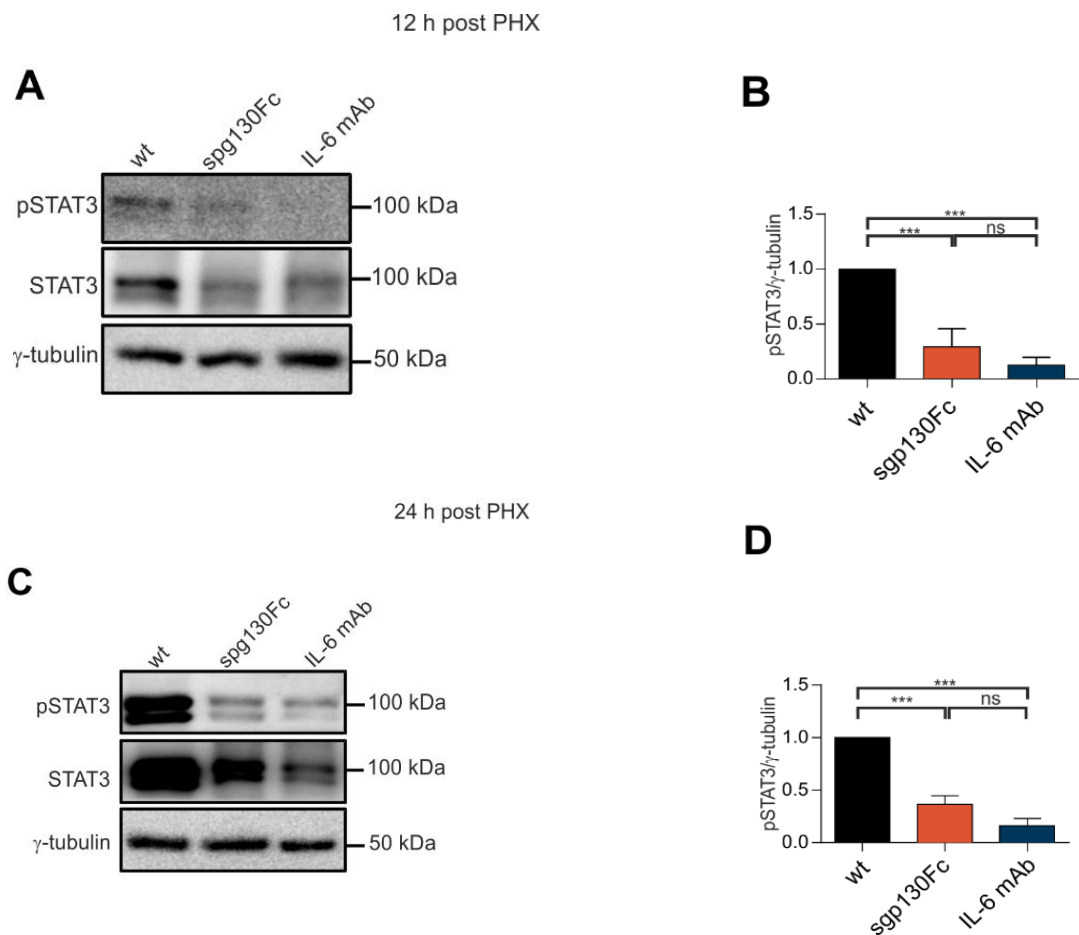


Fig. 28. Abrogated pSTAT3 in wt mice treated with sgp130Fc and IL-6 mAb after 70% PHX

(A) Lysates from liver tissues from wt mice, wt mice+sgp130Fc, and wt mice+IL-6 mAb mice were prepared and stained for pSTAT3 by Western blotting 12 h after PHX. Representative blots are shown (n=5 mice per group). (B) Quantification of (A) Western blots of 5 mice each. Relevant significances are displayed, *** $p \leq 0.001$. (C) Lysates from liver tissues from wt mice, wt mice+sgp130Fc and wt mice+IL-

6 mAb were stained for pSTAT3 by Western blotting 24 h after PHX. Representative blots are shown (n = 5 mice per group). (D) Quantification of (C) Western blot analyses of 5 mice each. Relevant significances are displayed, *** $p \leq 0.001$. These figures were taken from *Fazel Modares, N., et al. J hepatology, 2019*.

Liver regeneration was impeded upon blockade of IL-6 signaling in treated mice with either IL-6 mAb or sgp130Fc. Impaired liver regeneration coincided with low levels of STAT3 phosphorylation, a higher number of necrotic areas, and higher mortality after PHX. These results indicate that blockade of IL-6 signaling and abrogated STAT3 signaling target cell proliferation during liver damage. Therefore, liver cell proliferation was further investigated. To this end, wt mice, wt mice treated with IL-6 mAb and wt mice treated with sgp130Fc were subjected to 70% PHX. Samples were collected from five different animals from each group at different time points: 0 h and 12 h and 24 h postoperation. Paraffin-embedded liver sections were prepared. To evaluate cell proliferation, an antibody directed against proliferating cell nuclear antigen (PCNA) was used. DAPI was employed to stain the cell nucleus (Fig. 29A-B).

PCNA positive cells were rarely observed directly after PHX by immunohistochemistry. Twelve hours after PHX, the number of positive cells for PCNA was increased, resulting in significantly enhanced PCNA expression ($p < 0.001$) compared to detected positive cells 0 h after PHX. Consistent with this finding, the number of positive cells for PCNA gradually increased until 24 h after PHX and reached significance.

Few cells were positive for PCNA 0 h after PHX. However, PHX did not induce positive cells in the remaining liver of treated mice with sgp130Fc 12 h after PHX. The number of PCNA positive cells also continuously decreased until 24 h after PHX compared to wt control mice. Blockade of IL-6 signaling with IL-6 mAb resulted in fewer PCNA-positive cells 12 h after PHX, and even fewer positive cells were observed 24 h after PHX in treated mice with IL-6 mAb.

Taken together, these data illustrated that liver regeneration was not impaired in the presence of IL-6 in wt mice. In the presence of IL-6 and active signaling of IL-6, PHX enhanced the survival rate in wt mice accompanied by less necrotic areas, and higher STAT3 phosphorylation, resulting in a higher number of proliferating cells 12 h and 24 h post PHX.

The blockade of IL-6 trans-signaling was consistent with impaired liver regeneration. Blockade of IL-6 trans-signaling resulted in less survival rate after PHX, accompanied by a higher number of

necrotic scores, and a lower amount of STAT3 phosphorylation, which resulted in lower proliferation and impaired liver regeneration. This observation confirmed that IL-6 trans-signaling positively contributes to liver regeneration after PHX, which was concluded in the first part of the presented work.

The blockade of IL-6 trans-signaling and classic signaling by IL-6 mAb resulted also in lower survival rate after PHX. Impaired IL-6 signaling led to less STAT3 phosphorylation, and less PCNA positive cells resulted in impaired liver regeneration accompanied by higher necrotic areas.

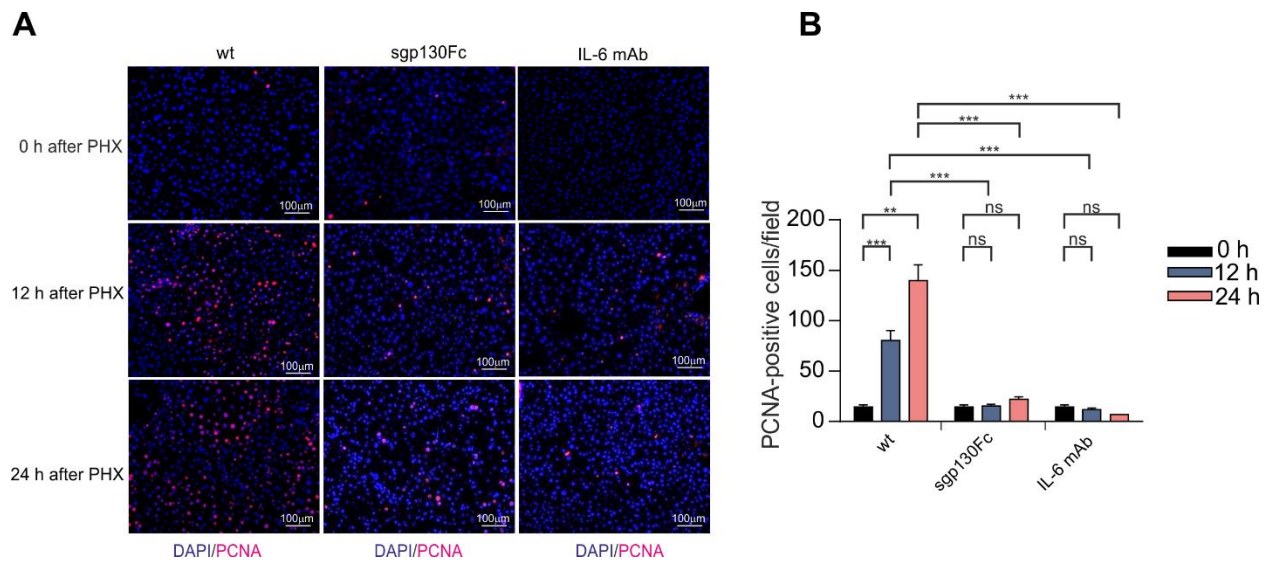


Fig. 29. Abrogated PCNA signals in wt mice treated with sgp130Fc and IL-6 mAb after 70% PHX

(A) Sections of paraffin-embedded liver tissues from wt mice, wt mice +sgp130Fc and wt mice +IL-6 mAb were stained for PCNA at 12 h and 24 h after PHX. Representative slides are shown (n=5 mice per group).

(B) Quantification of (A) from 10 visual fields of every mouse (n=5). Data are displayed, **p ≤ 0.01, ***p ≤ 0.001. All results are displayed as the mean ± SEM. These figures were taken from *Fazel Modares, N., et al. J hepatology, 2019.*

3.8 Effect of IL-6 on the function of HSC in liver regeneration upon liver damage

It has been shown that HGF induces hepatocyte proliferation and liver regeneration when injected into naïve mice and rats [185-187]. Also, recently it has been shown that treatment with HGF and HIL-6, resulted in an increase in hepatocyte proliferation after PHX [174]. In the liver, HGF is mainly produced by hepatic stellate cells [188]. HGF affects hepatocytes through its unique receptor, namely, the Met receptor, which is expressed on hepatocytes and epithelial cells [189, 190]. It has been shown that c-MET receptor-deficient mice result in liver failure after treatment with CCl₄ [191]. Therefore, knowing the contribution of HGF/c-met to hepatocyte proliferation upon injury raises the question of whether IL-6 through trans-signaling could affect HSC functions, resulting in an alteration of HGF production. To date, we have shown that blockade of IL-6 signaling leads to impaired liver regeneration, which was consistent with the low survival rate after PHX.

Furthermore, the novel mouse model described in this study, sIL-6R^{+/+} mice, helped us to survey the contribution of only IL-6 trans-signaling on the level of a single substrate to liver regeneration after PHX. sIL-6R^{+/+} mice exhibited 80% survival, accompanied by higher STAT phosphorylation and cell proliferation. However, blockade of IL-6 trans-signaling resulted in a lower survival rate and less STAT3 phosphorylation, which was associated with reduced proliferation and regeneration failure. These observations incorporate the impact of IL-6 through its trans-signaling to liver regeneration upon PHX. To investigate the effect of IL-6 on HSC function, HGF production and c-met expression after PHX were assessed.

3.9 Induced *Hgf* expression of hepatic stellate cells via IL-6 trans-signaling in mice following PHX

To analyze HGF production during liver regeneration, wt mice, wt mice treated with IL-6 mAb and wt mice treated with sgp130Fc were subjected to 70% PHX. At 12 h and 24 h after PHX, the liver was isolated, and RNA was extracted. RT-PCR was performed to analyze the expression levels of *Hgf* and *c-Met* after PHX. Directly after the operation, PHX did not induce the mRNA expression of *Hgf*. However, the level of *Hgf* expression continuously increased until 24 h after PHX in wt mice. In the absence of IL-6 trans-signaling, PHX did not induce the expression level of *Hgf* compared to time point 0. Specific blockade of IL-6 trans-signaling with sgp130Fc resulted in a significant decrease in *Hgf* mRNA expression levels 12 h and 24 h after PHX as compared to wt mice.

Furthermore, blockade of IL-6 signaling by IL-6 mAb resulted in a significant decrease in *Hgf* expression 12 h and 24 h after PHX as compared to wt. The *Hgf* expression level 24 h after PHX was comparable to the expression level observed directly after PHX in treated mice with IL-6 mAb (Fig. 30A).

Furthermore, the expression of the HGF receptor *c-Met* was analyzed directly at 12 h and 24 h after PHX. The wt expression of *c-Met* gradually increased from time point 0 to 24 h after PHX. However, mice treated with sgp130Fc exhibited comparable expression levels, as observed in wt mice 12 h after PHX. Twelve hours after PHX, a similar pattern was observed when mice were treated with IL-6 mAb and subjected to PHX. However, PHX did not induce *c-Met* expression in mice treated with sgp130Fc at 24 h after PHX as compared to time point 0 after PHX. Blockade of IL-6 classic or trans-signaling resulted in the reduction of *c-Met* expression level 24 h after operation as compared to wt mice (Fig. 30B).

This observation indicates that IL-6 signaling might affect the function of HSCs, resulting in the alteration of HGF production. As presented, blockade of IL-6 signaling led to a reduction in HGF production compared to wt mice. Concerning *c-Met*, mRNA expression levels were comparable to basal levels observed directly after PHX in the absence of IL-6 signaling.

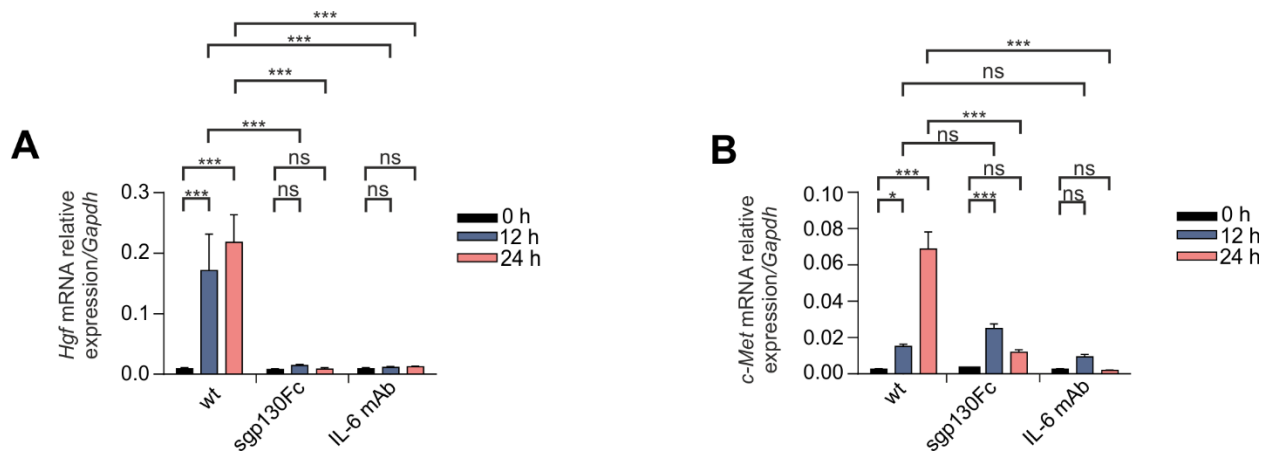


Fig. 30. Abrogated *Hgf/c-Met* expression in mice treated with sgp130Fc and IL-6 mAb after 70% PHX

(A) Total RNA was extracted from liver tissues of wt, wt+sgp130Fc and wt+IL-6 mAb mice 0,12 h and 24 h after PHX. Subsequently, the RNA levels of *Hgf* were determined by quantitative RT-PCR (n = 5). Relevant significances are displayed, *** $p \leq 0.001$. (B) Total RNA was extracted from liver tissues of wt mice, wt+sgp130Fc mice and wt+IL-6 mAb mice 0,12 h and 24 h after PHX. Subsequently, the RNA levels of *c-Met* were determined by quantitative RT-PCR (n=5). Relevant significances are displayed, *** $p \leq 0.001$ and * $p \leq 0.05$. Data are presented as the mean \pm SEM. These figures were taken from *Fazel Modares, N., et al. J hepatology, 2019.*

Furthermore, the expression levels of HGF and *c-Met* were analyzed in sIL-6R^{+/+} mice and IL-6R^{-/-} mice.

To this end, IL-6^{-/-} and sIL-6R^{+/+} mice were subjected to 70% PHX. RNA was isolated, and RT-PCR was performed. The mRNA levels of *Hgf* increased gradually from time point 0 until 24 h after PHX in sIL-6R^{+/+} mice. The kinetics of *Hgf* expression during PHX in sIL-6R^{+/+} mice was comparable to the expression kinetics observed in wt mice. However, the absence of IL-6R resulted in a reduction of *Hgf* expression 12 h after PHX as compared to wt mice. Levels of *Hgf* expression were comparable to expression observed directly after PHX in IL-6R^{-/-} mice.

Furthermore, analysis of *c-Met* expression in sIL-6R^{+/+} mice revealed a gradual increase in its expression pattern until 24 h after PHX, leading to a significant increase in expression level.

Concerning *c-Met* expression level in IL-6R^{-/-} mice, an unexplained initial increase in expression was found directly after PHX. However, the mRNA expression level of *c-Met* gradually

decreased 12 h and 24 h after PHX, resulting in a significant reduction compared to the expression level observed directly after PHX.

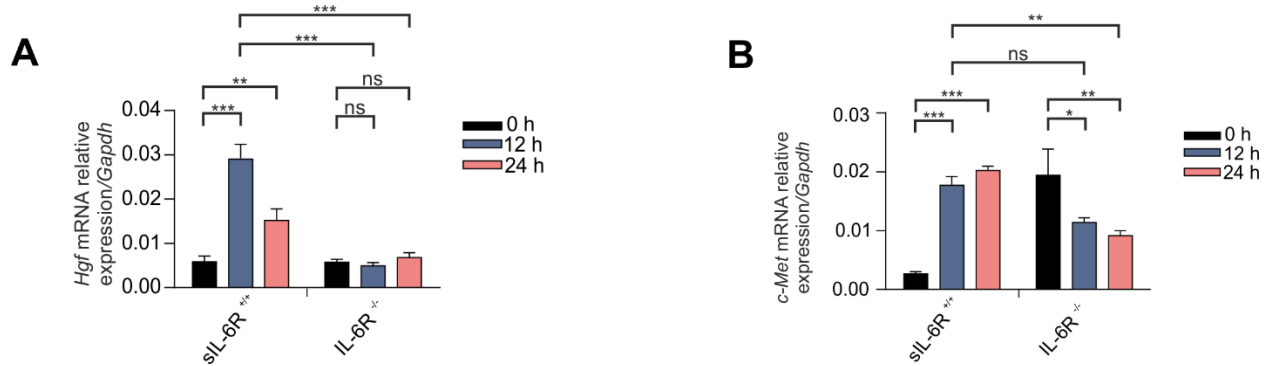


Fig. 31. Abrogated *Hgf/c-Met* expression in sIL-6R^{+/+} and IL-6R^{-/-} mice after 70% PHX

(A) Total RNA was extracted from liver tissues of sIL-6R^{+/+} and IL-6R^{-/-} mice 0, 12 h and 24 h after PHX. Subsequently, the RNA levels of *Hgf* were determined by quantitative RT-PCR (n = 5). Relevant significances are displayed, **p ≤ 0.01, ***p ≤ 0.001. (B) Total RNA was extracted from liver tissues of sIL-6R^{+/+} and IL-6R^{-/-} mice 0, 12 h and 24 h after PHX. Subsequently, the RNA levels of *c-Met* were determined by quantitative RT-PCR (n = 5). Relevant significances are displayed, *p ≤ 0.05, **p ≤ 0.01, ***p ≤ 0.001. Data are presented as the mean ± SEM. These figures were taken from *Fazel Modares, N., et al. J hepatology, 2019.*

Furthermore, we analyzed the production levels of HGF at the protein level. ELISA was performed. To this end, liver lysates were prepared from wt mice, wt mice treated with sgp130Fc, wt mice treated with IL-6 mAb, sIL-6R^{+/+} mice, and IL-6R^{-/-} mice.

Analysis of HGF protein levels showed an upregulation 12 h after PHX in wt mice. The expression of HGF gradually decreased until 24 h after PHX in wt mice. In contrast, levels of HGF were upregulated gradually from 0 h after the operation until 24 h after PHX and reached significance as early as 24 h after PHX in sIL-6R^{+/+} mice (Fig. 32)

A slight increase in HGF was detected 12 h postsurgery compared to the expression level observed directly after the surgery in treated mice with sgp130Fc. However, the pattern remained unchanged until 24 h after the operation upon blockade of IL-6 trans-signaling (Fig. 32).

HGF was slightly upregulated 12 h after PHX, however, did not reach its significance in comparison to the level observed directly after PHX in treated mice with IL-6 mAb. The expression level of HGF, 24 h after PHX was comparable to basal levels observed 0 h after PHX in treated mice with IL-6 mAb (Fig. 32).

In IL-6R^{-/-} mice, the production of HGF was comparable to the expression level observed 0 h after PHX. PHX did not induce the expression level of HGF in the absence of IL-6R.

Taken together, these results indicate that HGF was upregulated in the early phase of liver regeneration in wt mice. Similarly, sIL-6R^{+/+} also displayed an increased level in HGF expression. However, in mice with abrogated IL-6 signaling, PHX failed to induce the production of HGF in HSCs.

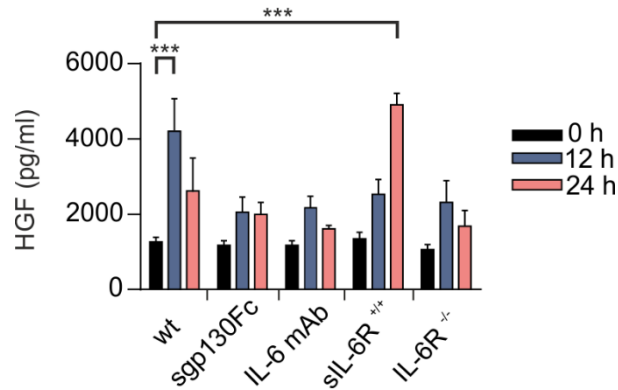


Fig. 32. Enhanced *HGF* production in sIL-6R^{+/+} mice after 70% PHX

Total HGF protein levels in liver lysates of wt mice, wt+sgp130Fc mice, wt+IL-6 mAb mice, sIL-6R^{+/+} mice, and IL-6R^{-/-} mice 0, 12 h and 24 h after PHX were determined by ELISA (n=5). Relevant significances are displayed, ***p ≤ 0.001. Data are presented as the mean ± SEM. This figure was taken from *Fazel Modares, N., et al. J hepatology, 2019.*

3.10 IL-6 Trans-signaling regulates *Hgf* production

The above results illustrated that IL-6 and its signaling might affect HSCs and, subsequently, HGF production. First, the expression of IL-6 and gp130 was assessed by RT-PCR and immune staining to confirm that IL-6 could trigger HSCs. To this end, freshly isolated rat HSCs were kept for one day in the culture. RNA was isolated, and RT-PCR was performed. mRNA expression of *IL-6R* and *gp130* was detected in total RNA of rat HSCs (Fig. 33A).

Furthermore, the expression of IL-6R was visualized by immunostaining. Freshly isolated HSCs were kept for one day in culture and fixed. HSCs were stained positively for IL-6R, as shown in Fig. 33B.

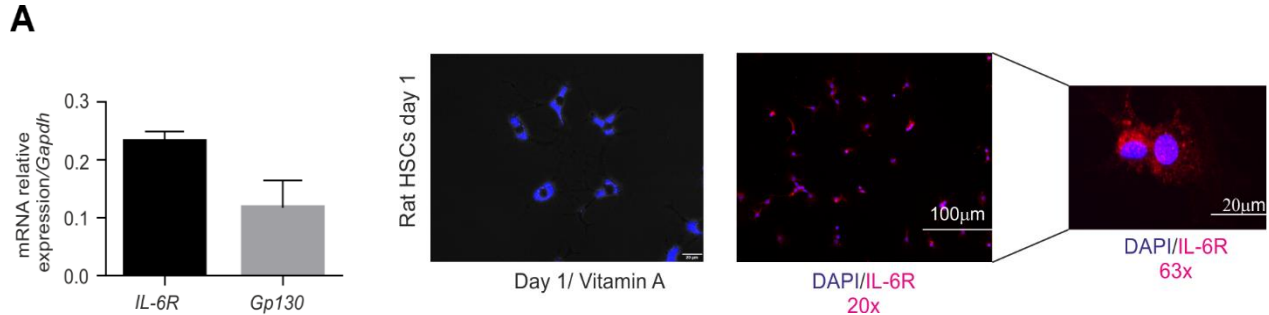


Fig. 33. Expression of *IL-6R* and *gp130* in hepatic stellate cells

(A) Total RNA was extracted from rat HSCs, and the mRNA levels of IL-6R and gp130 were determined by quantitative PCR (n=3). (B) Immunohistochemistry of IL-6R and DAPI in rat hepatic stellate cells. These figures were taken from *Fazel Modares, N., et al. J hepatology, 2019.*

Knowing that the IL-6R and gp130 were expressed on HSCs, HGF production was assessed by RT-PCR and ELISA. Therefore, HSCs were isolated and kept for one day in culture. Cells were stimulated with HIL-6 (100 ng/ml), IL-6 (100 ng/ml), and sgp130Fc (1 µg/ml) and left untreated for two days. At the end of the experiments, supernatants (sp) were collected, and the cells were harvested. RNA was extracted, and RT-PCR was first performed. As already mentioned, HIL-6 is a fusion protein consisting of IL-6 and sIL-6R that triggers IL-6 trans-signaling. Stimulation of HSCs with HIL-6 induced mRNA expression of *Hgf* two days after stimulation. However, stimulation with sgp130Fc did not completely abolish the mRNA expression of *Hgf* in rat HSCs. Interestingly, stimulation with IL-6 also did not result in the induction of *Hgf* mRNA expression. Notably, the observed expression level of HGF after treatment with HIL-6 and sgp130Fc was comparable to the expression observed in control cells (Fig. 34). This observation illustrates that IL-6 trans-signaling could affect the expression of HGF in HSCs.

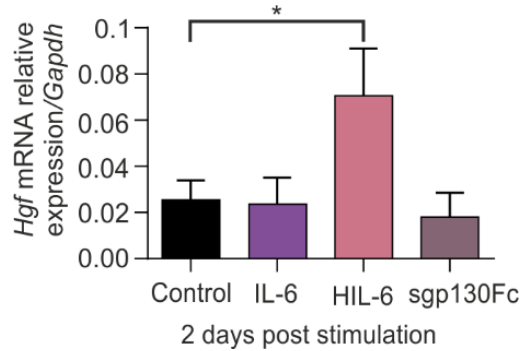


Fig. 34. Enhanced *Hgf* mRNA expression in hepatic stellate cells through IL-6 Trans-signaling

Rat HSCs were stimulated for 48 h with IL-6 (100 ng/ml), Hyper IL-6 (100 ng/ml) or sgp130Fc (1 µg/ml). Total RNA was extracted from rat HSCs, and the mRNA level of *Hgf* was determined by quantitative PCR (n=7). Relevant significances are displayed * $p \leq 0.05$. Data are presented as the mean \pm S.E.M. These figures were taken from *Fazel Modares, N., et al. J hepatology, 2019.*

Knowing that HGF expression levels increased after stimulation of IL-6 trans-signaling by HIL-6, HGF protein levels were measured by ELISA. As before, cells were stimulated under similar conditions with HIL-6 (100 ng/ml), IL-6 (100 ng/ml), and sgp130Fc (1 µg/ml) and those left untreated for two days. Cells were harvested, and lysates were prepared. ELISA was performed. In the lysate of treated HSCs with HIL-6, HGF expression was enhanced, which was consistent with higher expression at the mRNA level. However, stimulation with IL-6 did not induce the production of HGF in cell lysates of HSCs. Moreover, using sgp130Fc was used as an internal control and as expected did not affect the production of HGF in HSCs (Fig. 35).

This observation confirmed the expression pattern of HGF on the mRNA levels and confirmed that IL-6 trans-signaling induced HGF synthesis in HSCs.

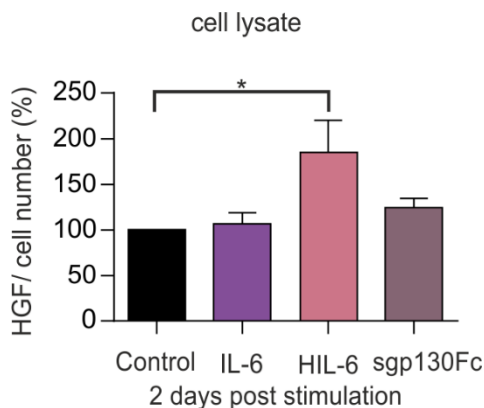


Fig. 35. Enhanced HGF production in hepatic stellate cells through IL-6 Trans-signaling

Total HGF protein in lysates of rat HSCs stimulated for 48 h with IL-6, Hyper IL-6 or sgp130Fc was determined by ELISA (n= 4). Relevant significances are displayed * $p \leq 0.05$. Data are presented as the mean \pm SEM. These figures were taken from *Fazel Modares, N., et al. J hepatology, 2019.*

Furthermore, ELISA was performed to analyze the release of HGF after stimulation. In keeping with previous findings, HSCs were stimulated with HIL-6 (100 ng/ml), IL-6 (100 ng/ml), and sgp130Fc (1 µg/ml) or left untreated. At the end of the experiment, supernatant was collected, and ELISA was performed.

In supernatants of cells treated with HIL-6, no increase of HGF was detected, and the HGF level was comparable to the level observed in the control group (Fig. 36).

However, a slight increase was observed after treatment with IL-6 alone, which did not reach significance (Fig. 36).

Concerning sgp130Fc, no affect was observed in the expression of HGF in collected sp. And a comparable amount of HGF was observed in the supernatants compared to the untreated group (Fig. 36).

Taken together, the results of this study indicated that exogenous induction of IL-6 trans-signaling might increase the synthesis of HGF in HSCs. However, we did not observe a significant reduction in its level upon stimulation with sgp130Fc. These observations demonstrate that HSC might need further factors to release induced HGF (Fig. 36).

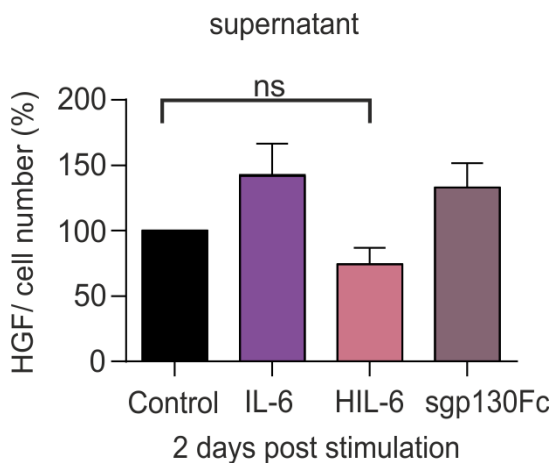


Fig. 36. No induction of HGF release from hepatic stellate cells through IL-6 trans-signaling

Total HGF protein in cell culture supernatants of rat HSCs stimulated for 48 h with IL-6, Hyper IL-6 or sgp130Fc was determined by ELISA (n = 3). Relevant significances are displayed * $p \leq 0.05$. Data are displayed as the mean \pm SEM. These figures were taken from *Fazel Modares, N., et al. J hepatology, 2019.*

4 Discussion

IL-6 belongs to the IL-6 cytokine family. IL-6 targets cells through two pathways: classic and trans-signaling. In classic signaling, IL-6 binds to IL-6R and mediates homodimerization of gp130. IL-6R expression is restricted to a few cell types, including macrophages, neutrophils, and hepatocytes [4]. Therefore, classic IL-6 signaling causes limited activation of cells. Another signaling pathway of IL-6 is known as IL-6 trans-signaling. In trans-signaling, IL-6 binds to the soluble form of IL-6R, resulting in homodimerization of gp130. Gp130 is ubiquitously expressed on target cells. Therefore, IL-6, through trans-signaling, has a broad spectrum of target cells in the body. In humans, sIL-6R is generated through mRNA splicing or ectodomain shedding via ADAM proteases, primarily mediated by ADAM17 and ADAM10 [192]. In mice, the production of IL-6R is different, and the soluble form of IL-6R is generated only by ectodomain shedding by ADAM 10 and 17 [193]. IL-6 is involved in both anti-inflammatory and inflammatory responses. IL-6 trans-signaling is associated with various autoimmune diseases, such as RA. In contrast, it has been shown that classic signaling of IL-6 promotes homeostatic and regenerative processes in liver, brain, heart, and bone marrow [31].

As the largest organ in the body, the liver has essential biological functions, such as detoxification, protein synthesis, and metabolism [194]. Since the liver is in direct contact with various nutrients, including toxic substances, the risk of injury is also high. However, the liver has a remarkable capacity to regenerate upon damage and its original size could be restored [148, 164]. Liver fibrosis is a chronic liver injury resulting from accumulation of ECM proteins, which is characteristic of most chronic liver diseases [195, 196]. By persistent hepatic damage and progression of fibrosis, liver becomes cirrhotic. Cirrhosis is mostly accompanied by loss of function and hepatocellular death which results in some cases into hepatocellular carcinoma [197, 198]. A better understanding of liver regeneration process and liver physiology are essential to improve medical interventions to treat patients diagnosed with an advanced stage of liver disease.

Partial hepatectomy (PHX) was described as a preclinical model in rodents to understand the underlying mechanisms that contribute to the regeneration of the liver [155, 199].

Importantly, it has been shown that IL-6 plays a vital role in liver regeneration [57, 122]. IL-6 in the liver promotes three main functions. First, IL-6 promotes the production of acute-phase proteins [168]. Second, IL-6 promotes hepatocyte proliferation [174]. Third, IL-6 reduces cell

death and protects the liver. Subjecting IL-6 deficient mice to 70% PHX resulted in lower survival and less DNA synthesis [41, 169]. Consistent with this finding, it was also shown that exogenous induction of IL-6 improved the outcome after PHX [169]. It has been demonstrated that PHX could induce expression levels of IL-6 and IL-6R [174, 200, 201]. Based on the vital role of IL-6 in liver regeneration, the question arises of which IL-6 signaling (trans-signaling or classic signaling) is needed for liver regeneration upon injury. To date, no clear answer to this question has been obtained. To answer this question, a model with only IL-6 trans-signaling is required. A model with a hyperactive ADAM protease could fail because ADAM protease activity not only results in ectodomain shedding of IL-6R but also TNF, EGFR-ligand, and Notch cleavage. Therefore, as a mouse model with ADAM hyperactivity is associated with different signaling pathways. In the current study, we aimed to investigate the role of IL-6 trans-signaling in liver regeneration by a novel mouse model in which all the membrane-bound IL-6R was genetically converted to the soluble form of IL-6R through Cre-deletion. Therefore, in these mice, IL-6 only initiates the signal through trans-signaling in target cells.

4.1 Generation of IL-6 trans-signaling mice

The genetic modification was performed on the original reading frame of IL-6R to induce expression of sIL-6R transcriptionally in these mice. On the original gene structure of IL-6R, exon 9 encodes the transmembrane and intracellular domain, and exon 10 encodes the last part of the intracellular domain. In transgenic mice, exon 9 and exon 10 were fused. Additionally, the 2A-peptide GFP cassette was fused and replaced with the stop codon, which is in exon 10 in the original frame of the IL-6R gene. First, PCR data confirmed that exon 9 and exon 10 were deleted in the generated mice (Fig. 8). The detection of GFP protein in the liver and spleen lysates of sIL-6R^{fl/fl} mice demonstrated that the modified sequence was correctly inserted in sIL-6R^{fl/fl} mice (Fig. 5). Furthermore, the absence of GFP protein in the liver and spleen lysate confirmed that the E9-E10c-GFP-E10u cassette was successfully deleted from the modified IL-6R gene in sIL-6R^{+/+} mice (Fig. 5).

Furthermore, analysis of the IL-6R mRNA expression levels and the production of IL-6R protein illustrated that genetic modification of IL-6R did not influence the overall expression of IL-6R (Fig. 7). Next, to examine whether classic IL-6 signaling was inactive and that cells were targeted only through trans-signaling, the expression of membrane-bound IL-6R was analyzed in

monocytes and CD3-positive T cells that express membrane-bound IL-6R. In sIL-6R^{+/+} mice, a significant reduction of IL-6R was observed compared to sIL-6R^{fl/fl} and wild-type mice. However, the levels of IL-6R were comparable to the levels observed in the IL-6R^{-/-} control group. Therefore, membrane-bound IL-6R was not expressed in sIL-6R^{+/+}, confirming the absence of IL-6 classic signaling through complete deletion of IL-6R [201]. To further confirm the expression of IL-6R, membrane-bound IL-6R was visualized on liver sections. The lack of IL-6R-expressing cells on the liver section of sIL-6R^{+/+} mice illustrated that all transmembrane-bound IL-6R were converted to the soluble form of IL-6R. Using IL-6R-deficient mice as a negative control, we demonstrated that the observed signal for IL-6R was specific, since no IL-6R-expressing cells were observed in IL-6R^{-/-} mice (Fig. 6).

Interestingly, the expression of IL-6R was higher compared to wt mice confirmed by RT-PCR, which correlated with higher amounts of sIL-6R in the serum of sIL-6R^{+/+} mice under steady-state conditions (Fig. 9A). It was shown that small noncoding RNAs, known as microRNAs, target the expression of genes such as IL-6R. By binding to the complementary sequences of the mRNA of the target gene, these microRNAs negatively control the gene expression at the posttranscriptional level [202]. In this study, the IL-6R genetic modification was accompanied by partial deletion of the 3'UTR in sIL-6R^{+/+} mice. An explanation for the enhanced expression of IL-6R in sIL-6R^{+/+} mice might be the deletion of the 3'UTR on the modified IL-6R gene in sIL-6R^{+/+} mice. Concerning IL-6R, it has been shown that miR-590-5p and miR-21 target the 3'UTR of IL-6R and negatively regulate the expression of IL-6R [203, 204]. Lack of the 3'UTR on the modified IL-6R gene may interfere with regulatory microRNAs, such as miR-590-5p and miR-21. Thus, upregulation of IL-6R supported the hypothesis that the absence of the 3'UTR results in IL-6R mRNA stability, leading to significant expression of IL-6R protein in sIL-6R^{+/+} mice. Further investigation is needed to understand which potential microRNAs precisely regulate IL-6R expression (the binding sites of microRNAs to the E10-3'UTR of IL-6R gene is shown at the end section 4.10).

4.2 sIL-6R in sIL-6R^{+/+} mice targets the cells through trans-signaling

Are the enhanced levels of sIL-6R biologically active in sIL-6R^{+/+} mice?

To answer this question, sIL-6R^{+/+} mice were injected with recombinant IL-6. STAT3 phosphorylation was monitored in the liver, lung, and colon. Injection with IL-6 resulted in enhanced STAT3 phosphorylation (Fig 10 -12). In the liver, lung, and colon of sIL-6R^{+/+} mice, IL-6 was able to target the cells through IL-6 trans-signaling, resulting in enhanced STAT3 phosphorylation. IL-6 is an important stimulatory factor that produces acute-phase proteins [168]. As a response to exogenous induction of IL-6, the production of acute-phase proteins was assessed in sIL-6R^{+/+} and compared to wt mice. mRNA expression levels of *Saa* after injection with IL-6 showed that IL-6 through trans-signaling could induce the production of *Saa* in sIL-6R^{+/+} mice compared to the level observed in wt mice, in which classic signaling and trans-signaling were active (Fig. 13). These data suggest that IL-6 trans-signaling compensates for the lack of classic signaling in sIL-6R^{+/+} mice.

The level of sIL-6R is 11 ng/ml in wt mice; however, under the pathophysiological situations, it can rise to 2- or 3-fold [205]. It has been reported that sIL-6R in the serum mainly originates from neutrophils/macrophages and hepatocytes, illustrating that these cells are also significant producers of membrane-bound IL-6R [181]. However, in the present study, analysis of IL-6R expression in mice with deletion of IL-6R on hepatocytes or neutrophils/macrophages, namely, sIL-6R^{+/+} Alb Cre⁺ and sIL-6R^{+/+} LysM Cre⁺, revealed that only 70.8% of circulating sIL-6R amounts originated from these cells, and the remaining 29.2% originated from different sources (Fig. 9B).

Our data showed that hepatocytes and neutrophils/macrophages produce less membrane-bound IL-6R, contradicting the hypothesis that these cells could be the main source of membrane-bound IL-6R. It has been shown that ADAM activities are upregulated during apoptosis, resulting in more ectodomain shedding of IL-6R such that neutrophils release higher amounts of sIL-6R before undergoing apoptosis [192]. Therefore, these cells might release more elevated amounts of sIL-6R compared to other cells, which also express membrane-bound IL-6R. In mice using different IL-

6R Cre in a specific cell might help to further investigate the contribution of each cell to the total amounts of membrane-bound IL-6R.

4.3 Liver regeneration was normal in sIL-6R^{+/+} mice

Knowing that sIL-6R is biologically active and that trans-signaling is the only pathway by which IL-6 could target the cells, the question arose of whether upregulated IL-6 after PHX could promote liver regeneration through IL-6 trans-signaling in sIL-6R^{+/+} mice.

To this end, sIL-6R^{+/+} mice were subjected to 70% PHX. Based on reported studies, wt mice subjected to 70% showed 70% to 100% survival [206, 207]. A similar observation was obtained by subjecting wt mice to PHX in the current study (Fig. 14).

Interestingly, sIL-6R^{+/+} mice showed an 80% survival rate after PHX, which was comparable to the survival rate observed in wt mice (Fig 14). A higher survival rate was accompanied by an increase in the amounts of circulating sIL-6R after PHX in the serum of wt mice and sIL-6R^{+/+} mice, respectively. In wt mice, levels of sIL-6R increased from 11 ng/ml to 15 ng/ml, which was previously reported [174] (Fig. 18A). Concerning sIL-6R^{+/+} mice, the basal level of sIL-6R detected in sIL-6R^{+/+} mice under steady-state conditions was 363 ng/ml. Interestingly, PHX induced the level of sIL-6R in the serum of partially hepatectomized mice to be 1600 ng/ml as early as 12 h after PHX and 620 ng/ml 24 h after PHX (Fig. 18C). The transcriptional expression of IL-6R in its soluble form might explain the early peak observed in the expression of IL-6 in sIL-6R^{+/+} mice. However, a peak for sIL-6R was observed with a slight delay in wt and only 24 h post-PHX in wt mice (Fig 18A). In wt mice, IL-6R is first expressed in the trans-membrane form, and on the protein level, ectodomain shedding occurs, which might explain the delay in enhanced expression of sIL-6R in wt mice. Therefore, the kinetics of ADAM activity after PHX by IF or ELISA might be matched to the dynamics of sIL-6R observed after PHX.

To confirm that IL-6R is expressed in its soluble form, the mRNA expression levels of IL-6R were also measured. The obtained data illustrated a gradual increase for *Il-6R* during PHX in sIL-6R^{+/+} mice as compared to wt, confirming the higher amount of IL-6R detected on the protein levels after PHX. In the spleens of sIL-6R^{+/+} mice, IL-6R was upregulated as early as 24 h post-PHX (Fig 19A-B). It has been shown that the proliferation of pro-inflammatory macrophages, which abundantly express membrane-bound IL-6R, is promoted by classic IL-6 signaling and not IL-6

trans-signaling in nephrotoxic nephritis (NTN) [208]. Therefore, it is possible that in the lack of IL-6 classic signaling, the proliferation of pro-inflammatory macrophages was delayed; thus, decreased expression was observed after PHX in the spleen of sIL-6R^{+/+} mice

4.4 IL-6 trans-signaling initiated JAK/STAT signaling in target cells

In the current study, the obtained data suggested a clear correlation between IL-6 trans-signaling and liver regeneration after PHX. It has been shown that IL-6 activated STAT3 signaling during liver regeneration [207]. In this study, the analysis of IL-6 trans-signaling activation was assessed by monitoring STAT3 phosphorylation. Upon PHX, the detected levels of STAT3 phosphorylation significantly increased at the early stage after PHX in sIL-6R^{+/+} mice, which was similar to the pattern observed in wt mice (Fig 20A-B). Consistently, it was reported that STAT3 DNA binding was induced after PHX. Higher STAT3 phosphorylation and DNA-binding resulted in the upregulation of target genes involved in the cell cycle, such as *c-myc* and *c-fos*, and subsequently, hepatocyte proliferation was induced [207, 209]. Therefore, in the current study, proliferating cell nuclear antigen (PCNA) was monitored in mice that were subjected to PHX. In sIL-6R^{+/+} mice, more cells were marked positively for PCNA, which indicates that more cells were entered into the G1 phase of the cell cycle (Fig 22A-B). Prospectively, global transcriptional profiling might help to identify which genes are upregulated in sIL-6R^{+/+} after PHX, resulting in higher proliferation.

4.5 IL-6 trans-signaling results in enhanced HGF production by HSCs after PHX

Liver regeneration is a complicated process in which different cells and signals collaborate to orchestrate the regeneration of the liver. In addition to the contribution of IL-6 to hepatocyte proliferation, growth factors, including hepatocyte growth factor (HGF) [210, 211], also play an essential role in hepatocytes proliferation, which is released by non-parenchymal cell in the liver mainly HSCs [212]. HSCs are in a quiescent state under normal conditions [109, 213]. However, liver damage activates HSCs. Activated HSCs express extracellular matrix and temporarily scarce tissue on the side of injury, which prevents the progression of injury [109].

A positive correlation between HGF and IL-6 was suggested by Kariv et al., who stimulated immortalizing cells with IL-6, and triiodothyronine resulted in HGF upregulation 48 h post-stimulation [214]. Another study showed that treatment with HIL-6 and HGF together, but not IL-6, could enhance hepatocyte proliferation after PHX [174].

In light of these findings, HGF expression was analyzed at the mRNA and protein levels after PHX. The obtained data suggest that IL-6 induces the production of HGF in HSCs through trans-signaling (Fig 32A). This observation drove the hypothesis that IL-6, through trans-signaling via STAT3 signaling, stimulates HSCs to produce more HGF after PHX. However, the cross-talk between IL-6 and PI3K activity, which resulted in hepatocyte proliferation in the presence of HIL-6 and HGF, was reported in wt mice [174]. To further investigate whether a cross-talk between JAK/STAT and PI3K could result in upregulation of HGF in sIL-6R^{+/+}, activation of PI3K signaling might be assessed by Western blotting.

In summary, the current study proposed a model in which IL-6 trans-signaling promotes liver regeneration in the lack of IL-6 classic signaling [201]. In detail, upon PHX, Kupffer cells are stimulated and produce higher amounts of IL-6 [162, 163, 215]. At the same time, sIL-6R expression is increased [201]. IL-6 binds to sIL-6R and initiates the signal through IL-6 trans-signaling [28]. On the other hand, upregulation of sIL-6R and IL-6 also might result in homodimerization of gp130 expressed on HSCs. As a result, the production of HGF is enhanced through JAK/STAT in sIL-6R^{+/+} mice after PHX. Enhanced HGF from one side and enhanced STAT activation results in the upregulation of genes responsible for the synthesis of acute-phase proteins, antiapoptotic genes (Bcl), and genes involved in regulating the cell cycle, such as c-myc and cyclins [216](Fig. 37).

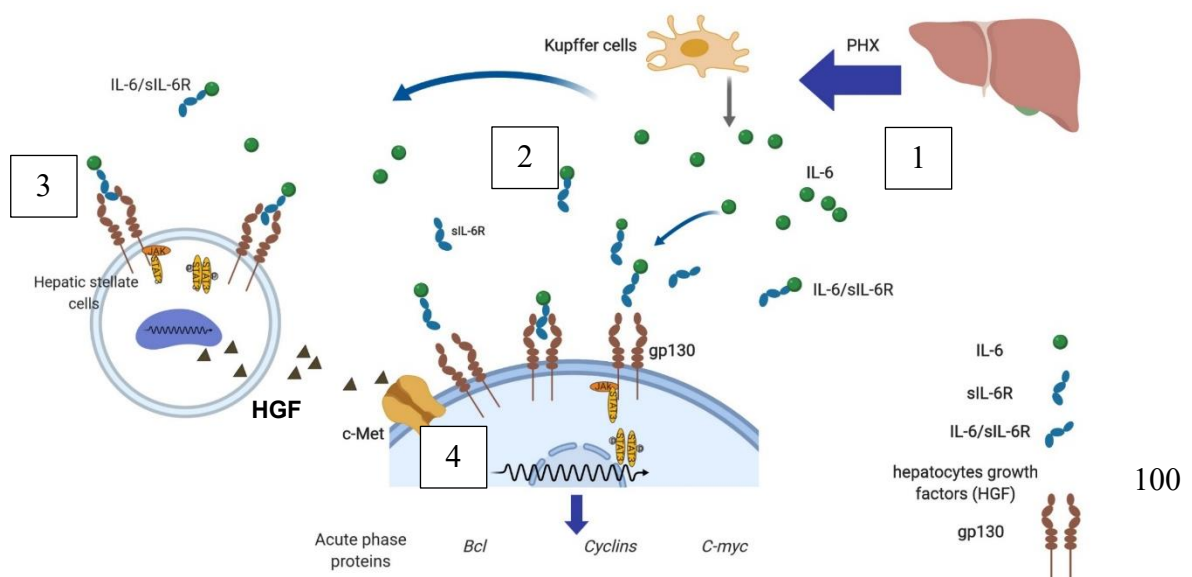


Fig. 37. Proposed model for IL-6 trans-signaling in liver regeneration after PHX

1) PHX induces the expression of IL-6 by stimulating macrophages. 2) IL-6 (in green), in complex with sIL-6R (in dark blue), interacts with expressed gp130 (in brown) on hepatocytes. 3) On the other hand, IL-6 (in green) binds to sIL-6R and interacts with expressed gp130 (brown) on HSCs. Subsequently, through the initiation of JAK/STAT, HGF expression and production were enhanced. 4) Finally, the production of HGF through c-Met and STAT3 phosphorylation in hepatocytes results in the upregulation of cyclins, acute phase proteins, Bcl and c-myc, which promotes hepatocytes to enter the cell cycle leading to liver regeneration [216]. Figure adopted from Nechemia et al. [174].

4.6 Abrogated liver regeneration upon blockade of IL-6 trans-signaling by sgp130Fc

To further investigate the decisive role of IL-6 trans-signaling in liver regeneration, IL-6 trans-signaling was inhibited by using a specific inhibitor, sgp130Fc. Previously, the sgp130Fc expression plasmid was injected into wt mice by hydrodynamic injection, which resulted in less DNA synthesis after PHX [174]. At the same time, using sgp130Fc enabled us to specifically block IL-6 trans-signaling [30]. Injected mice with 50 μ g of sgp130Fc were subjected to 70% PHX. The 20% survival rate after PHX coincided with less STAT3 phosphorylation, resulting in fewer proliferation rate after blockade of IL-6 trans-signaling. Fewer cell proliferation led to impaired liver regeneration after PHX in treated mice with sgp130Fc. In agreement with a previous report by Nechemia et al., we confirmed that IL-6 trans-signaling plays a vital role in liver regeneration after PHX [201].

The dosage of sgp130Fc was chosen according to a previous report, where five different dosages of sgp130Fc, including 0.01, 0.1, 0.5, 1, and 10 mg/kg, were tested in a murine CLP sepsis model [217]. Barkhausen et al. demonstrated that a moderate dosage of sgp130Fc (0.5-1 mg/kg) resulted in the survival of mice [217]. In contrast, either overly low (0.1, 0.01) or overly high doses of sgp130Fc (10 mg/ml) did not result in any alteration in the outcome [217]. These results suggested that an effective dose for sgp130Fc to block only trans-signaling should be in the range of 0.5-1

mg/kg. Therefore, in the present study, a low dose of sgp130Fc 50 $\mu\text{g}/\text{mouse}$ was applied to minimize the cross-inhibition of classic signaling.

To further investigate the effect of a lower dose of sgp130Fc on liver regeneration, mice were treated (10 $\mu\text{g}/\text{mouse}$ every two days) and subjected to PHX (Fig. 35). The low dose of sgp130Fc did not impair liver regeneration, and these mice survived after PHX, which is in consistent with the previous study from Barkhausen et al., where they demonstrated that low doses of sgp130Fc is not sufficient to block IL-6 trans-signaling [217]. Therefore, the effective dose of sgp130Fc to inhibit trans-signaling was 50 $\mu\text{g}/\text{mouse}$ in the current study [201].

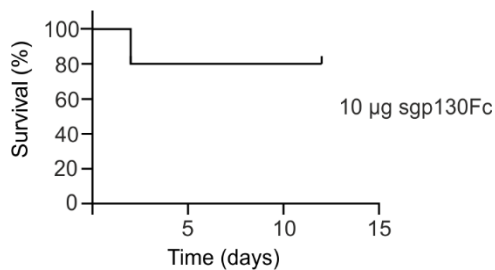


Fig 38. The low dose of sgp130Fc did not interfere with liver regeneration

Wt mice were injected with sgp130Fc 10 $\mu\text{g}/\text{mouse}$ every two days, subjected to 70% PHX. Every two days injection was repeated. Mice were monitored until the end of the experiment.

Furthermore, to confirm the effect of IL-6 trans-signaling blockade on HGF production, analysis of HGF levels sgp130Fc was measured by ELISA and RT-PCR. The analysis showed that HGF amounts were significantly reduced after blockade of IL-6 trans-signaling (Fig 30A-B).

Based on the results obtained in this study, a model was proposed for IL-6 trans-signaling in liver regeneration after PHX in wt mice by IL-6 trans-signaling blockade via sgp130Fc. In detail upon PHX, Kupffer cells are stimulated and produce higher amounts of IL-6 [162, 215]. At the same time, the generation of sIL-6R occurs by ADAM proteases [192]. IL-6 binds to sIL-6R. sgp130Fc traps the complex of IL-6/sIL-6R and inhibits trans-signaling in hepatocytes and HSCs [81]. This result in less STAT3 phosphorylation, resulting in less HGF and proliferating cells leading to abrogated liver regeneration (Fig. 39).

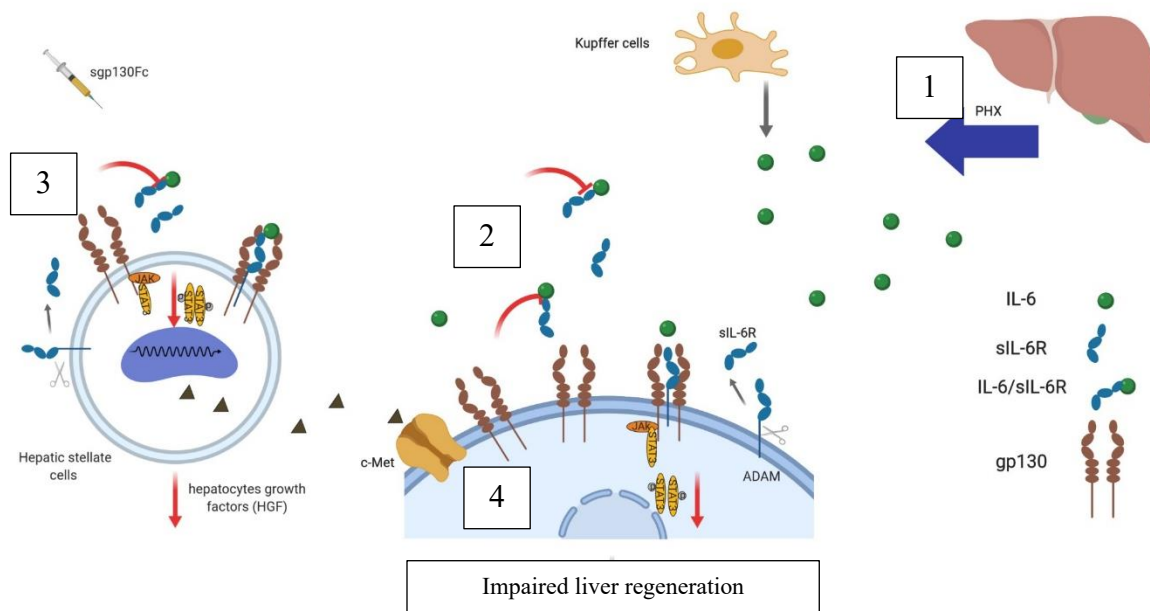


Fig. 39. Proposed model for IL-6 trans-signaling blockade in liver regeneration after PHX by sgp130Fc

1) PHX induces the expression of IL-6 by stimulating macrophages. 2) IL-6 (in green) binds to the sIL-6R (in dark blue). The complex is trapped with sgp130Fc. The binding of IL-6/sIL-6R with gp130 (brown) on hepatocytes is hampered, resulting in less STAT3 phosphorylation. 3) On the other hand, IL-6 (in green) binds to sIL-6R. The complex of IL-6/sIL-6R is trapped with sgp130Fc, resulting in hampered trans-signaling in HSCs and less HGF production. 4) Finally, less production of HGF and less STAT3 phosphorylation resulted in abrogated hepatocyte proliferation, which led to impaired liver regeneration in these mice. from Nechemia et al. [174]

4.7 Blockade of IL-6 classic and trans-signaling results in impaired liver regeneration

To further investigate the role of IL-6 in liver regeneration, IL-6 classic and trans-signaling was blocked by IL-6 mAb. Mice were injected with 250 μ g IL-6 mAb/mouse (6.25 mg IL-6 mAb/kg) and subjected to 70% PHX. Blockade of IL-6 signaling resulted in 10% survival after PHX. Ten percent of survival was accompanied by abrogated STAT3 phosphorylation. Continuously proliferating cells were monitored after PHX on the liver sections of these mice. Less STAT3

phosphorylation also resulted in less proliferation of cells leading to impaired liver regeneration after PHX, which was consistent with observed outcome in IL-6-deficient mice after PHX [41].

Furthermore, the impact of IL-6 blockade on HGF production by HSCs was analyzed. Therefore, HGF levels were measured by RT-PCR and ELISA after PHX. The obtained results demonstrated that the level of HGF was significantly decreased at the protein level, as well as at the mRNA level, after blockade of IL-6 classic and trans-signaling in these mice (Fig. 30-32).

Based on the data obtained in this study, the proposed model is presented as Figure 40. After PHX, Kupffer cells are stimulated and produce higher amounts of IL-6 [162, 215]. At the same time, IL-6 mAb neutralizes expressed IL-6. By neutralizing IL-6, all IL-6 signaling is enabled. This effect results in a significant reduction of STAT3 phosphorylation, with reduced HGF production by HSCs leading to decreased cell proliferation and regeneration.

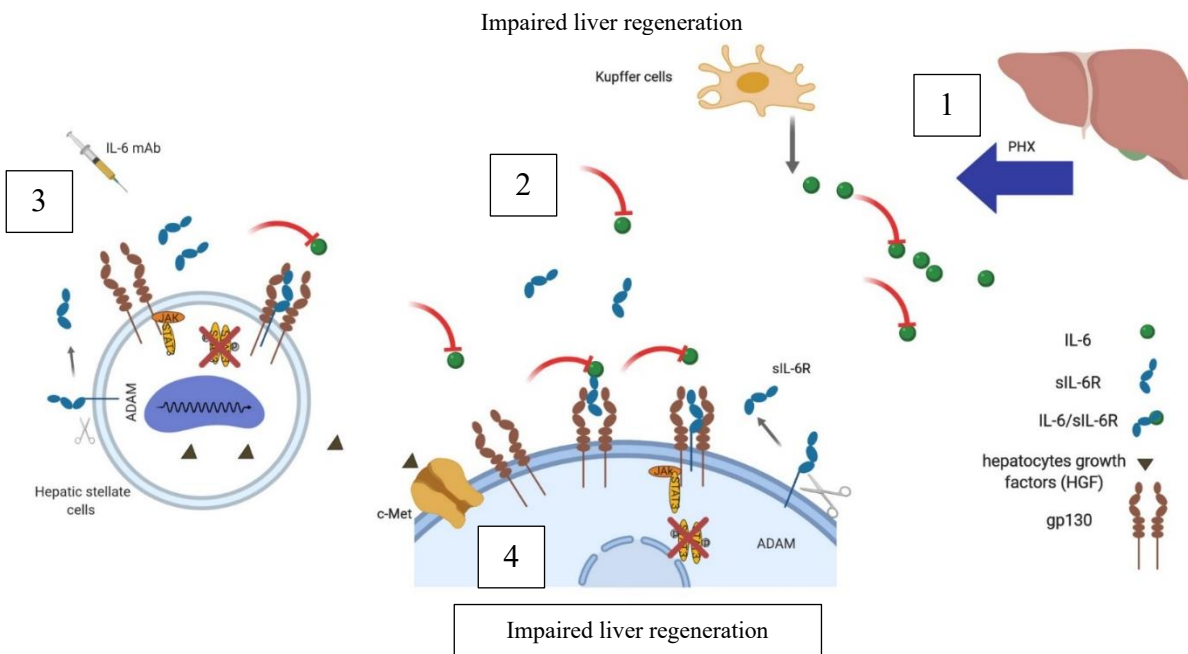


Fig. 40. A model for blockade of IL-6 signaling by IL-6 mAb in liver regeneration after PHX

1) PHX induces the expression of IL-6 by stimulating macrophages. 2) IL-6 mAb neutralizes IL-6 (in green) and inhibits the binding of IL-6 to IL-6R (in dark blue) or sIL-6R (in dark blue), resulting in blockade of both IL-6 signaling (classic and trans-signaling). 3) On the other hand, IL-6 signaling is also inhibited on HSCs, resulting in less production of HGF. 4) Finally, reduced production of HGF and abrogated STAT3 phosphorylation resulted in abrogated hepatocyte

proliferation, which led to impaired regeneration process in these mice. Figure adopted from Nechemia et al. [174]

4.8 The absence of IL-6R results in impede liver regeneration after PHX

To date, only IL-6-deficient mice but not IL-6R-deficient mice have been used in liver regeneration models, such as PHX [41]. In the current study, IL-6R-deficient mice were subjected to PHX, and liver regeneration was analyzed. Interestingly, only 10% of IL-6R^{-/-} mice survived (Fig. 14).

To further investigate the underlying mechanism, which resulted in 90% death after PHX, IL-6-mediated STAT3 signaling was evaluated. The obtained data showed that the amount of STAT3 phosphorylated cells was significantly reduced after PHX (Fig. 20-21).

Subsequently, the proliferation of liver cells was analyzed by IF. Observations showed a significant decrease in the number of PCNA-positive cells after PHX in the absence of IL-6R, which resulted in impaired liver regeneration in these mice (Fig 22).

Previous reports showed that IL-6R-deficient mice in opposite to IL-6^{-/-} mice did not show delay in the wound-healing model as compared to IL-6 deficient mice, and the outcome was comparable to wt mice [181]. The reason might be that other family members of the IL-6 cytokine family, such as CNTF, could bind to IL-6R and compensate for the lack of IL-6R [181]. In another study where colitis was induced by dextran sodium sulfate (DSS), IL-6R^{-/-} mice did not show any severe phenotype compared to IL-6-deficient mice [218]. In contrast, the role of IL-6/IL-6R in liver regeneration was studied by M. Xu et al. in 2015 [219]. Liver is the main source of Lipocalin-2 (LCN2), an acute phase response protein, which is highly upregulated in the setting of injury, infection [220, 221]. It has been shown that LCN2 has antibacterial function by suppressing bacterial growth [222-224]. M. Xu et al. in 2015 demonstrated that impaired IL-6 signaling led to lower production of LCN2 after PHX which was confirmed by subjecting hepatocytes-specific IL-6R deficient mice to 70% PHX [219]. Lower amount of LCN2 resulted to higher bacterial translocation to the MLNs upon PHX [219, 225]. Current study suggested a vital role for the presence of IL-6R during liver regeneration after PHX [201].

Furthermore, the correlation between impaired IL-6 signaling and HGF expression was analyzed. Expression analysis and ELISA results illustrated that in the absence of IL-6R and impaired IL-6

signaling, production of HGF was abrogated, resulting in a significant reduction in protein levels, as well as mRNA expression levels, after PHX (Fig 31-32).

Among the IL-6 cytokine family, similarities between IL-11 and IL-6 were previously reviewed by Garbers et al. IL-11 could stimulate the cells in a similar way as IL-6. IL-11 can bind to IL-11R, resulting in homodimerization of gp130 expressed on target cells [226]. The similarity between IL-6 and IL-11 raises the question of whether IL-11/IL-11R might promote liver regeneration in the absence of IL-6R. To further investigate whether IL-11 signaling could be induced exogenously and subsequent events after PHX could be analyzed. The obtained data demonstrated that blockade of IL-6 trans-signaling or blockade of both IL-6 signaling results in impaired liver regeneration after PHX.

4.9 IL-6 trans-signaling promotes HGF production in rat HSCs

We have shown that IL-6-targeted HSCs resulted in the upregulation of HGF after PHX. Similarly, impaired IL-6 was consistent with abrogated HGF production. The positive correlation between IL-6 signaling and HGF was suggested *in vivo* by the data obtained from this study [201].

The question raised in this study was whether HSCs express IL-6 compartments, including IL-6R and gp130. Therefore, for further investigation, rat HSCs were isolated and cultured. RNA was isolated from cultured HSCs, and the data showed that *Il-6R* and *gp130* were expressed in HSCs (Fig 33A).

Moreover, the expression of IL-6R was assessed by immunohistochemistry. Freshly isolated HSCs were maintained for one day in culture and then fixed. IF staining results showed that IL-6R was expressed in HSCs, and further investigation with confocal microscopy might help to visualize the localization of IL-6R in HSCs (Fig 33B).

Furthermore, to examine whether IL-6 trans-signaling could also upregulate HGF *in vitro*, HSCs were stimulated with HIL-6, IL-6, and sgp130Fc. Stimulation with HIL-6 but not IL-6 alone resulted in the upregulation of *Hgf* mRNA levels. To further investigate this phenomenon, the amounts of HGF produced in lysates of HSCs were measured. Interestingly, the amounts of HGF were enhanced after stimulation with HIL-6 in lysates of HSCs, confirming that IL-6 trans-signaling stimulates HSCs to produce more HGFs. Moreover, the amount of HGF released into the culture medium was measured by ELISA. The amount of HGF did not differ after stimulation with HIL-6 or IL-6 and sgp130Fc in the supernatant poststimulation. However, sgp130Fc used in this *in vitro* setup served as an internal control. Sgp130Fc alone has no affinity toward IL-6 or sIL-6R; therefore, proper costimulation with sgp130Fc and HIL-6 might be needed for further investigation.

The different outcome observed poststimulation drove the hypothesis that IL-6 trans-signaling could induce the synthesis of HGF in HSCs; however, to release the synthesized HGF, altered signaling might be needed. For example, during PHX, by removing 2/3 of the liver, the original amounts of blood have to circulate in smaller space in the liver, resulting in stretched cells and veins, which might result in increased HGF release [227]. However, in the *in vitro* setup, the absence of mechanical factors might result in a different kinetic of HGF release.

On the other hand, it has been shown that hepatocyte exosomes might be needed for intracellular communication among resident cells in the liver [228]. In this *in vitro* setup, the hepatocytes and factors that are released from hepatocytes are lacking. Therefore, coculture system and the presence of hepatocytes in the culture might correct the outcome.

4.10 Clinical relevance of the presented work in the context of liver regeneration

Yearly, liver cirrhosis causes 1 million deaths and liver hepatitis, and HCC results in 1 million deaths per year [229]. Liver cirrhosis and liver cancer currently rank 11th and 16th among causes of death worldwide, respectively, accompanied by 3.5% of all deaths worldwide [230]. As a clinical intervention, liver transplantation was established to rescue patients diagnosed with HCC [198]. High-risk donors, a limited number of donors, and rapid tumor growth before undergoing transplantation are some of the reasons that cause patients to drop out of the liver-transplant waiting list [231].

Therefore, as an alternative therapeutic intervention, liver resection was established. Liver resection retains a vital role in the therapeutic strategy of HCC in patients with an adequate liver function [232]. It has been reported that patients with early cirrhosis accompanied by normal liver function without parenchyma disorders could relate 80% to 70% resection of the liver [233]. Different factors, such as environmental variables, post-operation care, immune suppression, associated diseases, severity of cirrhosis, and progression of HCC, could profoundly alter the outcome and survival after PHX in patients [234-236].

All the reports of liver regeneration on different rodent models and characterization of underlying mechanisms might have a beneficial effect and might result in improvement of surgical resection in patients. The data presented in the current study show that in the process of liver regeneration, any dysregulation of IL-6 and IL-6 signaling might interfere with after live resection. This finding was confirmed in the case of tocilizumab (TCZ), which bind to IL-6R or sIL-6R and inhibits IL-6 trans-signaling and classic signaling [74]. Remarkably, it was reported that patients treated with TCZ showed abnormalities in liver parameters, such as ALT and AST. Another study also showed hepatotoxicity upon treatment with TCZ [83]. Recently, the official report warned that the use of TCZ in patients diagnosed with RA, systemic juvenile idiopathic arthritis (sJIA), and giant cell

arteritis (RZA) in adults could be consistent with liver abnormalities and liver failure (Red hand letter, 26 Jun 2019, Roche).

Patients treated with different antibodies against IL-6, IL-6R, or sIL-6R upon liver injury might have the risk of developing liver disorders. Subsequently, due to the blockade of IL-6 trans-signaling, the liver might not be able to overcome the injury, leading to liver failure.

Importantly, the current study clearly illustrated that IL-6 initiates liver regeneration mainly through IL-6 trans-signaling. The pro-inflammatory role of IL-6 trans-signaling has been extensively studied and confirmed that IL-6 trans-signaling is involved in such diseases as RA, cancer, and metabolic disorders. Therefore, new inhibitory drugs are designed to sufficiently block IL-6 trans-signaling. Recently, sgp130Fc, a specific blocker of IL-6 trans-signaling, was designed and described in various models. The DSS colitis model [65, 237], antigen-induced arthritis [238], the acute inflammation model [239], and murine asthma models [240] confirmed the efficiency of sgp130Fc in blocking trans-signaling and subsequently improving the outcome of diseases. However, in the presented model, the physiological contribution of IL-6 trans-signaling was highlighted by an exemplified liver regeneration model. Consistently, we showed that using sgp130Fc results in weakened regeneration upon liver injury followed by PHX. Therefore, the use of sgp130Fc, which recently entered clinical trial phase II, might result in a similar outcome upon treatment in patients.

In summary, three main findings were explained in this study: IL-6 promotes liver regeneration upon liver damage through trans-signaling. Second, generated sIL-6R^{+/+} mice could mimic hyperactivation of ADAM for only a single substrate. Generated sIL-6R^{+/+} mice are a novel tool to study the role of IL-6 trans-signaling in pathophysiological and physiological circumstances in greater detail. Third, along with illustrating the fundamental role of IL-6 trans-signaling in liver regeneration, these data suggested that IL-6 classic signaling might be insufficient to promote liver regeneration upon injury.

Binding sites of miR-204, 590-5p, 21 and 125 to Remaining part of 3'UTR of exon 10 in the original reading frame of IL-6R.

Exon10 (3'untranslated region)

...TCATCTGGATGGTACCTGGCAGCTGGCAGGGCACCACGAGATCAGCACACAAGTTTCTCATGCGGGTCCCATCCAC
CTGGGGTGGGGTGGGGCGGGCGGGGCTGCAGCTTCACTAACCCACAAGAGCTCTGCACAGGTTCTGAGTAGGTGCAG
CTGGTGCTGCATAGGCTCTGAAGGAAGGAAGGGGCTGTGAGGAACACAGGCCATTGTGAAGACAGCTTGTGATGACT
GAATAGAGATGCCCCTCAGCTCCACATCTGATAGTGGCTCACAAGCTGCACCCTCAGGAGGCCTCAGAAAGGGGCTC
CAAAGGCTGCCCCAGCTGCCTCGCTCTGCCTCACTGCCCAAGCCACCTTTTAGCTCTCGAACTCCTAAAGTCCAAG
CACTTTTGCCATTCTCTTTCCGAGGCCACTGAGGCCGGGTGGAAGCTTGGTTCCGATTTCTTCTCAACATCTGGAAA
GCAGCTGGGCCCCGGTGGTGGTACTAATATCTCAGGGCCTGATGGTTTACGCGAGTGACAATTTCTACAAGCAGTT
TTTAAATGTGAATGATGACCCAGGCACTGCTGGCTGCGGAGGCTTCATTTTCTCTTCGATCTCAGGACTTCAGGC
GAAAAGCGGAGTGGAAGTAGAGAGCGGATGGGTGTCCACCGTCTCATGGTACTTGCGGGAGGTACAGCCTGGAAAA
CACGTTTCTGTCCCCCTACTCTCCAGGAGAGGGATGATGGTAGGGGGTGCCTCTTCCAGGGCGGAGAGAACTACT
TTACCCAGCCTTGCCATTCTGATTTCAACTGGACTGGAGCTACTAGGAAAGTCGACATTCATGCAAAAAGAAAAA
ACGTTAACTAGCAAGAATGCACTTTTCAATTTGGTTTTTAGAGAAGTGTTCCTGTTTCTCTCAAGAGTCTGGAAGAG
GCCGCTCACTGCACACTACTGTATGAACCCTCACTGCCACCCTGGAGGACCAAGTGCAGTAACGGTAGCCCAAACA
CCAAGTCAAGTGAAGTCAAGGGAAAAAACAACAAGCAACAAAAAACAACAACAACAACAACAACAACAACAACAACA
AAATCACCCCCCAAAAAAACA
CAAACCAACCCGCTGTTTCTATAACAGAAAAGCCTTTGGTTTCAATTTTTATTTTTGATTTTTTTGTCTTAAAAAGT
ATAAAAATAGCCTGTCCATGCTCTGCTTCAGGGAATGAGCCTGTGAACACTCCAGGCGCAGGCAGGAAGGGTGTCT
GCTTCTGCTACAC

loxP

GTACGCCGGCTTAAGTGTACACGCGTACTAGTCTAGC**GAAGTTCCTATACTTTCTAGAGAATAGGAACTTC**GGTTCGA
AC**ATAACTTCGTATAGCATAACATTATACGAAGTTAT**GGTACCTGCAGAATTCATGCATAAGCTTGGATCCGTTCTTC
GGACGCCTCGTCAACACCGTACG

Remaining E10-3'UTR

**CTCACTGCCACCTTGGCCTTCTTGGCTTTACGTTTGACTGAGTGGCCTCAGATGCTTTCCCTGGGGCTTTGAGGAA
TCCAGTGATGTTAGTGGTACCAGGAGACCACAGAGCCACAGTGTGGTCTTAGATTAAGTACTTCTGCAACCA
CAGCACCCACACCTGCCGTCTTACTGAACTATGCCAGTAACTTGCCTTTTCTGCCACCACCACGAGACGAGACGGG
CAGAGCTCGGAAGCTGTCACCCATGCCCTCTGCTTGTCCGCTCTAGGGGCCACTGACCTAAGCATTAGTTATTTTA
TTTTATTTTATTTTTTTGTGGGTTTTGTACATTTTAGGTCCTGTTGCTGTCTTAGAAAAGGCTCTGTAGGTTGACAG
AAAATCAGGCCAAGTATTCATGTTTTTTTTTTTTTTTTTCTTCTTTCTCTTTGCTAAGTTTTTTGGGACTCAA
GGTAG**

miR-204-

CAAACTGCTGTGAAGGGAAATTTATTAATAAATGTTACAGATCGTGATCTTCAGGGGATCGGCGACTGTGCTCACT
CACAGTTCTTCAGTCCCTCACAGGGCTCTGCTGTTACCCAAGCCAGGCAGAGCAGGCAGACGGAAGACTGAAATCCA
GATAGCTCATTATCTCTGTGAGTTAAATGGCTTTGATCTCCAAGTTGTTTTCACTATTGTTGTAAGGGGATAGCCTC
CCC

miR-590-5p miR-21-

CCAACCCGTATCAAAGGATGCTTTTTCTTTT**ACTTTTTATAAGCTAA**GTCAACAAAGTCTGTTTCGTCCGGTTT
CGTTCACTTACACAGGTGTATGCCCTCAGCTGCTTCTGGTCTCAATTCTGTGCAAGCTGAATAGGTGTTCCATCCT
CGGGTCATTCTTACTGGAGTTTCTGCAGCCACAGGCTGCCTTGTCAACAGTACCACTTAACACCAGCATTACGCGA
CCAGGCAGCCAAATGCCTGGTCTAGACAGAGATGATTTAAACATGATCTTTGTTGCATGGTAGAAAGAGGGAAACACA
TACTGGTTCTAGTTCTAAGGTTCTTAGATGTTTGGTCTTCTGGCATTAGTGAATAGCTTTAAACTATTTCAAGGG
AGAAGCCTTGGCCACACCCACGACATTTGGCCGACAGTCCTTTCTCTCCATGAGCCTTGCCTTCCACCTGGCTGAA
AGCTCA

miR-204-

CACTGAATCTTTCTGTGCCTTGGTGTCTTGGGAGAAAGGGAAACCCCGGTGTGGGCTTTACTGCCGGCATTGGCTT
GGAGCCAGCGTGGAGCAGAGCCCAACAGGGTGGGCCAGGCTTAGTTATGGTGTGCCGGTTTAAAGGAATGCCTGGTTT
GCCTGGTTGCCTGGGCTCCGAGCTAGAGTTTCTAGTAGTTCTTTATGGCTGACCTAGTTGGGAAAGACTCCCATAC
TCAGCTTCAGGTAGAGGTGGTGAGAAACCTTTTCTTTGTAGAGGCAGCATCATCCCAAGAGCCTACAGTGAGGTGA
GGTGGGAGGGGCAGGCGCTGGGGAGGGTCTGCCAAAGTGGGAGGGGGCAGGCCAGCTGGGGAGGGTCTGCCAAAGTG
GGAGGGGGCAGGCCAGCTGGGGAGGGTCTGCCAAAGTGGGAGGGGGCAGGCCAGCTGGGGAGGGTCTGCCAAAGTGG
GAGGGGGCAGGCCAGCTGGGGAGGGTCTGCCAAAGTGGGAGGGGGCAGGCCAGCTGGGGAGGGTCTGCCAAAGTGGG
AGGGGCAGGCGCTGGGGAGGGTCTGCCAAAGTGGGAGGGGGCAGGCCAGCTGGGGAGGGTCTGCCAAAATGGGAGGG
GGCAGGCCAGCTGGGGAGGGTCTGCCAAAGTGGGAGGGACAGGCGCTGGGGAGGGTCTGCCAAAGTGGGAGGGGGCA
GGCCAGCTGGGGAGGGTCTGCCAAAGTGGGAGGGGGCAGGCCAGCTGGGGAGGGTCTGGGGCTGGCGCTGGGGAGG
GTCTGCCAAAGTCTCTCCAGCCTCTGCTGCTAGTGTAGTTGGGTGCCAGTTCAGGAAGTTTCTATGGCAACCTTA
ATGCGCCTTAAGGAACACTGTCAGGTTTGTGAACATATGCTCAGATGGAGATCTTGTTTCCAGGGAAAGGACTGGTA
CAGTGTGTAGCAAGCTGGAATGGACAGAGAGACTTTGGCAAGAGATCATATCCGTTAAAAACAGGATACCTCAATGC
TACATGTTTTTATCTTTGAGACAATATTTTTAAGTTTTTACGCTCTGTCCCCTGTGAGCTGATACCTAAGACCTAA
GTCAGTGCTTTTTTAATGCCTTTTTGCCTCTTGTTTGTCTTAAAGTGAATTTGTAAGTGTGGAAATAAATAATT
TCTAAAGTTGCACTGAGATGTTCTTCTGCTTTGGCAACCTGGTCATTAAAAGGAAAACCTTCCCTCCATGATGAGC
GAGGAGTAAAGAATGAGGAAGGCTAACTAACTAATTAATAGGACTGTCTCTGAGGGCACAGCGGCTCAGTCCTCTA
ACCCGGCTCGACACTAGGAAGGCAGAGGCGGGAGGATTTCTCCAAGTTTGGGCTAGTGAGGCCTTGTATGTCACTT
ATACTGCCCTCACAGACAGACAGACAGGCAGACACACACACACACACACACACACACACACACACTAAACC
TGGGACTAGCAATTTCTCAAAGGTTTTAGTTAGTAAACATTTCTCCCCAAACCAAGGCCTGGGATTTCTGGAAGGAA
ATCAGAGGCTCATGTGTCTGTCACGTTTGCATTGTTTCAGCATTACCAGATAGAGGCATGTTAGAAAAGTGAAGGAAG
GCCCCACTACTTAGGTGTGTACTGGACTATGGAGGTGAGAATGGGATCCTGAGAGCCATCCCGAGCTTTCTTGGTCT
CAGATGGCTGAGTCTGTCTCCACTGAAAAAGATCTTGGGCAAGAAAAACTTGGGACCCAGCCTTCTCTATGTCCCA
AACAGAAGGAAACCCATCATGTGGATGCTTTGCAGGTAAGAGTAGGGGTGGCTGCTGAGGGCCAGCCTCAGCTTGGT
TTGGGTTCTGAGAGAAGGGGTGTCTGGGAGCAGTACAAACAAATAACTTGAAGTCTAATCGTGGGTCCAAGCTGGCT
CTGTGGTTGAGACAGCTAATTTTTCTGCTAGCTGAGAGAGACCATTCTCTCTGCTAGTAAACATACTTCCCTACAAGCT
CTCTGGATAGCTCGTGGGTTTTCTGACCAAAGTCAGAAAAGCTGCTATATATATATAAAAAAAAAACCTCTTGATAT
TCTAACCAAATCAGAAACCTGTTTGAATAATTTCTAAAATTAATTTCTGGATTTTCCAATCAAAATCAGAAAGAAAA
AAAAAATCTCAAAGAGCCGTGCGCGCTCTTCAGACAACCTTCTCTGAATAGCTTCTGGAAAACATTGTAAAAGAGC
GACGTCGGCTCTCTAAGTAACTCTTAGTGGTCAGAAATCCATTAGAAAAAAATTTCTAAAAAGCTGAGTTTGCTCTC
CATGACTTTCCAGACTAAAATCAGGAATCCTGTTAGAAAAAAACCTAGAAGAGCTATGTTCCCTCTCCAGAGAT
CTTCAGACAGCTCAGCTCTCCTTGGTAGAGAAAAATTTAAGAACCATTATTGCTTTTTGCCAGCTCATCTCATGCA
GCCAAAAGCCTAGCTTTTTATTTACATATCAATTCAGTCATTTATTCCAGGTTCCCTCTTGACCACCCCGGGGAAT
CCACACTCCAGGACCTTAGCCCCTTGACTCACAGGAAAGGGATAGCAAGTCCATTTTTTCCCCTCTTTTATTAACAT
TGCAGAAGAATTAGAGATCTGCCTGCCTCTGTAAACATAGCTGGGTGGGACCTTGTCTGAGAGTACCATCTCCCA
CCACTCTTGACCTAAATTTGCTCTGACCCAGGCTGACCTTGAAGTCAAGAATCTGCCTGCATTTGTATCTGCCTGT
CTTTGCGTCTCTCTGGCAAGCCGGCTCACAGTGCAGCCGCTCTGCTCCTTACATCTGTGAAGCTCCTTATACAAT
TCATACTGCATTTTATATTTTTGCATAGCTGAGAAATTATACATTTCTGAACATGTCTTTAGAGTTCTTGTCTGAA
GATCCCAGTGTTTAGCATTTTGTGAGACATTAGTCACACCTTCCATCTGACTCACGGTGTCTCTGATTATCAT
GAAATCATTAAAGTTAACAGGGAGGACATTTCTTGGAGGAACATGAAAATATGTTTATTATACAAACAAGCCTT
ACTCCACAGCAGCCGTCAACTCTCGTGGAGGCCACGCTGCTGGCCCTGTTCCAGGGGCAGGAACCATGTCGTTT
TGTCTCTATCAAGGCCATGCCACAGCTGGTGGCAAGAAGTGTGCAAAGGCCCCCAACTCAGATGAAGCTGGGGTTGG
GTGGCACCCACTGCCCTTCACTTGGACCCCTGTTCCCGAAGCACAGCTGTTCTTCTCCACCCCAAGGCAGGTGCTGT
TTCCTTAGTATGAGCTCTGGTCCCATAGCTGTTGGTGCCTTGTATGCCCCCTTCTGCAGCCGTGTGCTCTCCAACCC
TGAACCACTCTCTCCAGCAAGGATCCCTGTGTCTCATTTGGTTTGTCTAAACTGAGGCTGGCAGCCGGCCAACCTGGG
AGTCTGATCCCCCGGGCAAAGGCATAGCACTTTTCCAGGGGTGACTTTGAAGAGGTCTGAGCACCAGGGGAGGTACAG
AGAGGAAGGACAGAAATCGGTTCCCTAAATTTTTCTCCCCTTTGGTTTTTCTGAGATACGGTTTTCTGTGTGGCCC
TGGCTATCCTAGAACCTGCTCTGTAGATCACAGCTGGCCTTGAAGTCAAGATCTGTCTGCCTCTGCCTCCAGAGTG
CTGGGACTAAAGGTGTGCGCCAACACAGCTCCGGCTAGATCCTTAAACTGAACCAGGGGCTTCCCTTTACCTCTGG
ACTTGCCGTGAGACTTTGATGCTTAGTTTGTATACACTTTAATGGACCTTTGAAAACGCCTCCCATTCTGTCCGGGA
TCGCAGGGCTCTGTACATGGAGTACAGGAGGGCAAACAACCTTAAAGAGCCCAACCTGAGAGTCTGAGTTGGATCTT

ACAGAGGCAGCAGAAGACAAAGTTTTGATTCTGGAAGTTTCTAACTATTTCCCTTAAGTTCATTCCCAGCTCTGCT
GGCCTCTTTGGGGGGACCTGCACACATGTGACAGGCACAGACAAATAAAATAAAATAAAATAAAATAAAATA
AAATAAAATAAAATAACATGTGTTAAAATCTTGACTGGAAAGATGGCTCAGTGGTTAAGAGCACTGGCTGCTCTTAC
AGAAGGTTAAAGTCAATGGAAAACCCAGAAATCTCGGAAATGTTTCATGCGGAGCGCTTGGAAATAAAATCACAGCCAT
TTCTGAGAAATATCTCTGTTACTTAAAGTACCTTACTGAGAAGGTCTTACTTAAGGGGAAGAGTCTCCACCCTGGC
TTCCTGTGGGTGTGTCTCACGGGGGATTTGTTCCCTTTAGATCTCCAGAGATGAAAGGAGACCGAGGGCCCCTTAGGA
GACTTTTGTTTTATTTTTTTTCTTGACAGAGTCTTGCTATGTAGCCCAGGCTGGCCTGCAGTTCACAGTTCTTGCCTC
TCAGCCTGACCCTTGTGGGAGTTACACCCAGCCAGTTTTAAGAAAAACAAGTTCTTGGTTTTATGGGCTGGCCTTCT
CAACTCTAGCCCCTTGTGTTCTCAGGACTCCCCTATTCCCCTTGAATAAACGATCACTATTTCCATTTCTAGCCA
AGTGTCTTGATGCAATCTTCTGGCCTAGGACAACAGCCTGGACCCAGATGCCCTCTGAACTCTGACTTGAAGCCTG
AAGTTAATCATGGTTCTTTATTTTCTCATCTCTTTTTTTGGATTCTAGTTAAAGCCTAAATATAGTTCTGAGACACTT
TGGGTTTTCTTACTGGTTCTTGACCGTCAAGCCAACTCAAAGGGCAGGACTTCCTCCTTCTGGCAGCTGACGGGAT
CTCTACTTTCTGCTTGTTTTTTGTTGAGTCAGAGCCCTGGCTGTCCTGGATCTCACTATGTAGACCAGGCGGCTGTT
CATGAATTCAGGGAGATCCACCTGTCTCTGCTTCCCACTGCTGGATTAAAGGTGTATGCTACCACAGCCAGCCTTG
CTCCACTGTCTGTCTGTCTCTTTCTTTCTTTCCATTTTTTTTTTAAGATCTATTGATGTATGTTATGTATATGG
GTGCTTTGACTGCAGATGTGTCTGTACATCAGAAGTGGGCATCAGATCACATTGAAGATGGTTGTG

miR-125-

AGCTGCCTCAGG...

5 References

1. Dendorfer, U., *Molecular biology of cytokines*. Artif Organs, 1996. **20**(5): p. 437-44.
2. Dinarello, C.A., *Historical insights into cytokines*. Eur J Immunol, 2007. **37 Suppl 1**: p. S34-45.
3. Garbers, C., et al., *Plasticity and cross-talk of interleukin 6-type cytokines*. Cytokine Growth Factor Rev, 2012. **23**(3): p. 85-97.
4. Rose-John, S., *Interleukin-6 Family Cytokines*. Cold Spring Harb Perspect Biol, 2018. **10**(2).
5. Murakami, M., D. Kamimura, and T. Hirano, *Pleiotropy and Specificity: Insights from the Interleukin 6 Family of Cytokines*. Immunity, 2019. **50**(4): p. 812-831.
6. Tanaka, T., et al., *Regulation of IL-6 in Immunity and Diseases*. Adv Exp Med Biol, 2016. **941**: p. 79-88.
7. Wolff, S.C., et al., *Charged residues in the C-terminus of the P2Y1 receptor constitute a basolateral-sorting signal*. J Cell Sci, 2010. **123**(Pt 14): p. 2512-20.
8. Bazan, J.F., *A novel family of growth factor receptors: a common binding domain in the growth hormone, prolactin, erythropoietin and IL-6 receptors, and the p75 IL-2 receptor beta-chain*. Biochem Biophys Res Commun, 1989. **164**(2): p. 788-95.
9. Bazan, J.F., *Haemopoietic receptors and helical cytokines*. Immunol Today, 1990. **11**(10): p. 350-4.
10. Hirano, T., et al., *Complementary DNA for a novel human interleukin (BSF-2) that induces B lymphocytes to produce immunoglobulin*. Nature, 1986. **324**(6092): p. 73-6.
11. Weissenbach, J., et al., *Two interferon mRNAs in human fibroblasts: in vitro translation and Escherichia coli cloning studies*. Proc Natl Acad Sci U S A, 1980. **77**(12): p. 7152-6.
12. May, L.T., D.C. Helfgott, and P.B. Sehgal, *Anti-beta-interferon antibodies inhibit the increased expression of HLA-B7 mRNA in tumor necrosis factor-treated human fibroblasts: structural studies of the beta 2 interferon involved*. Proc Natl Acad Sci U S A, 1986. **83**(23): p. 8957-61.
13. Sehgal, P.B., et al., *Regulation of the acute phase and immune responses in viral disease. Enhanced expression of the beta 2-interferon/hepatocyte-stimulating factor/interleukin 6 gene in virus-infected human fibroblasts*. J Exp Med, 1988. **167**(6): p. 1951-6.
14. Yamasaki, K., et al., *Cloning and expression of the human interleukin-6 (BSF-2/IFN beta 2) receptor*. Science, 1988. **241**(4867): p. 825-8.
15. Murakami, M., et al., *IL-6-induced homodimerization of gp130 and associated activation of a tyrosine kinase*. Science, 1993. **260**(5115): p. 1808-10.
16. Hibi, M., et al., *Molecular cloning and expression of an IL-6 signal transducer, gp130*. Cell, 1990. **63**(6): p. 1149-57.
17. Grotzinger, J., et al., *IL-6 type cytokine receptor complexes: hexamer, tetramer or both?* Biol Chem, 1999. **380**(7-8): p. 803-13.
18. Boulanger, M.J., et al., *Convergent mechanisms for recognition of divergent cytokines by the shared signaling receptor gp130*. Mol Cell, 2003. **12**(3): p. 577-89.
19. Heink, S., et al., *Trans-presentation of IL-6 by dendritic cells is required for the priming of pathogenic TH17 cells*. Nat Immunol, 2017. **18**(1): p. 74-85.

20. Varghese, J.N., et al., *Structure of the extracellular domains of the human interleukin-6 receptor alpha -chain*. Proc Natl Acad Sci U S A, 2002. **99**(25): p. 15959-64.
21. Sprecher, C.A., et al., *Cloning and characterization of a novel class I cytokine receptor*. Biochem Biophys Res Commun, 1998. **246**(1): p. 82-90.
22. Baran, P., et al., *Minimal interleukin 6 (IL-6) receptor stalk composition for IL-6 receptor shedding and IL-6 classic signaling*. J Biol Chem, 2013. **288**(21): p. 14756-68.
23. Gerhartz, C., et al., *Differential activation of acute phase response factor/STAT3 and STAT1 via the cytoplasmic domain of the interleukin 6 signal transducer gp130. I. Definition of a novel phosphotyrosine motif mediating STAT1 activation*. J Biol Chem, 1996. **271**(22): p. 12991-8.
24. Heinrich, P.C., et al., *Principles of interleukin (IL)-6-type cytokine signalling and its regulation*. Biochem J, 2003. **374**(Pt 1): p. 1-20.
25. Oberg, H.H., et al., *Differential expression of CD126 and CD130 mediates different STAT-3 phosphorylation in CD4+CD25- and CD25high regulatory T cells*. Int Immunol, 2006. **18**(4): p. 555-63.
26. Chalaris, A., et al., *The soluble Interleukin 6 receptor: generation and role in inflammation and cancer*. Eur J Cell Biol, 2011. **90**(6-7): p. 484-94.
27. Scheller, J. and S. Rose-John, *Interleukin-6 and its receptor: from bench to bedside*. Med Microbiol Immunol, 2006. **195**(4): p. 173-83.
28. Rose-John, S., *IL-6 trans-signaling via the soluble IL-6 receptor: importance for the pro-inflammatory activities of IL-6*. Int J Biol Sci, 2012. **8**(9): p. 1237-47.
29. Lokau, J., M. Agthe, and C. Garbers, *Generation of Soluble Interleukin-11 and Interleukin-6 Receptors: A Crucial Function for Proteases during Inflammation*. Mediators Inflamm, 2016. **2016**: p. 1785021.
30. Rose-John, S., *The Soluble Interleukin 6 Receptor: Advanced Therapeutic Options in Inflammation*. Clin Pharmacol Ther, 2017. **102**(4): p. 591-598.
31. Scheller, J., et al., *The pro- and anti-inflammatory properties of the cytokine interleukin-6*. Biochim Biophys Acta, 2011. **1813**(5): p. 878-88.
32. Wolf, J., S. Rose-John, and C. Garbers, *Interleukin-6 and its receptors: a highly regulated and dynamic system*. Cytokine, 2014. **70**(1): p. 11-20.
33. Kishimoto, T., et al., *Interleukin-6 family of cytokines and gp130*. Blood, 1995. **86**(4): p. 1243-54.
34. Erta, M., A. Quintana, and J. Hidalgo, *Interleukin-6, a major cytokine in the central nervous system*. Int J Biol Sci, 2012. **8**(9): p. 1254-66.
35. Gumusoglu, S.B., et al., *The role of IL-6 in neurodevelopment after prenatal stress*. Brain Behav Immun, 2017. **65**: p. 274-283.
36. Gadiant, R.A. and U. Otten, *Expression of interleukin-6 (IL-6) and interleukin-6 receptor (IL-6R) mRNAs in rat brain during postnatal development*. Brain Res, 1994. **637**(1-2): p. 10-4.
37. Gruol, D.L. and T.E. Nelson, *Physiological and pathological roles of interleukin-6 in the central nervous system*. Mol Neurobiol, 1997. **15**(3): p. 307-39.
38. Zhong, J., et al., *Sensory impairments and delayed regeneration of sensory axons in interleukin-6-deficient mice*. J Neurosci, 1999. **19**(11): p. 4305-13.
39. Cafferty, W.B., et al., *Conditioning injury-induced spinal axon regeneration fails in interleukin-6 knock-out mice*. J Neurosci, 2004. **24**(18): p. 4432-43.

40. Fontes, J.A., N.R. Rose, and D. Cihakova, *The varying faces of IL-6: From cardiac protection to cardiac failure*. Cytokine, 2015. **74**(1): p. 62-8.
41. Cressman, D.E., et al., *Liver failure and defective hepatocyte regeneration in interleukin-6-deficient mice*. Science, 1996. **274**(5291): p. 1379-83.
42. Kopf, M., et al., *Impaired immune and acute-phase responses in interleukin-6-deficient mice*. Nature, 1994. **368**(6469): p. 339-42.
43. Harmer, D., C. Falank, and M.R. Reagan, *Interleukin-6 Interweaves the Bone Marrow Microenvironment, Bone Loss, and Multiple Myeloma*. Front Endocrinol (Lausanne), 2018. **9**: p. 788.
44. Nowell, M.A., et al., *Soluble IL-6 receptor governs IL-6 activity in experimental arthritis: blockade of arthritis severity by soluble glycoprotein 130*. J Immunol, 2003. **171**(6): p. 3202-9.
45. Diehl, S. and M. Rincon, *The two faces of IL-6 on Th1/Th2 differentiation*. Mol Immunol, 2002. **39**(9): p. 531-6.
46. Bettelli, E., et al., *Reciprocal developmental pathways for the generation of pathogenic effector TH17 and regulatory T cells*. Nature, 2006. **441**(7090): p. 235-8.
47. Alexander, W.S., et al., *SOCS1 is a critical inhibitor of interferon gamma signaling and prevents the potentially fatal neonatal actions of this cytokine*. Cell, 1999. **98**(5): p. 597-608.
48. Diehl, S., et al., *Induction of NFATc2 expression by interleukin 6 promotes T helper type 2 differentiation*. J Exp Med, 2002. **196**(1): p. 39-49.
49. Dienz, O., et al., *The induction of antibody production by IL-6 is indirectly mediated by IL-21 produced by CD4+ T cells*. J Exp Med, 2009. **206**(1): p. 69-78.
50. Urashima, M., et al., *CD40 ligand triggers interleukin-6 mediated B cell differentiation*. Leuk Res, 1996. **20**(6): p. 507-15.
51. Tanaka, T., M. Narazaki, and T. Kishimoto, *IL-6 in inflammation, immunity, and disease*. Cold Spring Harb Perspect Biol, 2014. **6**(10): p. a016295.
52. Heikkila, K., S. Ebrahim, and D.A. Lawlor, *Systematic review of the association between circulating interleukin-6 (IL-6) and cancer*. Eur J Cancer, 2008. **44**(7): p. 937-45.
53. Ma, Y., et al., *IL-6, IL-8 and TNF-alpha levels correlate with disease stage in breast cancer patients*. Adv Clin Exp Med, 2017. **26**(3): p. 421-426.
54. Kotake, S., et al., *Interleukin-6 and soluble interleukin-6 receptors in the synovial fluids from rheumatoid arthritis patients are responsible for osteoclast-like cell formation*. J Bone Miner Res, 1996. **11**(1): p. 88-95.
55. Diaz-Torne, C., et al., *The combination of IL-6 and its soluble receptor is associated with the response of rheumatoid arthritis patients to tocilizumab*. Semin Arthritis Rheum, 2018. **47**(6): p. 757-764.
56. Andus, T., et al., *Regulation of synthesis and secretion of major rat acute-phase proteins by recombinant human interleukin-6 (BSF-2/IL-6) in hepatocyte primary cultures*. Eur J Biochem, 1988. **173**(2): p. 287-93.
57. Gauldie, J., et al., *Interferon beta 2/B-cell stimulatory factor type 2 shares identity with monocyte-derived hepatocyte-stimulating factor and regulates the major acute phase protein response in liver cells*. Proc Natl Acad Sci U S A, 1987. **84**(20): p. 7251-5.
58. Han, C., et al., *Association of anemia and physical disability among patients with rheumatoid arthritis*. J Rheumatol, 2007. **34**(11): p. 2177-82.

59. Srirangan, S. and E.H. Choy, *The role of interleukin 6 in the pathophysiology of rheumatoid arthritis*. Ther Adv Musculoskelet Dis, 2010. **2**(5): p. 247-56.
60. Tanaka, T. and T. Kishimoto, *Targeting interleukin-6: all the way to treat autoimmune and inflammatory diseases*. Int J Biol Sci, 2012. **8**(9): p. 1227-36.
61. Spencer, S., et al., *Loss of the interleukin-6 receptor causes immunodeficiency, atopy, and abnormal inflammatory responses*. J Exp Med, 2019. **216**(9): p. 1986-1998.
62. Papadaki, H.A., et al., *Anemia of chronic disease in rheumatoid arthritis is associated with increased apoptosis of bone marrow erythroid cells: improvement following anti-tumor necrosis factor-alpha antibody therapy*. Blood, 2002. **100**(2): p. 474-82.
63. Kim, G.W., et al., *IL-6 inhibitors for treatment of rheumatoid arthritis: past, present, and future*. Arch Pharm Res, 2015. **38**(5): p. 575-84.
64. Hirano, T., et al., *Excessive production of interleukin 6/B cell stimulatory factor-2 in rheumatoid arthritis*. Eur J Immunol, 1988. **18**(11): p. 1797-801.
65. Atreya, R., et al., *Blockade of interleukin 6 trans signaling suppresses T-cell resistance against apoptosis in chronic intestinal inflammation: evidence in crohn disease and experimental colitis in vivo*. Nat Med, 2000. **6**(5): p. 583-8.
66. Okuda, Y., et al., *IL-6-deficient mice are resistant to the induction of experimental autoimmune encephalomyelitis provoked by myelin oligodendrocyte glycoprotein*. Int Immunol, 1998. **10**(5): p. 703-8.
67. Scott, L.J., *Tocilizumab: A Review in Rheumatoid Arthritis*. Drugs, 2017. **77**(17): p. 1865-1879.
68. Calabrese, L.H. and S. Rose-John, *IL-6 biology: implications for clinical targeting in rheumatic disease*. Nat Rev Rheumatol, 2014. **10**(12): p. 720-7.
69. Kang, S., et al., *Targeting Interleukin-6 Signaling in Clinic*. Immunity, 2019. **50**(4): p. 1007-1023.
70. Raimondo, M.G., et al., *Profile of sarilumab and its potential in the treatment of rheumatoid arthritis*. Drug Des Devel Ther, 2017. **11**: p. 1593-1603.
71. Fleischmann, R., et al., *Sarilumab and Nonbiologic Disease-Modifying Antirheumatic Drugs in Patients With Active Rheumatoid Arthritis and Inadequate Response or Intolerance to Tumor Necrosis Factor Inhibitors*. Arthritis Rheumatol, 2017. **69**(2): p. 277-290.
72. Sarosiek, S., R. Shah, and N.C. Munshi, *Review of siltuximab in the treatment of multicentric Castleman's disease*. Ther Adv Hematol, 2016. **7**(6): p. 360-366.
73. Hunter, C.A. and S.A. Jones, *IL-6 as a keystone cytokine in health and disease*. Nat Immunol, 2015. **16**(5): p. 448-57.
74. Navarro, G., et al., *Tocilizumab in rheumatoid arthritis: a meta-analysis of efficacy and selected clinical conundrums*. Semin Arthritis Rheum, 2014. **43**(4): p. 458-69.
75. Morel, J., et al., *Risk factors of serious infections in patients with rheumatoid arthritis treated with tocilizumab in the French Registry REGATE*. Rheumatology (Oxford), 2017. **56**(10): p. 1746-1754.
76. Jostock, T., et al., *Soluble gp130 is the natural inhibitor of soluble interleukin-6 receptor transsignaling responses*. Eur J Biochem, 2001. **268**(1): p. 160-7.
77. Narazaki, M., et al., *Soluble forms of the interleukin-6 signal-transducing receptor component gp130 in human serum possessing a potential to inhibit signals through membrane-anchored gp130*. Blood, 1993. **82**(4): p. 1120-6.

78. Rose-John, S., et al., *Studies on the structure and regulation of the human hepatic interleukin-6 receptor*. Eur J Biochem, 1990. **190**(1): p. 79-83.
79. Schuett, H., et al., *Transsignaling of interleukin-6 crucially contributes to atherosclerosis in mice*. Arterioscler Thromb Vasc Biol, 2012. **32**(2): p. 281-90.
80. Ullah, M.A., et al., *Allergen-induced IL-6 trans-signaling activates gammadelta T cells to promote type 2 and type 17 airway inflammation*. J Allergy Clin Immunol, 2015. **136**(4): p. 1065-73.
81. Rose-John, S., et al., *The IL-6/sIL-6R complex as a novel target for therapeutic approaches*. Expert Opin Ther Targets, 2007. **11**(5): p. 613-24.
82. Hiura, M., et al., *Case of severe liver damage after the induction of tocilizumab therapy for rheumatoid vasculitis*. Hepatol Res, 2011. **41**(5): p. 492-6.
83. Mahamid, M., R. Mader, and R. Safadi, *Hepatotoxicity of tocilizumab and anakinra in rheumatoid arthritis: management decisions*. Clin Pharmacol, 2011. **3**: p. 39-43.
84. Abdel-Misih, S.R. and M. Bloomston, *Liver anatomy*. Surg Clin North Am, 2010. **90**(4): p. 643-53.
85. Michels, N.A., *The ever varied blood supply of the liver and its collateral circulation*. J Int Coll Surg, 1957. **27**(1): p. 1-17.
86. Eipel, C., K. Abshagen, and B. Vollmar, *Regulation of hepatic blood flow: the hepatic arterial buffer response revisited*. World J Gastroenterol, 2010. **16**(48): p. 6046-57.
87. Fiebig, T., et al., *Three-dimensional in vivo imaging of the murine liver: a micro-computed tomography-based anatomical study*. PLoS One, 2012. **7**(2): p. e31179.
88. Selden, C., M. Khalil, and H.J. Hodgson, *What keeps hepatocytes on the straight and narrow? Maintaining differentiated function in the liver*. Gut, 1999. **44**(4): p. 443-6.
89. Kmiec, Z., *Cooperation of liver cells in health and disease*. Adv Anat Embryol Cell Biol, 2001. **161**: p. III-XIII, 1-151.
90. Haussinger, D., H. Sies, and W. Gerok, *Functional hepatocyte heterogeneity in ammonia metabolism. The intercellular glutamine cycle*. J Hepatol, 1985. **1**(1): p. 3-14.
91. Lamers, W.H., et al., *Hepatic enzymic zonation: a reevaluation of the concept of the liver acinus*. Hepatology, 1989. **10**(1): p. 72-6.
92. Gumucio, J.J., *Hepatocyte heterogeneity: the coming of age from the description of a biological curiosity to a partial understanding of its physiological meaning and regulation*. Hepatology, 1989. **9**(1): p. 154-60.
93. Jungermann, K., *Metabolic zonation of liver parenchyma*. Semin Liver Dis, 1988. **8**(4): p. 329-41.
94. Gissen, P. and I.M. Arias, *Structural and functional hepatocyte polarity and liver disease*. J Hepatol, 2015. **63**(4): p. 1023-37.
95. Bilzer, M., F. Roggel, and A.L. Gerbes, *Role of Kupffer cells in host defense and liver disease*. Liver Int, 2006. **26**(10): p. 1175-86.
96. Dixon, L.J., et al., *Kupffer cells in the liver*. Compr Physiol, 2013. **3**(2): p. 785-97.
97. Blaner, W.S., et al., *Hepatic stellate cell lipid droplets: a specialized lipid droplet for retinoid storage*. Biochim Biophys Acta, 2009. **1791**(6): p. 467-73.
98. Kordes, C. and D. Haussinger, *Hepatic stem cell niches*. J Clin Invest, 2013. **123**(5): p. 1874-80.
99. Rui, L., *Energy metabolism in the liver*. Compr Physiol, 2014. **4**(1): p. 177-97.
100. Michalopoulos, G.K. and M.C. DeFrances, *Liver regeneration*. Science, 1997. **276**(5309): p. 60-6.

101. Grant, D.M., *Detoxification pathways in the liver*. J Inherit Metab Dis, 1991. **14**(4): p. 421-30.
102. Bataller, R. and B. Gao, *Liver fibrosis in alcoholic liver disease*. Semin Liver Dis, 2015. **35**(2): p. 146-56.
103. Tripodi, A., *Hemostasis in Acute and Chronic Liver Disease*. Semin Liver Dis, 2017. **37**(1): p. 28-32.
104. Thawley, V., *Acute Liver Injury and Failure*. Vet Clin North Am Small Anim Pract, 2017. **47**(3): p. 617-630.
105. Rowe, I.A., *Lessons from Epidemiology: The Burden of Liver Disease*. Dig Dis, 2017. **35**(4): p. 304-309.
106. Than, N.N., et al., *Clinical effectiveness of cell therapies in patients with chronic liver disease and acute-on-chronic liver failure: a systematic review protocol*. Syst Rev, 2016. **5**: p. 100.
107. Friedman, S.L., *Seminars in medicine of the Beth Israel Hospital, Boston. The cellular basis of hepatic fibrosis. Mechanisms and treatment strategies*. N Engl J Med, 1993. **328**(25): p. 1828-35.
108. Geerts, A., *History, heterogeneity, developmental biology, and functions of quiescent hepatic stellate cells*. Semin Liver Dis, 2001. **21**(3): p. 311-35.
109. Tsuchida, T. and S.L. Friedman, *Mechanisms of hepatic stellate cell activation*. Nat Rev Gastroenterol Hepatol, 2017. **14**(7): p. 397-411.
110. Friedman, S.L., *Mechanisms of hepatic fibrogenesis*. Gastroenterology, 2008. **134**(6): p. 1655-69.
111. Higashi, T., S.L. Friedman, and Y. Hoshida, *Hepatic stellate cells as key target in liver fibrosis*. Adv Drug Deliv Rev, 2017. **121**: p. 27-42.
112. Iredale, J.P., *Hepatic stellate cell behavior during resolution of liver injury*. Semin Liver Dis, 2001. **21**(3): p. 427-36.
113. Soyer, M.T., R. Ceballos, and J.S. Aldrete, *Reversibility of severe hepatic damage caused by jejunoileal bypass after re-establishment of normal intestinal continuity*. Surgery, 1976. **79**(5): p. 601-4.
114. Blachier, M., et al., *The burden of liver disease in Europe: a review of available epidemiological data*. J Hepatol, 2013. **58**(3): p. 593-608.
115. Talwani, R., B.L. Gilliam, and C. Howell, *Infectious diseases and the liver*. Clin Liver Dis, 2011. **15**(1): p. 111-30.
116. Tag, C.G., et al., *Bile duct ligation in mice: induction of inflammatory liver injury and fibrosis by obstructive cholestasis*. J Vis Exp, 2015(96).
117. Alison, M.R., S. Islam, and S. Lim, *Stem cells in liver regeneration, fibrosis and cancer: the good, the bad and the ugly*. J Pathol, 2009. **217**(2): p. 282-98.
118. Haglund, U.H., et al., *Right hemihepatectomy*. J Gastrointest Surg, 2008. **12**(7): p. 1283-7.
119. Viveiros, A., H. Zoller, and A. Finkenstedt, *Hepatocellular carcinoma: when is liver transplantation oncologically futile?* Transl Gastroenterol Hepatol, 2017. **2**: p. 63.
120. Francavilla, A., et al., *Regulation of liver size and regeneration: importance in liver transplantation*. Transplant Proc, 1988. **20**(1 Suppl 1): p. 494-7.
121. Perlman, R.L., *Mouse models of human disease: An evolutionary perspective*. Evol Med Public Health, 2016. **2016**(1): p. 170-6.
122. Schmidt-Arras, D. and S. Rose-John, *IL-6 pathway in the liver: From physiopathology to therapy*. J Hepatol, 2016. **64**(6): p. 1403-15.

123. Zhang, D., et al., *STAT3 participates in transcriptional activation of the C-reactive protein gene by interleukin-6*. J Biol Chem, 1996. **271**(16): p. 9503-9.
124. Wuestefeld, T., et al., *Lack of gp130 expression results in more bacterial infection and higher mortality during chronic cholestasis in mice*. Hepatology, 2005. **42**(5): p. 1082-90.
125. Streetz, K.L., et al., *Lack of gp130 expression in hepatocytes promotes liver injury*. Gastroenterology, 2003. **125**(2): p. 532-43.
126. Klein, C., et al., *The IL-6-gp130-STAT3 pathway in hepatocytes triggers liver protection in T cell-mediated liver injury*. J Clin Invest, 2005. **115**(4): p. 860-9.
127. Bergmann, J., et al., *IL-6 trans-signaling is essential for the development of hepatocellular carcinoma in mice*. Hepatology, 2017. **65**(1): p. 89-103.
128. Bosch, F.X., et al., *Primary liver cancer: worldwide incidence and trends*. Gastroenterology, 2004. **127**(5 Suppl 1): p. S5-S16.
129. Lemos, B., et al., *Evolution of proteins and gene expression levels are coupled in Drosophila and are independently associated with mRNA abundance, protein length, and number of protein-protein interactions*. Mol Biol Evol, 2005. **22**(5): p. 1345-54.
130. Sakurai, T., et al., *Loss of hepatic NF-kappa B activity enhances chemical hepatocarcinogenesis through sustained c-Jun N-terminal kinase 1 activation*. Proc Natl Acad Sci U S A, 2006. **103**(28): p. 10544-51.
131. Tirosh, I., et al., *A genetic signature of interspecies variations in gene expression*. Nat Genet, 2006. **38**(7): p. 830-4.
132. Ghebranious, N. and S. Sell, *Hepatitis B injury, male gender, aflatoxin, and p53 expression each contribute to hepatocarcinogenesis in transgenic mice*. Hepatology, 1998. **27**(2): p. 383-91.
133. Rifkin, S.A., et al., *A mutation accumulation assay reveals a broad capacity for rapid evolution of gene expression*. Nature, 2005. **438**(7065): p. 220-3.
134. Nakatani, T., et al., *Sex hormone dependency of diethylnitrosamine-induced liver tumors in mice and chemoprevention by leuprorelin*. Jpn J Cancer Res, 2001. **92**(3): p. 249-56.
135. Yeh, S.H. and P.J. Chen, *Gender disparity of hepatocellular carcinoma: the roles of sex hormones*. Oncology, 2010. **78 Suppl 1**: p. 172-9.
136. Weber, L.W., M. Boll, and A. Stampfl, *Hepatotoxicity and mechanism of action of haloalkanes: carbon tetrachloride as a toxicological model*. Crit Rev Toxicol, 2003. **33**(2): p. 105-36.
137. Kovalszky, I., et al., *Modification of DENA-induced hepatocarcinogenesis by CCl4 cirrhosis. Comparison of the marker enzyme patterns*. Carcinogenesis, 1992. **13**(5): p. 773-8.
138. Park, E.J., et al., *Dietary and genetic obesity promote liver inflammation and tumorigenesis by enhancing IL-6 and TNF expression*. Cell, 2010. **140**(2): p. 197-208.
139. Croker, B.A., et al., *SOCS3 negatively regulates IL-6 signaling in vivo*. Nat Immunol, 2003. **4**(6): p. 540-5.
140. Babon, J.J., L.N. Varghese, and N.A. Nicola, *Inhibition of IL-6 family cytokines by SOCS3*. Semin Immunol, 2014. **26**(1): p. 13-9.
141. Ogata, H., et al., *Deletion of the SOCS3 gene in liver parenchymal cells promotes hepatitis-induced hepatocarcinogenesis*. Gastroenterology, 2006. **131**(1): p. 179-93.
142. Naugler, W.E., et al., *Gender disparity in liver cancer due to sex differences in MyD88-dependent IL-6 production*. Science, 2007. **317**(5834): p. 121-4.

143. Streetz, K.L., et al., *Interleukin 6/gp130-dependent pathways are protective during chronic liver diseases*. Hepatology, 2003. **38**(1): p. 218-29.
144. Kovalovich, K., et al., *Increased toxin-induced liver injury and fibrosis in interleukin-6-deficient mice*. Hepatology, 2000. **31**(1): p. 149-59.
145. Gewiese-Rabsch, J., et al., *Role of IL-6 trans-signaling in CCl(4)induced liver damage*. Biochim Biophys Acta, 2010. **1802**(11): p. 1054-61.
146. Drucker, C., et al., *Interleukin-6 trans-signaling regulates glycogen consumption after D-galactosamine-induced liver damage*. J Interferon Cytokine Res, 2009. **29**(11): p. 711-8.
147. Galun, E., et al., *Liver regeneration induced by a designer human IL-6/sIL-6R fusion protein reverses severe hepatocellular injury*. FASEB J, 2000. **14**(13): p. 1979-87.
148. Michalopoulos, G.K., *Liver regeneration*. J Cell Physiol, 2007. **213**(2): p. 286-300.
149. Zimmermann, A., *Regulation of liver regeneration*. Nephrol Dial Transplant, 2004. **19 Suppl 4**: p. iv6-10.
150. Rozga, J., *Hepatocyte proliferation in health and in liver failure*. Med Sci Monit, 2002. **8**(2): p. RA32-8.
151. Diehl, A.M. and R. Rai, *Review: regulation of liver regeneration by pro-inflammatory cytokines*. J Gastroenterol Hepatol, 1996. **11**(5): p. 466-70.
152. Murata, S., et al., *Platelets promote liver regeneration in early period after hepatectomy in mice*. World J Surg, 2007. **31**(4): p. 808-16.
153. Furchtgott, L.A., C.C. Chow, and V. Periwal, *A model of liver regeneration*. Biophys J, 2009. **96**(10): p. 3926-35.
154. Fausto, N., *Liver regeneration: from laboratory to clinic*. Liver Transpl, 2001. **7**(10): p. 835-44.
155. Taub, R., *Liver regeneration: from myth to mechanism*. Nat Rev Mol Cell Biol, 2004. **5**(10): p. 836-47.
156. Skullman, S., I. Ihse, and J. Larsson, *Influence of malnutrition on regeneration and composition of the liver in rats*. Acta Chir Scand, 1990. **156**(10): p. 717-22.
157. Fausto, N., *Liver regeneration*. J Hepatol, 2000. **32**(1 Suppl): p. 19-31.
158. Stocker, E. and U. Pfeifer, *[On the manner of proliferation of the liver parenchyma after partial hepatectomy. Autoradiography studies using 3H-thymidine]*. Naturwissenschaften, 1965. **52**(24): p. 663.
159. Cornell, R.P., *Gut-derived endotoxin elicits hepatotrophic factor secretion for liver regeneration*. Am J Physiol, 1985. **249**(5 Pt 2): p. R551-62.
160. Cornell, R.P., *Restriction of gut-derived endotoxin impairs DNA synthesis for liver regeneration*. Am J Physiol, 1985. **249**(5 Pt 2): p. R563-9.
161. Yamada, Y., et al., *Initiation of liver growth by tumor necrosis factor: deficient liver regeneration in mice lacking type I tumor necrosis factor receptor*. Proc Natl Acad Sci U S A, 1997. **94**(4): p. 1441-6.
162. Cornell, R.P., B.L. Liljequist, and K.F. Bartizal, *Depressed liver regeneration after partial hepatectomy of germ-free, athymic and lipopolysaccharide-resistant mice*. Hepatology, 1990. **11**(6): p. 916-22.
163. Takeishi, T., et al., *The role of Kupffer cells in liver regeneration*. Arch Histol Cytol, 1999. **62**(5): p. 413-22.
164. Koniaris, L.G., et al., *Liver regeneration*. J Am Coll Surg, 2003. **197**(4): p. 634-59.
165. Fausto, N., J.S. Campbell, and K.J. Riehle, *Liver regeneration*. Hepatology, 2006. **43**(2 Suppl 1): p. S45-53.

166. Su, A.I., et al., *Gene expression during the priming phase of liver regeneration after partial hepatectomy in mice*. Proc Natl Acad Sci U S A, 2002. **99**(17): p. 11181-6.
167. Kountouras, J., P. Boura, and N.J. Lygidakis, *Liver regeneration after hepatectomy*. Hepatogastroenterology, 2001. **48**(38): p. 556-62.
168. Trautwein, C., et al., *Acute-phase response factor, increased binding, and target gene transcription during liver regeneration*. Gastroenterology, 1996. **110**(6): p. 1854-62.
169. Blindenbacher, A., et al., *Interleukin 6 is important for survival after partial hepatectomy in mice*. Hepatology, 2003. **38**(3): p. 674-82.
170. Markiewski, M.M., et al., *The regulation of liver cell survival by complement*. J Immunol, 2009. **182**(9): p. 5412-8.
171. Skates, S.J. and D.E. Singer, *Quantifying the potential benefit of CA 125 screening for ovarian cancer*. J Clin Epidemiol, 1991. **44**(4-5): p. 365-80.
172. Hecht, N., et al., *Hyper-IL-6 gene therapy reverses fulminant hepatic failure*. Mol Ther, 2001. **3**(5 Pt 1): p. 683-7.
173. Peters, M., et al., *Combined interleukin 6 and soluble interleukin 6 receptor accelerates murine liver regeneration*. Gastroenterology, 2000. **119**(6): p. 1663-71.
174. Nechemia-Arbely, Y., et al., *Early hepatocyte DNA synthetic response posthepatectomy is modulated by IL-6 trans-signaling and PI3K/AKT activation*. J Hepatol, 2011. **54**(5): p. 922-9.
175. Rio, D.C., et al., *Purification of RNA using TRIzol (TRI reagent)*. Cold Spring Harb Protoc, 2010. **2010**(6): p. pdb prot5439.
176. Wilkinson, A.N., et al., *Granulocytes Are Unresponsive to IL-6 Due to an Absence of gp130*. J Immunol, 2018. **200**(10): p. 3547-3555.
177. Canfield, P.J. and S. Hemsley, *The roles of histology and immunohistology in the investigation of marsupial disease and normal lymphoid tissue*. Dev Comp Immunol, 2000. **24**(5): p. 455-71.
178. Feldman, A.T. and D. Wolfe, *Tissue processing and hematoxylin and eosin staining*. Methods Mol Biol, 2014. **1180**: p. 31-43.
179. Blancher, C. and A. Jones, *SDS -PAGE and Western Blotting Techniques*. Methods Mol Med, 2001. **57**: p. 145-62.
180. Konstantinou, G.N., *Enzyme-Linked Immunosorbent Assay (ELISA)*. Methods Mol Biol, 2017. **1592**: p. 79-94.
181. McFarland-Mancini, M.M., et al., *Differences in wound healing in mice with deficiency of IL-6 versus IL-6 receptor*. J immunol, 2010. **184**(12): p. 7219-28.
182. Greene, A.K. and M. Puder, *Partial hepatectomy in the mouse: technique and perioperative management*. J Invest Surg, 2003. **16**(2): p. 99-102.
183. Fang, J., et al., *Stable antibody expression at therapeutic levels using the 2A peptide*. Nat Biotechnol, 2005. **23**(5): p. 584-90.
184. Garbers, C., et al., *Inhibition of classic signaling is a novel function of soluble glycoprotein 130 (sgp130), which is controlled by the ratio of interleukin 6 and soluble interleukin 6 receptor*. J Biol Chem, 2011. **286**(50): p. 42959-70.
185. Patijn, G.A., et al., *Hepatocyte growth factor induces hepatocyte proliferation in vivo and allows for efficient retroviral-mediated gene transfer in mice*. Hepatology, 1998. **28**(3): p. 707-16.
186. Bucher, N.L., U. Patel, and S. Cohen, *Hormonal factors concerned with liver regeneration*. Ciba Found Symp, 1977(55): p. 95-107.

187. Igawa, T., et al., *Hepatocyte growth factor is a potent mitogen for cultured rabbit renal tubular epithelial cells*. *Biochem Biophys Res Commun*, 1991. **174**(2): p. 831-8.
188. Schirmacher, P., et al., *The role of Ito cells in the biosynthesis of HGF-SF in the liver*. *EXS*, 1993. **65**: p. 285-99.
189. Prat, M., et al., *The receptor encoded by the human c-MET oncogene is expressed in hepatocytes, epithelial cells and solid tumors*. *Int J Cancer*, 1991. **49**(3): p. 323-8.
190. Naldini, L., et al., *Hepatocyte growth factor (HGF) stimulates the tyrosine kinase activity of the receptor encoded by the proto-oncogene c-MET*. *Oncogene*, 1991. **6**(4): p. 501-4.
191. Huh, C.G., et al., *Hepatocyte growth factor/c-met signaling pathway is required for efficient liver regeneration and repair*. *Proc Natl Acad Sci U S A*, 2004. **101**(13): p. 4477-82.
192. Schumacher, N., et al., *Shedding of Endogenous Interleukin-6 Receptor (IL-6R) Is Governed by A Disintegrin and Metalloproteinase (ADAM) Proteases while a Full-length IL-6R Isoform Localizes to Circulating Microvesicles*. *J Biol Chem*, 2015. **290**(43): p. 26059-71.
193. Sommer, J., et al., *Alternative intronic polyadenylation generates the interleukin-6 trans-signaling inhibitor sgp130-E10*. *J Biol Chem*, 2014. **289**(32): p. 22140-50.
194. Trefts, E., M. Gannon, and D.H. Wasserman, *The liver*. *Curr Biol*, 2017. **27**(21): p. R1147-R1151.
195. Campana, L. and J.P. Iredale, *Regression of Liver Fibrosis*. *Semin Liver Dis*, 2017. **37**(1): p. 1-10.
196. Friedman, S.L., *Liver fibrosis -- from bench to bedside*. *J Hepatol*, 2003. **38 Suppl 1**: p. S38-53.
197. Williams, E.J. and J.P. Iredale, *Liver cirrhosis*. *Postgrad Med J*, 1998. **74**(870): p. 193-202.
198. Ramesh, H., *Resection for hepatocellular carcinoma*. *J Clin Exp Hepatol*, 2014. **4**(Suppl 3): p. S90-6.
199. Nevzorova, Y.A., et al., *Partial hepatectomy in mice*. *Lab Anim*, 2015. **49**(1 Suppl): p. 81-8.
200. Norris, C.A., et al., *Synthesis of IL-6 by hepatocytes is a normal response to common hepatic stimuli*. *PLoS One*, 2014. **9**(4): p. e96053.
201. Fazel Modares, N., et al., *IL-6 Trans-signaling Controls Liver Regeneration After Partial Hepatectomy*. *Hepatology*, 2019.
202. Bartel, D.P., *MicroRNAs: genomics, biogenesis, mechanism, and function*. *Cell*, 2004. **116**(2): p. 281-97.
203. Zhou, Y., et al., *Inducible microRNA-590-5p inhibits host antiviral response by targeting the soluble interleukin-6 (IL6) receptor*. *J Biol Chem*, 2018. **293**(47): p. 18168-18179.
204. Wang, W., et al., *Human cancer cells suppress behaviors of endothelial progenitor cells through miR-21 targeting IL6R*. *Microvasc Res*, 2018. **120**: p. 21-28.
205. Hoge, J., et al., *IL-6 controls the innate immune response against *Listeria monocytogenes* via classical IL-6 signaling*. *J Immunol*, 2013. **190**(2): p. 703-11.
206. Kuramitsu, K., et al., *Failure of fibrotic liver regeneration in mice is linked to a severe fibrogenic response driven by hepatic progenitor cell activation*. *Am J Pathol*, 2013. **183**(1): p. 182-94.
207. Cressman, D.E., R.H. Diamond, and R. Taub, *Rapid activation of the Stat3 transcription complex in liver regeneration*. *Hepatology*, 1995. **21**(5): p. 1443-9.

208. Luig, M., et al., *Inflammation-Induced IL-6 Functions as a Natural Brake on Macrophages and Limits GN*. J Am Soc Nephrol, 2015. **26**(7): p. 1597-607.
209. Braun-Dullaeus, R.C., M.J. Mann, and V.J. Dzau, *Cell cycle progression: new therapeutic target for vascular proliferative disease*. Circulation, 1998. **98**(1): p. 82-9.
210. Yin, C., et al., *Hepatic stellate cells in liver development, regeneration, and cancer*. J Clin Invest, 2013. **123**(5): p. 1902-10.
211. Tsai, M.T., et al., *Regulation of HGF-induced hepatocyte proliferation by the small GTPase Arf6 through the PIP2-producing enzyme PIP5K1A*. Sci Rep, 2017. **7**(1): p. 9438.
212. Matsumoto, K. and T. Nakamura, *Emerging multipotent aspects of hepatocyte growth factor*. J Biochem, 1996. **119**(4): p. 591-600.
213. Puche, J.E., Y. Saiman, and S.L. Friedman, *Hepatic stellate cells and liver fibrosis*. Compr Physiol, 2013. **3**(4): p. 1473-92.
214. Kariv, R., et al., *Triiodothyronine and interleukin-6 (IL-6) induce expression of HGF in an immortalized rat hepatic stellate cell line*. Liver Int, 2003. **23**(3): p. 187-93.
215. Streetz, K.L., et al., *Interleukin 6 and liver regeneration*. Gut, 2000. **47**(2): p. 309-12.
216. Li, W., et al., *Global changes in interleukin-6-dependent gene expression patterns in mouse livers after partial hepatectomy*. Hepatology, 2001. **33**(6): p. 1377-86.
217. Barkhausen, T., et al., *Selective blockade of interleukin-6 trans-signaling improves survival in a murine polymicrobial sepsis model*. Crit Care Med, 2011. **39**(6): p. 1407-13.
218. Sommer, J., et al., *Interleukin-6, but not the interleukin-6 receptor plays a role in recovery from dextran sodium sulfate-induced colitis*. Int J Mol Med, 2014. **34**(3): p. 651-60.
219. Xu, M.J., et al., *Liver is the major source of elevated serum lipocalin-2 levels after bacterial infection or partial hepatectomy: a critical role for IL-6/STAT3*. Hepatology, 2015. **61**(2): p. 692-702.
220. Li, C. and Y.R. Chan, *Lipocalin 2 regulation and its complex role in inflammation and cancer*. Cytokine, 2011. **56**(2): p. 435-41.
221. Zhao, P., C.M. Elks, and J.M. Stephens, *The induction of lipocalin-2 protein expression in vivo and in vitro*. J Biol Chem, 2014. **289**(9): p. 5960-9.
222. Goetz, D.H., et al., *The neutrophil lipocalin NGAL is a bacteriostatic agent that interferes with siderophore-mediated iron acquisition*. Mol Cell, 2002. **10**(5): p. 1033-43.
223. Flo, T.H., et al., *Lipocalin 2 mediates an innate immune response to bacterial infection by sequestering iron*. Nature, 2004. **432**(7019): p. 917-21.
224. Berger, T., et al., *Lipocalin 2-deficient mice exhibit increased sensitivity to Escherichia coli infection but not to ischemia-reperfusion injury*. Proc Natl Acad Sci U S A, 2006. **103**(6): p. 1834-9.
225. Wang, X., et al., *Bacterial translocation after major hepatectomy in patients and rats*. Arch Surg, 1992. **127**(9): p. 1101-6.
226. Garbers, C. and J. Scheller, *Interleukin-6 and interleukin-11: same same but different*. Biol Chem, 2013. **394**(9): p. 1145-61.
227. Lorenz, L., et al., *Mechanosensing by beta1 integrin induces angiocrine signals for liver growth and survival*. Nature, 2018. **562**(7725): p. 128-132.
228. Nojima, H., et al., *Hepatocyte exosomes mediate liver repair and regeneration via sphingosine-1-phosphate*. J Hepatol, 2016. **64**(1): p. 60-8.
229. Mokdad, A.A., et al., *Liver cirrhosis mortality in 187 countries between 1980 and 2010: a systematic analysis*. BMC Med, 2014. **12**: p. 145.

230. Asrani, S.K., et al., *Burden of liver diseases in the world*. J Hepatol, 2019. **70**(1): p. 151-171.
231. Yao, F.Y., et al., *Liver transplantation for hepatocellular carcinoma: analysis of survival according to the intention-to-treat principle and dropout from the waiting list*. Liver Transpl, 2002. **8**(10): p. 873-83.
232. Belghiti, J. and R. Kianmanesh, *Surgical treatment of hepatocellular carcinoma*. HPB (Oxford), 2005. **7**(1): p. 42-9.
233. Poon, R.T. and S.T. Fan, *Assessment of hepatic reserve for indication of hepatic resection: how I do it*. J Hepatobiliary Pancreat Surg, 2005. **12**(1): p. 31-7.
234. Belli, A., et al., *Liver resection for hepatocellular carcinoma in patients with portal hypertension: the role of laparoscopy*. Hepatobiliary Surg Nutr, 2015. **4**(6): p. 417-21.
235. Tsoulfas, G., et al., *Current and future challenges in the surgical treatment of hepatocellular carcinoma: a review*. Int Surg, 2014. **99**(6): p. 779-86.
236. Zamora-Valdes, D., T. Taner, and D.M. Nagorney, *Surgical Treatment of Hepatocellular Carcinoma*. Cancer Control, 2017. **24**(3): p. 1073274817729258.
237. Mitsuyama, K., et al., *STAT3 activation via interleukin 6 trans-signalling contributes to ileitis in SAMPI/Yit mice*. Gut, 2006. **55**(9): p. 1263-9.
238. Nowell, M.A., et al., *Therapeutic targeting of IL-6 trans signaling counteracts STAT3 control of experimental inflammatory arthritis*. J Immunol, 2009. **182**(1): p. 613-22.
239. Rabe, B., et al., *Transgenic blockade of interleukin 6 transsignaling abrogates inflammation*. Blood, 2008. **111**(3): p. 1021-8.
240. Doganci, A., et al., *The IL-6R alpha chain controls lung CD4+CD25+ Treg development and function during allergic airway inflammation in vivo*. J Clin Invest, 2005. **115**(2): p. 313-25.

6 Zusammenfassung

IL-6 ist durch seine pleiotrope Eigenschaft an verschiedenen physiologischen und pathophysiologischen Prozessen im Körper beteiligt. Der klassische Signalweg, hervorgerufen durch die Bindung von IL-6 an den membranständigen IL-6R und die Interaktion mit gp130, ist in regenerative und homöostatische Prozesse involviert. Da nur wenige Zelltypen, wie z.B. Hepatozyten, den IL-6R exprimieren, ist der klassische Signalweg von IL-6 auf diese Zelltypen beschränkt. Das durch IL-6 und die lösliche Form des IL-6R (sIL-6R) und gp130 vermittelte Trans-Signal spielt bei pathophysiologischen Prozessen eine große Rolle. In Mäusen wird die lösliche Form des IL-6R durch die Aktivität von ADAM-Proteasen, hauptsächlich ADAM10 und ADAM17, erzeugt. In der Leber ist IL-6 der Hauptregulator der Akute-Phase-Reaktion. Darüber hinaus spielt IL-6 eine wichtige Rolle bei der Proliferation von Hepatozyten und der Leberregeneration. Vorangegangene Arbeiten haben gezeigt, dass IL-6 defiziente Tiere eine verringerte Leberregeneration und erhöhte Mortalität nach partieller Hepatektomie (PHX) zeigen. Allerdings ist der Beitrag der verschiedenen Signalwege von IL-6 zur Leberregeneration bisher noch unklar.

In Übereinstimmung mit publizierten Daten, konnte in dieser Arbeit eine reduzierte Regeneration und erhöhte Mortalität nach PHX in IL-6R defizienten Mäusen und in Mäusen, denen ein neutralisierender IL-6 Antikörper gespritzt wurde, nachgewiesen werden. Obwohl Hepatozyten den IL-6R exprimieren und daher als typische Zielzellen für das klassische IL-6 Signal gelten, führte eine selektive Blockade des IL-6 Trans-Signals durch lösliches gp130Fc (sgp130Fc) ebenfalls in einer reduzierten Regeneration und erhöhten Mortalität nach PHX. Um das Ergebnis, dass das IL-6 Trans-Signaling die Leberregeneration nach PHX steuert, zu untermauern, wurde die neue Mauslinie sIL-6R^{+/+} generiert, in der der gesamte membranständige IL-6R in den löslichen IL-6R überführt wurde. sIL-6R^{+/+} Mäuse können nur noch das IL-6 Trans-Signal ausführen. Regeneration und Mortalität nach PHX war in sIL-6R^{+/+} Mäusen und Wildtyp-Mäuse nicht unterscheidbar, was darauf hindeutete, dass das IL-6 Trans-Signal irgendwie die Proliferation von Hepatozyten durch den JAK/STAT Weg in sIL-6R^{+/+} Mäusen anregt. Eine mechanistische Erklärung ist, dass das IL-6 Trans-Signal die Expression von Hepatocyte Growth Factor (HGF) in

Hepatischen Sternzellen induziert. Es bleibt zu zeigen, ob das IL-6 Trans-Signal komplett indirekt über HGF oder auch direkt die Proliferation von Hepatozyten steuert.

Zusammenfassend zeigen die Daten, dass das IL-6 Trans-Signal die Leberregeneration nach PHX kontrolliert.

7 Summary

IL-6 through its pleiotropic features is involved in different physiological and pathophysiological processes in the body. Classic signaling mediated by IL-6 through the membrane-bound IL-6R and gp130 is involved in regenerative and homeostatic processes. Few cell types express IL-6R such as hepatocytes, therefore classic signaling of IL-6 is limited to these cell types. Trans-signaling mediated by IL-6 through the soluble form of IL-6R and gp130 is involved in pathophysiological processes. In mice, the soluble form of IL-6R is generated through ADAM protease activity mainly ADAM10 and ADAM17. In the liver IL-6 is the main driver of the acute phase response. Furthermore, IL-6 is important for hepatocyte proliferation and subsequent liver regeneration. Previous reports highlighted the role of IL-6 in liver regeneration by subjecting IL-6 deficient mice to partial hepatectomy (PHX). Absence of IL-6 resulted in less hepatocyte proliferation leading to higher mortality after PHX. To date, contribution of each signaling pathway of IL-6 in liver regeneration after PHX is not clear.

In agreement with published data, we also observed higher mortality and reduced regeneration after injection of neutralizing IL-6 monoclonal antibodies and in IL-6R deficient mice after PHX. Albeit hepatocytes express IL-6R and are considered as cells targeted by classic signaling, selective blockade of IL-6 trans-signaling by soluble gp130Fc (sgp130Fc), resulted also in higher mortality and less proliferation in wildtype mice after PHX. To support our finding that IL-6 trans-signaling controls liver regeneration after PHX, we generated and characterized a novel mouse model in which all membrane-bound IL-6 receptors were converted to the soluble form of IL-6R (sIL-6R^{+/+} mice). These mice are only able to execute IL-6 trans-signaling. Regeneration and mortality of sIL-6R^{+/+} mice was undistinguishable from wild-type mice after PHX, suggesting that IL-6 trans-signaling somehow induced hepatocyte proliferation through JAK/STAT pathway resulting in liver regeneration in sIL-6R^{+/+} mice after PHX. Mechanistically, IL-6 trans-signaling induced hepatocyte growth factor (HGF) expression in hepatic stellate cells. It remains to be shown, if IL-6 directly induces hepatocyte regeneration or whether the detour via hepatic stellate cells and HGF expression is more important.

In conclusion, the results showed that IL-6 trans-signaling is controlling liver regeneration following PHX.

8 Abbreviations

3'UTR 3'untranslated region

ADAM a disintegrin and metalloproteinase

BSA bovine serum albumin

CCl₄ carbon tetrachloride

cDNA copy DNA

CLC cardiotrophin-like-cytokine

CLF-1 cytokine-like factor 1 cm centimetre

CNTF ciliary neurotrophic factor α -receptor CT-1 cardiotrophin-1 C-terminal carboxy-terminal

DEN diethyl nitrosamine

DMEM Dulbecco's modified Eagle's Medium

DMSO dimethylsulfoxid

DNA deoxyribonucleic acid

dNTP deoxynucleotide

EDTA ethylenediaminetetraacetat

EGFR epidermal growth factor receptor

ELISA enzyme-linked immunosorbent assay

ER endoplasmic reticulum

Fc fragment crystallizable

FCS fetal calf serum

FNIII fibronectin Type III

FRT flippase recognition target

g gram

GAPDH glyceraldehyde 3-phosphate dehydrogenase

GFP green fluorescent protein

GFP green fluorescent protein

gp130 glycoprotein 130

GPI glycosylphosphatidylinositol

h hour

H&E staining

HCC hepatocellular carcinoma

HFD high-fat diet

HGF hepatocyte growth factor

HIL-6 hyper IL-6

HSC hepatic stellate cell

IBD inflammatory bowel diseases

IF Immunofluorescence staining

IFN interferon Ig immunoglobulin

Ig-like immunoglobulin like

IL interleukin

IL-6 interleukin 6

IL-6R interleukin 6 receptor

IZM intracellular domain

Jak janus kinase

kb kilo base

kDa kilodalton

LIF leukaemia inhibitory factor m murine M molar

LPS lipopolysaccharide

mAb monoclonal antibody

MAPK mitogen-activated protein kinase

MEF mouse embryonic fibroblast

mg milligram

min minute

miRNA microRNA

ml milliliter

mM millimolar

ng nanogram
NLS nuclear localization signal
nm nanomolar
ns not significant
N-terminal amino-terminal
OSM oncostatinM
PAGE polyacrylamide gel electrophoresis
PBS phosphate buffer saline
PCNA proliferating cell nuclear antigen
PCR polymerase chain reaction
PHX partial hepatectomy

PI3K phosphoinositide 3-kinase
PIAS protein inhibitor activated
PVDF Polyvinylidene fluoride
qPCR quantitative PCR R receptor
RA rheumatoid arthritis

RNA ribonucleic acid
RNase ribonuclease
rpm rounds per minute
RT room temperature
s second

SDS sodium dodecyl sulphate

sgp130 soluble gp130
sgp130 soluble gp130
SH2 containing phosphatase

SH2 src-homology 2 SHP2

sIL-6R soluble IL-6 receptor
sIL-6R soluble IL-6R

sIL-6R^{+/+} soluble IL-6R

SOCS suppressor of cytokine signaling

sp supernatant

STAT signal transducer and activator of transcription

STAT signal transducer and activator of transcription

TAE tris-acetat-EDTA buffer

TBS tris-buffered saline

TCZ tocilizumab

TEMED N,N,N',N'-tetramethylenediamine Tris tris-(hydroxymethyl-)aminomethane

TNF tumor necrosis factor

V volt

WB Western blot

WT wild

ZBM cytokine binding domain

µg microgram

µl microliter

µM micromolar

9 Publications

1. IL-6 Trans-signaling Controls Liver Regeneration After Partial Hepatectomy. Fazel *Modares N, *Polz R, Haghighi F, Lamertz L, Behnke K, Zhuang Y, Kordes C, Häussinger D, Sorg UR, Pfeffer K, Floss DM, Moll JM, Piekorz RP, Ahmadian MR, Lang PA, Scheller J. *Hepatology*, 2019, doi: 10.1002/hep.30774

(* shared authorship)
2. Cell-Mediated Maintenance of Cluster of Differentiation 169–Positive Cells Is Critical for Liver Regeneration. Behnke K, Zhuang Y, Xu HC, Sundaram B, Reich M, Shinde PV, Huang J, Modares NF, Tumanov AV, Polz R, Scheller J, Ware CF, Pfeffer K, Keitel V, Häussinger D, Pandyra AA, Lang KS, Lang PA. *Hepatology* May 2018, doi:10.1002/hep.30088
3. IL-23R Signaling Plays No Role in Myocardial Infarction. Engelowski E, Modares NF, Gorressen S, Bouvain P, Semmler D, Alter C, Ding Z, Flögel U, Schrader J, Xu H, Lang PA, Fischer J, Floss DM, Scheller J. *Sci Rep*. 2018, doi: 10.1038/s41598-018-35188-8

10 Acknowledgement

First and foremost, I would like to express my sincerest gratitude to my main supervisor Prof. Dr. Jürgen Scheller. I specially thanks him for giving the opportunity to do my Ph.D. in his research group and for all the enthusiasm about my work. Thanks for your support and guidance. I am grateful for the time I have spent in your group and the chance of meeting great group members. Thanks also to Prof. Dr. Philipp Lang for his great support during my Ph.D. I am looking forward to work with you in future.

I would like to thank Dr. Roland Piekorz, who have been supportive of my career goals and who supported me actively to pursue those goals. It was great to work with you.

Special thanks to all members of the Scheller's lab for scientific support and the fun provided on daily basis. Particularly I would like to thank Dr. Doreen Floss for taking care of me at the beginning of my Ph.D. and for mental support during these years. Thanks to Dr. Erika Engelowski for taking care and guiding me through the basic things in the lap needed to startup my project. Moreover, being great friend for me during those years. Erika hope to see you soon in Canada.

Thanks to Dr. Ursula Sorg and Dr. Kristina Behnke for their help with operations. Thanks to Sofie Moßner, Dr. Paul Baran for their support and the fun we had in the lab and most importantly helping me to improving my German skills. Thanks to Dr. Alexander Lang for the great discussions. Thanks to Dr. Fereshteh Haghighi for her endless support when nothing was working and for her help to do western blots. Thanks to Robin Polz and Dr. Jens Moll for their help in different challenges during my Ph.D.

Especial thanks to Petra Oprea Jeremic for all her kind support, her efforts to solve any kind of problems and issues for me, for her invaluable mental support and for her great heart. Petra you are the best.

Anna Masiarz, Marcus Kuchner, Denise Heise and Artur Schneider, thank you for your daily support and being my best friends. I will miss you so much and hope to see you very soon.

Thanks to Freshteh Kamrani for encouraging, me all the time. Great thanks to Sebastian Fye for handling the chaos in the lab and helping me whenever I needed help. Also, thanks to Prof. Dr. Ahmdian and all his group members particularly Parivash Nouri, Neda Jasemi, Marcel Buchholzer, Oliver Krumbach and Farhad Bazgir for the fun and their support.

Here, I would like to thank my master thesis supervisor Prof. Dr. Mathias Hornef for his great support since then until now. I want to thank Dr. Aline Dupont. She was the most influential teacher I ever had. With her brilliant advice and endless support, I improved and progressed in my academic career. Thanks to my best friend Dr. Kaiyi Zhang and Martin Jongejan for great time and their unconditional love and support. Thanks to Zohre Soltani for being with me all the time while being in Iran and helping me to calm down in my difficult times.

I am also thankful to all my lovely friends in Iran and Germany: Parisa, Roya, Hajar, Ziba, Praivash, Mahyar, Neda, Amir, Mona, Kazem, Ehsan, Liela, Yuan Kaiyi, Aline, Chris, Saeideh, Fereshteh, Parasto, Hamed, Afsoon, Mahsa, Fahime, Farzam I and II, Sina, Golanz, Milad, Darja, Marago, Afshin, Hossein, Sandra and all my other friends around the world who have made for me these four years memorable for me. This Ph.D. thesis would not have been possible without the guidance, encouragement and help from all the kind people around me.

The last but not least, an honorable mention goes to my greatest loves of my life, my parents and my sister, Nasim, for their dedication, understanding and many years of invaluable support in all the ups and downs of my life. Nasim; without your great support since my childhood until now, I could not achieve my goals, thanks for being there always for me and make me feel I am home while being far from home.

Great thanks to Faraz- you are my soul mate and my home. Thanks for providing me with unfailing support and continuous encouragement through these years and writing process. Looking forward to building our life and write great chapters of life together.

To Dad, Mom, Nasim and Faraz from deep of my heart I say that I love you all.